Development of an Improved and Internally-Consistent Framework for Evaluating Liquefaction Damage Potential

Sneha Upadhyaya

Dissertation submitted to the faculty of the Virginia Polytechnic Institute and State University in partial fulfillment of the requirements for the degree of

Doctor of Philosophy
In
Civil Engineering

Russell A. Green, Co-Chair
Adrian Rodriguez-Marek, Co-Chair
Brett W. Maurer
Ioannis Koutromanos

1 November 2019
Blacksburg, VA

Keywords: soil liquefaction, liquefaction triggering, manifestation severity index

Development of an Improved and Internally-Consistent Framework for Evaluating Liquefaction Damage Potential

Sneha Upadhyaya

ABSTRACT (Academic)

Soil liquefaction continues to be one of the leading causes of ground failure during earthquakes, resulting in significant damage to infrastructure around the world. The study presented herein aims to develop improved methodologies for predicting liquefaction triggering and the consequent damage potential such that the impacts of liquefaction on natural and built environment can be minimized. Towards this end, several research tasks are undertaken, with the primary focus being the development of a framework that consistently and sufficiently accounts for the mechanics of liquefaction triggering and surface manifestation. The four main contributions of this study include: (1) development of a framework for selecting an optimal factor of safety (*FS*) threshold for decision making based on project-specific costs of mispredicting liquefaction triggering, wherein the existing stress-based "simplified" model is used to predict liquefaction triggering; (2) rigorous investigation of manifestation severity index (*MSI*) thresholds for distinguishing cases with and without manifestation as a function of the average inferred soil-type within a soil profile, which may be employed to more accurately estimate liquefaction damage potential at sites having high fines-content, high plasticity soils; (3) development of a new manifestation model, termed Ishihara-inspired Liquefaction Severity Number (*LSNish*), that more fully accounts for the effects of non-liquefiable crust thickness and the effects of contractive/dilative tendencies of soil on the occurrence and severity of manifestation; and (4) development of a framework for deriving a "true" liquefaction triggering curve that is consistent with a defined manifestation model such that factors influential to triggering and manifestation are handled more rationally and consistently. While this study represents significant conceptual advance in how risk due to liquefaction is evaluated, additional work will be needed to further improve and validate the methodologies presented herein.

Development of an Improved and Internally-Consistent Framework for Evaluating Liquefaction Damage Potential

Sneha Upadhyaya

ABSTRACT (General Audience)

Soil liquefaction continues to be one of the leading causes of ground failure during earthquakes, resulting in significant damage to infrastructure around the world (e.g., the 2010-2011 Canterbury earthquake sequence in New Zealand, 2010 Maule earthquake in Chile, and the 2011 Tohoku earthquake in Japan). Soil liquefaction refers to a condition wherein saturated sandy soil loses strength as a result of earthquake shaking. Surface manifestations of liquefaction include features that are visible at the ground surface such as sand boils, ejecta, cracks, and settlement. The severity of manifestation is often used as a proxy for damage potential of liquefaction. The overarching objective of this dissertation is to develop improved models for predicting triggering (i.e., occurrence) and surface manifestation of liquefaction such that the impacts of liquefaction on the natural and built environment can be minimized. Towards this end, this dissertation makes the following main contributions: (1) development of an approach for selecting an appropriate factor of safety (*FS*) against liquefaction for decision making based on project-specific consequences, or costs of mispredicting liquefaction; (2) development of an approach that allows better interpretations of predictions of manifestation severity made by the existing models in profiles having high fines-content, high plasticity soil strata (e.g., clayey and silty soils), given that the models perform poorly in such conditions; (3) development of a new model for predicting the severity of manifestation that more fully accounts for factors controlling manifestation; and (4) development of a framework for predicting liquefaction triggering and surface manifestation such that the distinct factors influential to each phenomenon are handled more rationally and consistently.

ACKNOWLEDGEMENTS

I would like to express a deep sense of gratitude to my advisors, Dr. Russell A. Green, Dr. Adrian Rodriguez-Marek, and Dr. Brett W. Maurer, for their proficient guidance, support and encouragement throughout my PhD studies at Virginia Tech. They are not just great research advisors but also outstanding mentors and a great source of inspiration. Thank you for all that you have done for me and most importantly, for believing in me.

I would also like to thank Dr. Ioannis Koutromanos for reviewing this dissertation and providing useful feedback. I am also thankful to the entire geotechnical faculty at Virginia Tech who have in many ways contributed to the knowledge and experience that I have gained during my time here. Further, I would like to thank Dr. Binod Tiwari, who was my advisor during my master’s studies at California State University, Fullerton, for encouraging me to pursue a PhD at Virginia Tech.

I am also grateful for the good friends I have made during my PhD studies, who have been always very helpful and supportive, personally as well as intellectually. Special thanks to Mahdi Bahrampouri, Kristin Ulmer, and Tyler Quick for all the stimulating and insightful research discussions. Also thanks goes to Grace Huang, Dennis Kiptoo, Ali Albatal, and Cagdas Bilici, who were not just good friends but also great officemates. I am thankful for the Nepalese friends in Blacksburg who were like family to me, for all the good times we have shared together and the memories we have made.

I would like to greatly acknowledge the funding support provided by the National Science Foundation (NSF) grants CMMI-1435494, CMMI-1724575, CMMI-1751216, and CMMI-1825189, as well as Pacific Earthquake Engineering Research Center (PEER) grant 1132-NCTRBM and U.S. Geological Survey (USGS) award G18AP-00006. I would also like to thank our collaborators from New Zealand, especially Dr. Sjoerd van Ballegooy for his contributions towards the development of the New Zealand Geotechnical Database that is utilized by this study.

Finally, I would like to thank my family, especially my husband Santosh Bhattarai for his immense love, support and encouragement, my parents for all they have done to make me the person I am today, as well as my brother, parents-in-law, and brother-in-law for their love and moral support.

TABLE OF CONTENTS

LIST OF FIGURES

LIST OF TABLES

Chapter 1: Introduction

1.1 Problem Statement

Soil liquefaction continues to be one of the leading causes of ground failure during earthquakes, resulting in significant damage to infrastructure around the world (e.g., the 2010-2011 Canterbury earthquake sequence in New Zealand, 2010 Maule earthquake in Chile, and the 2011 Tohoku earthquake in Japan, among others). As such, accurate prediction of the occurrence and consequences of liquefaction is essential for reducing the risks due to liquefaction in a cost-effective manner (National Academies of Sciences, Engineering, and Medicine 2016). The present study aims at reducing the impacts of earthquake induced soil liquefaction by developing improved methodologies to evaluate liquefaction triggering and damage potential. In particular, the research presented herein is largely motivated by the need to address shortcomings in the existing methodologies to properly account for the mechanics of liquefaction triggering and the severity of surficial liquefaction manifestations within a consistent framework. Towards this end, this dissertation addresses the following pertinent issues:

1. The stress-based simplified model, originally proposed by Whitman (1971) and Seed and Idriss (1971), is the most commonly used approach for predicting liquefaction triggering at a site. Although probabilistic variants of this model have been developed, deterministic models still represent the standard of practice. In a deterministic liquefaction triggering model, the normalized cyclic stress ratio (CSR^*) or seismic demand, and the normalized cyclic resistance ratio ($CRR_{M7.5}$) are used to compute a factor of safety (FS) against liquefaction triggering (i.e., $FS = CRR_{M7.5}/CSR^*$). Towards this end, "rules of thumb" are often used to select an appropriate FS for decision making, which are largely based on heuristic approaches. Due to the lack of a standardized approach for selecting an appropriate FS, guidelines have been proposed in the literature, often without any consideration for the costs of mispredicting liquefaction, which could vary among different engineering projects. Accordingly, this dissertation investigates the relationship between the costs of misprediction and appropriate FS for decision making using a quantitative, standardized approach. While this study focuses on FS, similar relationships are also investigated between the costs of misprediction and probability of liquefaction triggering (PL).

2. While the "simplified" model predicts the occurrence of liquefaction at a specific depth in a profile, it does not predict the severity of surficial liquefaction manifestation, which relates to the damage potential at the ground surface. Manifestation severity index (*MSI*) models have been proposed to tie liquefaction triggering to the occurrence and severity of surficial manifestations (e.g., Liquefaction Potential Index, *LPI*; Ishihara-inspired *LPI*, *LPIish*; and Liquefaction Severity Number, *LSN*). Retrospective evaluations of such models during the 2010-2016 Canterbury, New Zealand earthquakes have shown that they systematically over-predicted a large number of case histories that were generally comprised of profiles having high fines-content, high plasticity soil strata. Accordingly, this dissertation further investigates the effects of high fines-content, high plasticity soil strata on the predictive performance of *LPI*, *LPIish*, and *LSN*. Specifically, for each of these models, manifestation severity thresholds as well as their predictive efficiencies are investigated as a function of the soil behavior type index (I_c) averaged over the upper 10 m of the soil profile (I_{c10}). The I_{c10} parameter is used to infer the extent to which a soil profile contains high fines-content, high plasticity strata.

3. Furthermore, existing manifestation models have inherent limitations such that they may not fully account for the factors influencing surface manifestations. In this dissertation, a new manifestation model is derived using insights from the existing models and the understanding of the mechanics of manifestation from the literature. This model is derived as a conceptual and mathematical merger of the *LSN* formulation (van Ballegooy et al. 2012; 2014) and Ishihara's relationship for predicting surface manifestation as a function of the relative thicknesses of the non-liquefied crust and underlying liquefied layer (Ishihara 1985), hence termed *LSNish*. As such, *LSNish* accounts for the influences of contractive/dilative tendencies of soils as well as the non-liquefied crust thickness in predicting the occurrence and severity of manifestation.

4. Lastly, it will be shown that the existing methodology for developing liquefaction triggering models is inconsistent with how it is used in predicting the occurrence and severity of surficial liquefaction manifestations. The manifestation models often assume that the triggering curves are "true triggering" curves (i.e., free of factors influencing surface manifestation). However, because of the way the triggering curves are being

developed, some of the factors influencing surface manifestations (e.g., dilative tendencies of dense soils) may already be embedded in the curve, making them combined "triggering" and "manifestation" curves. As a result, their use in conjunction with the manifestation model may double-count such factors. This dissertation presents an approach to derive a "true" liquefaction triggering curve that is consistent with a defined manifestation model.

1.2 Dissertation Structure and Contents

The four issues stated above are addressed in a series of four manuscripts, presented in Chapters 2 through 5, which forms the main body of this dissertation. These manuscripts will be submitted to recognized peer-reviewed journals in geotechnical and/or earthquake engineering. Chapter 6 presents the summary and key findings of this dissertation. Appendices A and B are two peer-reviewed conference papers that are included in the proceedings of the 7th International Conference on Earthquake Geotechnical Engineering (7ICEGE) and the 13th Australia New Zealand Conference on Geomechanics 2019, respectively. The two conference papers are presented as appendices since their main findings are discussed in the main body of this dissertation.

Chapter 2 presents a framework that relates optimal *FS* thresholds for decision making to the costs of mispredicting liquefaction triggering. As such, the framework presented in this chapter can be used to select a project-specific optimal *FS* decision threshold based on the costs of liquefaction risk-mitigation schemes relative to the costs associated with the consequences of liquefaction. Additionally, it is shown that the framework proposed herein can be similarly used to select optimal *PL* thresholds based on the relative costs of misprediction.

Chapter 3 investigates the influence of high fines-content, high plasticity soils on the predictive performance of three different *MSI* models. Specifically, receiver operating characteristic (ROC) analyses are performed on liquefaction case-histories compiled from the 2010-2016 Canterbury, New Zealand, earthquakes to investigate manifestation severity classification thresholds for the *LPI*, *LPIish*, and *LSN* models as well as their predictive efficiencies as a function of I_{c10}. Additionally, probabilistic models are proposed for assessing the severity of manifestations as a function of *MSI* and I_{c10}.

Chapter 4 presents the development of *LSNish*. *LSNish* is evaluated using the Canterbury earthquake liquefaction case histories and its predictive efficiency is compared to those of *LPI* and

LSN. Despite *LSNish* accounting for the mechanics of manifestation in a more appropriate manner, its predictive efficiency is shown to be less than that of the existing models. One likely reason for this is the double counting of the dilative tendencies of dense soils by *LSNish*. The post-liquefaction volumetric strain potential (ε_v) included in the *LSNish* formulation uses *FS* as an input which inherently accounts for the dilative tendencies of dense soils via the shape of the triggering curve that tends to vertical at higher penetration resistance. These findings indicate that the existing methodology for developing liquefaction triggering curves is inconsistent with how it is used in predicting the occurrence and severity of surficial liquefaction manifestation.

Accordingly, Chapter 5 presents an internally-consistent approach to developing models that predict triggering and surface manifestation of liquefaction. Specifically, this chapter presents a methodology to derive a "true" liquefaction triggering curve that is consistent with a defined manifestation model (e.g., *LSNish*). Utilizing the liquefaction case histories from the 2010-2016 Canterbury earthquakes, deterministic and probabilistic variants of the "true" triggering curve are derived within the *LSNish* formulation, for predominantly clean to silty sand profiles. The "true" triggering curve is shown to perform better than the existing triggering curves when operating within the *LSNish* formulation.

1.3 Attribution

The following provides the list of coauthors and their contributions to each manuscript included in this dissertation:

Chapter 2: Selecting optimal factor of safety and probability of liquefaction triggering thresholds for decision making based on misprediction costs

Sneha Upadhyaya, PhD candidate at the Department of Civil and Environmental Engineering, Virginia Tech, Blacksburg, Virginia, USA.

- Lead author; performed literature review; compiled liquefaction case history databases from the literature; performed all analyses; wrote the draft manuscript; prepared all figures and tables; incorporated comments from the coauthors to prepare a final draft of the manuscript.

Brett W. Maurer, PhD, Assistant Professor at the Department of Civil and Environmental Engineering, University of Washington, Seattle, Washington, USA.

- Research co-advisor to the lead author; provided guidance and made intellectual contributions throughout the study; proposed using the Receiver Operating Characteristic (ROC) methodology to develop the framework presented in this chapter; reviewed the draft manuscript and provided useful feedback.

Russell A. Green, PhD, Professor at the Department of Civil and Environmental Engineering, Virginia Tech, Blacksburg, Virginia, USA.

- Research co-advisor to the lead author; provided guidance and made intellectual contributions throughout the study; reviewed the draft manuscript and provided useful feedback.

Adrian Rodriguez-Marek, PhD, Professor at the Department of Civil and Environmental Engineering, Virginia Tech, Blacksburg, Virginia, USA.

- Research co-advisor to the lead author; provided guidance and made intellectual contributions throughout the study; reviewed the draft manuscript and provided useful feedback.

Chapter 3: Surficial liquefaction manifestation severity thresholds for profiles having high fines-content, high plasticity soils

Sneha Upadhyaya, PhD candidate at the Department of Civil and Environmental Engineering, Virginia Tech, Blacksburg, Virginia, USA.

- Lead author; performed literature review; added to the existing liquefaction case-history database from the 2010-2016 Canterbury, New Zealand, earthquakes that was largely compiled by Dr. Brett W. Maurer; performed all analyses; wrote the draft manuscript; prepared all figures and tables; incorporated comments from the coauthors to prepare a final draft of the manuscript.

Brett W. Maurer, PhD, Assistant Professor at the Department of Civil and Environmental Engineering, University of Washington, Seattle, Washington, USA.

- Research co-advisor to the lead author; provided guidance and made intellectual contributions throughout the study; provided the compiled liquefaction case-history database from the 2010-2016 Canterbury, New Zealand, earthquakes; provided matlab scripts for processing/analyzing the case-history data; reviewed the draft manuscript and provided useful feedback. In addition, Dr. Maurer's PhD research formed the basis of this study.

Russell A. Green, PhD, Professor at the Department of Civil and Environmental Engineering, Virginia Tech, Blacksburg, Virginia, USA.

- Research co-advisor to the lead author; provided guidance and made intellectual contributions throughout the study; contributed to the post-earthquake ground reconnaissance following the Canterbury earthquakes; initiated the idea of investigating the performance of different liquefaction triggering models and *MSI* models using the Canterbury earthquakes liquefaction case histories; reviewed the draft manuscript and provided useful feedback.

Adrian Rodriguez-Marek, PhD, Professor at the Department of Civil and Environmental Engineering, Virginia Tech, Blacksburg, Virginia, USA.

- Research co-advisor to the lead author; provided guidance and made intellectual contributions throughout the study; reviewed the draft manuscript and provided useful feedback.

Sjoerd van Ballegooy, PhD, Technical Director at Tonkin + Taylor Ltd., Newmarket, New Zealand.

- Led the post-earthquake reconnaissance efforts following the Canterbury earthquakes; oversaw the extensive geotechnical site characterization program in Christchurch and surroundings; designed the online New Zealand Geotechnical Database from which the case histories for this study were derived.

Chapter 4: Ishihara-inspired Liquefaction Severity Number (LSNish)

Sneha Upadhyaya, PhD candidate at the Department of Civil and Environmental Engineering, Virginia Tech, Blacksburg, Virginia, USA.

- Lead author; performed literature review; performed all analyses; wrote the draft manuscript; prepared all figures and tables; incorporated comments from the coauthors to prepare a final draft of the manuscript.

Russell A. Green, PhD, Professor at the Department of Civil and Environmental Engineering, Virginia Tech, Blacksburg, Virginia, USA.

- Research co-advisor to the lead author; provided guidance and made intellectual contributions throughout the study; derived the *LSNish* formulation; reviewed the draft manuscript and provided useful feedback.

Brett W. Maurer, PhD, Assistant Professor at the Department of Civil and Environmental Engineering, University of Washington, Seattle, Washington, USA.

- Research co-advisor to the lead author; provided guidance and made intellectual contributions throughout the study; reviewed the draft manuscript and provided useful feedback.

Adrian Rodriguez-Marek, PhD, Professor at the Department of Civil and Environmental Engineering, Virginia Tech, Blacksburg, Virginia, USA.

- Research co-advisor to the lead author; provided guidance and made intellectual contributions throughout the study; reviewed the draft manuscript and provided useful feedback.

Sjoerd van Ballegooy, PhD, Technical Director at Tonkin and Taylor, Ltd., Newmarket, New Zealand.

- Developed the *LSN* formulation; led the post-earthquake reconnaissance efforts following the Canterbury earthquakes; oversaw the extensive geotechnical site characterization program in Christchurch and surroundings; designed the online New Zealand Geotechnical Database from which the case histories for this study were derived.

Chapter 5: Development of a "true" liquefaction triggering curve

Sneha Upadhyaya, PhD candidate at the Department of Civil and Environmental Engineering, Virginia Tech, Blacksburg, Virginia, USA.

- Lead author; performed literature review; added to the existing liquefaction case-history database from the 2010-2016 Canterbury earthquakes that was largely compiled by Dr. Brett W. Maurer; contributed to the development of the framework for deriving the "true" triggering curve; performed all analyses; wrote the draft manuscript; prepared all figures and tables; incorporated comments from the coauthors to prepare a final draft of the manuscript.

Russell A. Green, PhD, Professor at the Department of Civil and Environmental Engineering, Virginia Tech, Blacksburg, Virginia, USA.

- Research co-advisor to the lead author; provided guidance and made intellectual contributions throughout the study; developed the conceptual framework for deriving the "true" triggering curve; reviewed the draft manuscript and provided useful feedback.

Adrian Rodriguez-Marek, PhD, Professor at the Department of Civil and Environmental Engineering, Virginia Tech, Blacksburg, Virginia, USA.

- Research co-advisor to the lead author; provided guidance and made intellectual contributions throughout the study; contributed largely to the development of the probabilistic framework presented in this study; reviewed the draft manuscript and provided useful feedback.

Brett W. Maurer, PhD, Assistant Professor at the Department of Civil and Environmental Engineering, University of Washington, Seattle, Washington, USA.

- Research co-advisor to the lead author; provided guidance and made intellectual contributions throughout the study; provided the compiled liquefaction case-history database from the 2010-2016 Canterbury, New Zealand, earthquakes; provided matlab scripts for processing/analyzing the case histories; contributed to the development of the framework for deriving the "true" triggering curve; reviewed the draft manuscript and provided useful feedback.

References

Ishihara, K. (1985). "Stability of natural deposits during earthquakes." *Proceedings of the 11th International Conference on Soil Mechanics and Foundation Engineering,* San Francisco, CA, USA, 1: 321-376.

National Academies of Sciences, Engineering, and Medicine (2016). *State of the art and practice in the assessment of earthquake-induced soil liquefaction and its consequences*. Washington, DC: The National Academies Press. https://doi.org/10.17226/23474.

Seed, H.B. and Idriss, I.M. (1971). "Simplified procedure for evaluating soil liquefaction potential." *Journal of the Soil Mechanics and Foundations Division*, 97(SM9): 1249–1273.

van Ballegooy, S., Malan, P.J., Jacka, M.E., Lacrosse, V.I.M.F., Leeves, J.R., Lyth, J.E., and Cowan, H. (2012). "Methods for characterising effects of liquefaction in terms of damage severity." *Proc. 15th World Conference on Earthquake Engineering* (15 WCEE), Lisbon, Portugal, September 24-28.

van Ballegooy, S., Malan, P., Lacrosse, V., Jacka, M.E., Cubrinovski, M., Bray, J.D., O'Rourke, T.D., Crawford, S.A., and Cowan, H. (2014). "Assessment of liquefaction-induced land damage for residential Christchurch." *Earthquake Spectra*, 30(1): 31-55.

Whitman, R.V. (1971). "Resistance of soil to liquefaction and settlement." *Soils and Foundations*, 11: 59-68.

Chapter 2: Selecting optimal factor of safety and probability of liquefaction triggering thresholds for decision making based on misprediction costs

Sneha Upadhyaya[1]; Brett W. Maurer[2]; Russell A. Green[3]; and Adrian Rodriguez-Marek[3]

[1]Graduate Student, Department of Civil and Environmental Engineering, Virginia Tech, Blacksburg, VA 24061.

[2]Assistant Professor, Department of Civil and Environmental Engineering, University of Washington, Seattle, WA 98195.

[3]Professor, Department of Civil and Environmental Engineering, Virginia Tech, Blacksburg, VA 24061.

2.1 Abstract

In deterministic liquefaction evaluations, the liquefaction triggering potential at a site is evaluated using factor of safety (*FS*) against liquefaction. In any engineering project, a minimum acceptable *FS* is required for design. While some guidelines are available in the literature for selecting an appropriate *FS*, there is no quantitative, standard approach. Moreover, such guidelines do not acknowledge that the choice of *FS* should be affected by the costs of mispredicting liquefaction which could differ from project to project. Herein, Receiver Operating Characteristic (ROC) analyses are used to select project-specific *FS* based on the relative costs of mispredictions. Towards this end, utilizing different liquefaction triggering models and their associated case-history databases, relationships are established between optimal *FS* threshold for decision making and the ratio of the cost of a false-positive prediction to the cost of a false-negative prediction (i.e., cost ratio, *CR*). It is shown that the optimal *FS-CR* relationships are specific to the triggering model and the database used. Additionally, it is shown that the deterministic triggering curves recommended by each model inherently corresponds to a certain *CR*, indicative of the degree of conservatism inherent to the position of the triggering curve. As an alternative to using *FS* to quantify liquefaction triggering potential, probabilistic variants of the triggering models were used to develop similar relationships between *CR* and probability of liquefaction triggering (*PL*) decision thresholds.

2.2 Introduction

The main objective of this study is to develop a framework that relates optimal factor of safety against liquefaction triggering (*FS*) thresholds to the cost of mispredicting liquefaction triggering; "optimal" herein should be understood as "optimal for decision making." As such, the framework proposed herein can be used to select project-specific *FS* thresholds based on the costs of liquefaction risk-mitigation schemes relative to the costs associated with the consequences of liquefaction. While the present study focuses on *FS*, it is shown that the framework proposed herein can also be used to relate optimal probability of liquefaction triggering (*PL*) threshold to the relative costs of mispredicting liquefaction triggering.

The stress-based "simplified" model is the most-widely used approach for predicting liquefaction triggering at a site. This model was originally developed by Whitman (1971) and Seed and Idriss (1971) for Standard Penetration Test (SPT) and has been subsequently updated for use with other in-situ testing methods such as the Cone Penetration Test (CPT) and shear-wave velocity (V_s) (e.g., Robertson and Wride 1998; Cetin et al. 2004; 2018; Moss et al. 2006; Idriss and Boulanger 2008; 2010; Kayen et al. 2013; Boulanger and Idriss 2012; 2014; Green et al. 2019; among others). Moreover, both deterministic and probabilistic variants of the simplified model have been proposed, where the latter accounts for the uncertainties in the model and its input parameters. In a deterministic liquefaction triggering model, the normalized cyclic stress ratio (CSR^*), or the seismic demand, and the normalized cyclic resistant ratio ($CRR_{M7.5}$), or soil capacity, are used to compute an *FS* against liquefaction:

$$FS = \frac{CRR_{M7.5}}{CSR^*} \tag{2.1}$$

where: CSR^* is the cyclic stress ratio normalized to a M7.5 event and corrected to an effective overburden stress of 1 atm and level-ground conditions and $CRR_{M7.5}$ is the cyclic resistant ratio normalized to the same conditions as CSR^* and is computed using the semi-empirical relationships that are a function of in-situ test metrics, which have been normalized to the effective overburden stress and corrected for fines-content. These metrics include SPT blow count ($N_{1,60cs}$); CPT tip resistance (q_{c1Ncs}); and small strain V_s (V_{s1}). Liquefaction is predicted to trigger when $FS \leq 1$ (i.e., when the demand equals or exceeds the capacity).

In a probabilistic liquefaction triggering model, a probability of liquefaction triggering (*PL*) is estimated generally as a function of the predictor variables that correlate to the capacity of the soil (e.g., $N_{1,60cs}$; q_{c1Ncs}; or V_{s1}), the demand imposed by the earthquake shaking (e.g., CSR^*), as well as the uncertainties in the triggering model. Often deterministic $CRR_{M7.5}$ curves correspond to $PL \approx$ 15% (e.g., Cetin et al. 2004; Moss et al. 2006; Boulanger and Idriss 2014). Although probabilistic liquefaction triggering models are preferred for a performance-based engineering framework, the deterministic model (i.e., *FS*) still represents the standard of practice for predicting liquefaction triggering at a site. Although in theory, liquefaction should not trigger for $FS > 1$, *FS* ranging from 1 to 1.5 are generally used for design, typically based on "rules of thumb." While such rules-of-thumb are somewhat guided by factors such as the uncertainty in the triggering model, importance of the structure, and consequences of liquefaction, they have been based largely on heuristic approaches. Due to the lack of a standardized approach for selecting *FS*, various guidelines have been proposed in the literature. For example, according to the 2009 NEHRP recommended seismic provisions by the Building Seismic Safety Council (2009), *FS* of 1.1 to 1.3 is generally appropriate for building sites to account for the chance that liquefaction occurred at depth, but did not manifest at the ground surface, for some of the case histories from previous events having *FS* in this range. Moreover, they refer to Martin and Lew (1999) (e.g., Table 2.1) for additional guidance on selecting *FS*, which considers different ground failure mechanisms (i.e., "settlement," "surface manifestation," and "lateral spreading") as well as the post-liquefaction strain potential of soil having an associated penetration resistance (e.g., $N_{1,60cs}$).

In any engineering project, the choice of *FS* (i.e., the desired degree of conservatism) should account for the consequence, or cost, of mispredicting liquefaction. However, the existing guidelines for selecting an appropriate *FS* do not account for such misprediction costs. These include the costs of false-negative predictions (i.e., liquefaction occurs, but was not predicted in the design event), which are the costs of liquefaction-induced damage (e.g., property damage, reconstruction and rehabilitation costs, etc.); and the costs of false-positive predictions (i.e., liquefaction is predicted, but did not occur in the design event), which could be those of unnecessary or over-designed liquefaction risk-mitigation schemes (e.g., ground improvement, stronger foundation design and construction, etc.). Clearly, these costs can vary among different engineering projects. For example, the costs associated with mispredicting liquefaction beneath a one-story residential building will be likely very different than those from a similar misprediction beneath a large earthen dam. As such, optimal, project-specific *FS* can be selected based on associated costs of mispredicting liquefaction triggering.

Accordingly, the present study uses a quantitative, standardized approach to select optimal *FS* thresholds for decision making, based on the costs of mispredicting liquefaction triggering. Towards this end, Receiver Operating Characteristic (ROC) analyses are performed on five liquefaction triggering models, using the field case-history databases from which the respective models were developed. Specifically, for each model, the ROC analyses are used to relate the optimal *FS* decision threshold to the ratio of false-positive costs to false-negative costs. This ratio is referred to herein as the cost ratio (*CR*). As a secondary focus, this study also derives relationships between misprediction costs and optimal *PL* thresholds.

In the following, overviews of the liquefaction triggering models and the associated databases are presented first, which is followed by an overview of the ROC analysis and a demonstration of how it can be used in deriving relationships between *CR* and optimal *FS* threshold. Next, optimal *FS*-*CR* relationships specific to different liquefaction triggering models, as well as a generic optimal *FS*-*CR* relationship, are presented and discussed. Finally, similar relationships are derived using *PL* as an alternative to *FS*.

2.3 Data and Methodology

2.3.1 Liquefaction triggering models and associated databases used

In the present study, five different liquefaction triggering models based on three different in-situ testing methods are analyzed using the field case-history databases from which the respective models were developed. These include the SPT-based models of Boulanger and Idriss (2014) [BI14-SPT] and Cetin et al. (2018) [Cea18], CPT-based models of Boulanger and Idriss (2014) [BI14-CPT] and Green et al. (2019) [Gea19], and V_s-based model of Kayen et al. (2013) [Kea13]. Each of these studies present both deterministic and probabilistic variants of the $CRR_{M7.5}$ curve, except for Gea19, which only presents the former.

Underlying each liquefaction triggering model is the case-history database from which the model was derived. Figure 2.1(a-e) contain the probabilistic $CRR_{M7.5}$ curves (except Figure 2.1d for Gea19, which only contains their deterministic $CRR_{M7.5}$ curve) and the associated liquefaction case-history data for BI14-SPT, Cea18, BI14-CPT, Gea19, and Kea13. Moreover, Table 2.1

summarizes the number of "liquefaction," "no liquefaction," and "marginal" cases in the database associated with each model. Note that, in this study, the "marginal" case histories are also treated as "liquefaction" cases. The deterministic $CRR_{M7.5}$ curves recommended by BI14-SPT, BI14-CPT, and Kea13 correspond to a *PL* of approximately 15%. However, Cea18 recommend their median (i.e., *PL* = 50%) $CRR_{M7.5}$ curve as their deterministic curve. The deterministic $CRR_{M7.5}$ for each of the above models are indicated in red in Figure 2.1(a-e).

ROC analyses were performed on each model using their associated case-history database, to relate optimal *FS* and *PL* to the relative costs of mispredicting liquefaction triggering, which is expressed as *CR*. The following section presents an overview of ROC analysis and how it can be used to derive such relationships.

2.3.2 Overview of ROC analysis

Receiver Operating Characteristics (ROC) analysis is a widely adopted tool to evaluate the performance of diagnostic tests. While ROC analysis has been extensively use in medical diagnostics (e.g., Zou 2007), its use in geotechnical engineering is relatively limited (e.g., Oommen et al. 2010; Maurer et al. 2015a,b,c; 2017a,b; 2019; Green et al. 2015; 2017; Zhu et al. 2017; Upadhyaya et al. 2018; 2019). In particular, in cases where the distribution of "positives" (e.g., liquefaction cases) and "negatives" (e.g., no liquefaction cases) overlap when plotted as a function of diagnostic test results (e.g., *FS* values, see Figure 2.2a), ROC analyses can be used (1) to identify the optimum diagnostic threshold (e.g., *FS* threshold); and (2) to assess the relative efficacy of competing diagnostic models, independent of the thresholds used. A ROC curve is a plot of the True Positive Rate (R_{TP}) versus the False Positive Rate (R_{FP}) for varying threshold values (e.g., *FS*). Here, R_{TP} is defined as the ratio of number of cases where liquefaction is predicted and was observed to the total number of cases with observed liquefaction, and R_{FP} is defined as the ratio of number of cases where liquefaction is predicted, but was not observed to the total number of cases with no observed liquefaction. A conceptual illustration of ROC analysis, including the relationship among the distributions for positives and negatives, the threshold value, and the ROC curve, is shown in Figure 2.2.

In ROC curve space, a diagnostic test that has no predictive ability (i.e., a random guess) results in a ROC curve that plots as 1:1 line through the origin. In contrast, a diagnostic test that has a perfect predictive ability (i.e., a perfect model) plots along the left vertical and upper horizontal axes, connecting at the point (0,1) and indicates the existence of a threshold value that perfectly segregates the dataset (e.g., all cases with liquefaction have *FS* below this threshold and all cases without liquefaction have *FS* above this threshold). The area under the ROC curve (*AUC*) is equivalent to the probability that "liquefaction" cases have a lower computed *FS* than "no liquefaction" cases. As such, higher *AUC* indicates better predictive capabilities (e.g., Fawcett 2005). To put this into perspective, a random guess returns an *AUC* of 0.5 whereas a perfect model returns an *AUC* of 1.

The optimum operating point (*OOP*) in a ROC analyses is defined as the threshold value (e.g., threshold *FS*) that minimizes the misprediction cost, where cost is computed as (Maurer et al. 2015c):

$$cost = C_{FP} \times R_{FP} + C_{FN} \times R_{FN} \tag{2.2}$$

where C_{FP} and R_{FP} are the cost and rate of false-positive predictions, respectively, and C_{FN} and R_{FN} are the cost and rate of false-negative predictions, respectively. Normalizing Eq. 2.2 with respect to C_{FN}, and equating R_{FN} to 1-R_{TP}, cost may alternatively be expressed as:

$$cost_n = \frac{cost}{C_{FN}} = CR \times R_{FP} + (1 - R_{TP}) \tag{2.3}$$

where *CR* is the cost ratio defined by $CR = C_{FP}/C_{FN}$ (i.e., the ratio of the cost of a false-positive prediction to the cost of a false-negative prediction).

As may be surmised, Eq. 2.3 plots as a straight line in ROC space with slope of *CR* and can be thought of as a contour of equal performance (i.e., an iso-performance line). Thus, each *CR* corresponds to a different iso-performance line. One such line, with *CR* = 1 (i.e., false positives costs are equal to false-negative costs) is shown in Figure 2.2b. The point where the iso-performance line is tangent to the ROC curve corresponds to the *OOP* (e.g., the "optimal" *FS* threshold corresponding to a given *CR*). Thus, by varying the *CR* values, a relationship between optimal *FS* and *CR* can be developed.

2.4 Results and Discussion

2.4.1 Optimal FS versus CR relationships

ROC analyses were performed on the distributions of *FS* for "liquefaction" and "no liquefaction" case histories for each of the five liquefaction triggering models used in this study (i.e., BI14-SPT, Cea18, BI14-CPT, Gea19, and Kea13), as shown in Figure 2.3. The resulting ROC curves are shown in Figure 2.4a. Using each of these ROC curves, optimal threshold *FS* values were determined in conjunction with Eq. 2.3 for a range of *CR* values (i.e., *CR* ranging from 0.001 to 2). The relationship between *CR* and optimal threshold *FS* for BI14-SPT, Cea18, BI14-CPT, Gea19, and Kea13 are shown in Figure 2.4b.

As may be observed from Figure 2.4b, the optimal threshold *FS* is inversely proportional to the *CR* such that, the lower the *CR*, the higher the optimal threshold *FS* (i.e., the degree of conservatism required), as was expected. Moreover, it can be seen that the optimal *FS*-*CR* relationships are specific to the liquefaction triggering model being used and the associated case-history database. In other words, at a given *CR*, the optimal *FS* could vary as a function of the liquefaction triggering model being used. For example, at *CR* = 1, the optimal threshold *FS* for BI14-SPT, Cea18, BI14-CPT, Gea19, and Kea13 are 0.94, 1.16, 0.94, 0.91, and 0.71, respectively (e.g., Figure 2.4b).

Additionally, it can be seen that the deterministic $CRR_{M7.5}$ curves (i.e., *FS* = 1) for BI14-SPT, Cea18, BI14-CPT, Gea19, and Kea13 have associated *CR*s of ~0.38, 1.1, 0.26, 0.29, and 0.28, respectively. This is indicative of the degree of conservatism inherent to the positioning of the deterministic $CRR_{M7.5}$ curve for each model, as well as differences in the range of scenarios represented in the liquefaction case-history databases from which the respective triggering models were derived. As shown, the associated *CRs* at *FS* = 1 are significantly lower than one for BI14-SPT, BI14-CPT, Gea19, and Kea13, suggesting that these models implicitly treated the cost of false negatives to be significantly higher than the cost of false positives. On the other hand, the associated *CR* at *FS* = 1 for Cea18 is very close to one (i.e., for *CR* = 1.1 at *FS* = 1), suggesting that Cea18 implicitly assumed that the costs of false negatives and false positives were similar, which is expected, since Cea18 recommend their median (i.e., *PL* = 50%) curve as the deterministic $CRR_{M7.5}$ curve.

As discussed in the Introduction, the choice of optimal *FS* decision threshold for any engineering project should be guided by the associated costs (or consequences) of mispredicting liquefaction. As such, the optimal *FS-CR* relationships derived herein can be used to determine project-specific optimal *FS* for decision making. However, there are limitations in using the optimal *FS-CR* curves shown in Figure 2.4b. It can be observed that these optimal *FS-CR* curves have a jagged (non-smooth) nature. Therefore, the relationship between optimal *FS* and *CR* may not be unique. In other words, for a given *CR*, there could be a range of *FS* that can be considered optimal and similarly, a given *FS* threshold may be optimal for a range of *CR* values. For example, consider the optimal *FS-CR* curve for BI14-SPT as shown in Figure 2.4b. It can be observed that $FS \approx 0.95$ is optimal for *CR* ranging from 0.28 to 1.4. Similarly, at $CR \approx 0.05$, any *FS* threshold ranging from 1.05 to 1.7 could be considered optimal. This is an artifact of the non-smooth nature of the ROC curve from which the optimal *FS-CR* curves were derived, which is likely a result of the limited number of case histories and the distribution of *FS* data in each case-history database. Additionally, the optimal *FS-CR* curves in Figure 2.4b only represent a limited range of *FS*, particularly, the maximum *FS* that can be determined using these curves could be lower than the *FS* that may be desired in practice. For example, using the optimal *FS* versus *CR* curve for BI14-SPT, the maximum value of $FS = 1.25$, however the minimum required *FS* for some critical projects could be as high as 2. The upper bound *FS* from each model is dictated by the largest *FS* for the "liquefaction" case histories in the associated database. However, the deterministic $CRR_{M7.5}$ curves in these models are generally conservatively positioned such that most of the "liquefaction" case histories fall above or to the left of the curve; as a result, none of the "liquefaction" case histories have large *FS*. Inherently, selecting a minimum required *FS* that is greater than the upper bound *FS* from an optimal *FS-CR* relationship implies that the damage to the infrastructure due to liquefaction are intolerable, regardless of cost.

Accordingly, it was hypothesized that combining the *FS* data from all the triggering models analyzed herein would result in a smoother ROC curve and the derivative optimal *FS-CR* curve. In combining the *FS* data, Cea18 was excluded since their deterministic $CRR_{M7.5}$ corresponds to $PL = 50\%$ (i.e., median $CRR_{M7.5}$ curve), as opposed to the often recommended $PL = 15\%$. Figure 2.5a contains the ROC curve for the *FS* data combined from BI14-SPT, BI14-CPT, Gea19, and Kea13 and Figure 2.5b contains the derivative optimal *FS-CR* curve. It can be observed that combining the *FS* data from different models results in relatively smoother ROC curve, as well as a smoother optimal *FS-CR* curve. Additionally, this generic *FS-CR* curve (i.e., developed from the combined *FS* data) represents a wider range of *FS* than some of the individual *FS-CR* curves. As a result, the generic *FS-CR* curve might be preferred over the individual *FS-CR* curves. However, even the generic *FS-CR* curve is not without limitations. As can be observed from Figure 2.5b, even after combining the *FS* data, the jagged nature of the *FS-CR* curve still remains, suggesting that additional case histories are needed to derive a more-refined curve in the future. Moreover, it should be noted that, by combining the *FS* data from different models, the degree of conservatism inherent to the associated deterministic $CRR_{M7.5}$ curves is also being averaged out. As a result, it could be argued that the use of triggering model-specific optimal *FS-CR* curves is preferred over the use of the generic curve in forward analyses.

To illustrate how an optimal *FS-CR* curve can be used to select a project-specific optimal *FS* threshold based on cost-considerations, an example is presented using the generic optimal *FS-CR* curve shown in Figure 2.5b. Consider a site that has a computed *FS* of 1 for a design earthquake scenario. If a one-story residential building is to be built at this site, for which the *CR* is estimated as 0.7, using Figure 2.5b, the optimal *FS* for decision making would be 0.94. Since, the computed *FS* is greater than the optimal *FS* for this scenario, it is more economical to leave the site unimproved and pay for the cost of repairs due to damages from liquefaction, if it occurs (note that liquefaction triggering and lateral spreading generally does not pose a risk to life-safety, e.g., Green and Bommer 2019). On the other hand, if a critical facility (e.g., a hospital building) is to be built at the site and has an estimated *CR* of 0.05, using Figure 2.5b the optimal *FS* decision threshold would be 1.25. In this case, the computed *FS* is lower than the optimal *FS* and thus performing ground improvement upfront is favorable.

2.4.2 Optimal PL versus CR relationships

Using an approach similar to deriving the optimal *FS-CR* relationships, optimal *PL-CR* relationships were also derived for BI14-SPT, Cea18, BI14-CPT, and Kea13. The ROC curves derived using the *PL* data from each of these models are presented in Figure 2.6a and the derivative optimal *PL-CR* curves are presented in Figure 2.6b. As may be observed from Figure 2.6b, the optimal *PL* threshold is directly proportional to *CR* such that as *CR* decreases, the corresponding optimal *PL* threshold for decision making decreases. As with the optimal *FS-CR* curves, the optimal *PL-CR* curves are also specific to the probabilistic liquefaction triggering models and the respective databases used in deriving them. Additionally, these optimal *PL-CR* curves also tend to be jagged, which is expected, since the underlying case-history database for the *FS* and *PL* data is the same. A generic optimal *PL-CR* curve was also derived by performing ROC analysis on the combined *PL* data from BI14-SPT, Cea18, BI14-CPT, and Kea13. Figure 2.7a shows the ROC curve for the combined *PL* data and Figure 2.7b shows the derivative optimal *PL-CR* curve. The optimal *PL-CR* curves are recommended to be used in a similar manner as the optimal *FS-CR* curves (i.e., the initial *PL* at a site can be compared with the optimal *PL* decision threshold at the *CR* of interest to determine whether or not liquefaction mitigation is worth the expense). It should be noted that, however, for each of the liquefaction triggering model used in this study, there is a one-to-one relationship between *FS* and *PL* (i.e., each *FS* corresponds to a certain *PL*). Therefore, the optimal *FS-CR* curves and optimal *PL-CR* curves contain similar information; as such, there is no additional benefits of using one over the other.

Finally, the approaches presented in this study are simplistic in the sense that they do not consider the complexity and probabilistic nature of life-cycle cost analyses (e.g., the response of an infrastructure asset to earthquake motions having a range of return periods). Additionally, the analyses presented herein are based on the assumption that the risk mitigation schemes completely eliminate the liquefaction hazard, which may not always be the case. Regardless, the study demonstrates that some consideration should be given to the relative consequences of misprediction when selecting an *FS* or *PL* threshold upon which decisions will be made.

2.5 Conclusions

This study demonstrated how project-specific costs of mispredicting liquefaction triggering can be utilized in selecting an appropriate factor of safety (*FS*) against liquefaction for decision making. Specifically, relationships between the optimal *FS* decision threshold and the ratio of false-positive prediction costs to false-negative prediction costs (i.e., cost ratio, *CR*) were derived by performing ROC analyses on five recently proposed liquefaction triggering models (i.e., BI14-SPT, Cea18, BI14-SPT, Gea19, and Kea13), used in conjunction with their respective case-history databases. The optimal *FS-CR* relationships were found to be specific to the liquefaction triggering models and the associated case-history database being used. Additionally, it was shown that the individual relationships were not very smooth due to limited number of case histories in the corresponding database as well as the distribution of *FS* in the database. Consequently, generic optimal *FS-CR* were derived by combining *FS* data from the individual models. However, it was shown that, even after using the combined *FS* data, the optimal *FS-CR* curves were not completely smooth, suggesting that additional liquefaction case histories will be needed to derive more refined relationships in the future. Using probability of liquefaction (*PL*) as an alternative to *FS*, relationships between *CR* and optimal *PL* thresholds were also derived using the same approach that was used to derive the optimal *FS-CR* curves. The optimal *PL-CR* curves, however, did not provide any additional information over the optimal *FS-CR* curves. This is because, there is a direct correlation between *FS* and *PL,* given the way the triggering models are currently developed.

2.6 Acknowledgements

The authors greatly acknowledge the funding support through the National Science Foundation (NSF) grants CMMI-1435494, CMMI-1724575, CMMI-1751216, and CMMI-1825189, as well as Pacific Earthquake Engineering Research Center (PEER) grant 1132-NCTRBM and U.S. Geological Survey (USGS) award G18AP-00006. However, any opinions, findings, and conclusions or recommendations expressed in this paper are those of the authors and do not necessarily reflect the views of NSF, PEER, or USGS.

References

Boulanger, R.W. and Idriss, I.M. (2012). "Probabilistic standard penetration test-based liquefaction-triggering procedure." *Journal of Geotechnical and Geoenvironmental Engineering*, 138(10): 1185-1195.

Boulanger, R.W. and Idriss, I.M. (2014). *CPT and SPT based liquefaction triggering procedures*. Report No. UCD/CGM-14/01, Center for Geotechnical Modelling, Department of Civil and Environmental Engineering, UC Davis, CA, USA.

Building Seismic Safety Council (BSSC). (2009). *NEHRP recommended seismic provisions for new buildings and other structures (FEMA P-750).* Federal Emergency Management Agency, Washington, DC.

Cetin, K. O., Seed, R. B., Der Kiureghian, A., Tokimatsu, K., Harder, L.F., Jr., Kayen, R. E., and Moss, R. E. S. (2004). "Standard penetration test-based probabilistic and deterministic assessment of seismic soil liquefaction potential." *Journal of Geotechnical and Geoenvironmental Engineering*, 130(12): 1314–1340.

Cetin, K.O., Seed, R.B., Kayen, R.E., Moss, R.E.S., Bilge, H.T., Ilgac, M., and Chowdhury, K. (2018). "SPT-based probabilistic and deterministic assessment of seismic soil liquefaction triggering hazard." *Soil Dynamics and Earthquake Engineering*, 115: 698-709.

Fawcett, T. (2005). "An introduction to ROC analysis." *Pattern recognition letters*, *27*(8): 861-874.

Green, R.A., Maurer, B.W., Cubrinovski, M. and Bradley, B.A. (2015). "Assessment of the relative predictive capabilities of CPT-based liquefaction evaluation procedures: Lessons learned from the 2010-2011 Canterbury earthquake sequence". *Proc. 6th Intern. Conf. on Earthquake Geotechnical Engineering* (6ICEGE), Christchurch, New Zealand, 2-4 November.

Green, R.A., Upadhyaya, S., Wood, C.M., Maurer, B.W., Cox, B.R., Wotherspoon, L., Bradley, B.A., and Cubrinovski M. (2017). "Relative efficacy of CPT- versus Vs-based simplified liquefaction evaluation procedures," *Proc. 19th Intern. Conf. on Soil Mechanics and Geotechnical Engineering*, Seoul, Korea, 17-22 September.

Green, R.A., Bommer, J.J., Rodriguez-Marek, A., Maurer, B.W., Stafford, P., Edwards, B., Kruiver, P.P., de Lange, G., and van Elk, J. (2019). "Addressing limitations in existing 'simplified' liquefaction triggering evaluation procedures: application to induced seismicity in the Groningen gas field." *Bulletin of Earthquake Engineering*, 17: 4539-4557.

Green, R.A. and Bommer, J.J. (2019). "What is the smallest earthquake magnitude that needs to be considered in assessing liquefaction hazard?" *Earthquake Spectra*, 35(3): 1441-1464.

Idriss, I.M. and Boulanger, R.W. (2008). *Soil liquefaction during earthquakes*. Monograph MNO-12, Earthquake Engineering Research Institute, Oakland, CA, 261 pp.

Idriss, I.M. and Boulanger, R.W. (2010). *SPT-based liquefaction triggering procedures*. Rep. UCD/CGM-10, 2.

Kayen, R., Moss, R., Thompson, E., Seed, R., Cetin, K., Kiureghian, A., Tanaka, Y., and Tokimatsu, K. (2013). "Shear-wave velocity–based probabilistic and deterministic assessment of seismic soil liquefaction potential." *Journal of Geotechnical and Geoenvironmental Engineering*, 139(3): 407-419.

Martin, G.R. and Lew, M. (eds). (1999). *Recommended procedures for implementation of DMG Special Publication 117 guidelines for analysing and mitigating liquefaction in California*. Southern California Earthquake Center, University of Southern California, Los Angeles, CA.

Maurer, B.W., Green, R.A., Cubrinovski, M., and Bradley, B. (2015a). “Fines-content effects on liquefaction hazard evaluation for infrastructure during the 2010-2011 Canterbury, New Zealand earthquake sequence.” *Soil Dynamics and Earthquake Engineering*, 76: 58-68.

Maurer, B.W., Green, R.A., Cubrinovski, M., and Bradley, B. (2015b). “Assessment of CPT-based methods for liquefaction evaluation in a liquefaction potential index framework.” *Géotechnique*, 65(5): 328-336.

Maurer, B.W., Green, R.A., Cubrinovski, M., and Bradley, B. (2015c). “Calibrating the Liquefaction Severity Number (LSN) for Varying Misprediction Economies: A Case Study in Christchurch, New Zealand.” *Proc. 6th International Conference on Earthquake Geotechnical Engineering*, Christchurch, New Zealand, 1-4 November 2015.

Maurer, B.W., Green, R.A., van Ballegooy, S., Bradley, B.A., and Upadhyaya, S. (2017a). “Performance comparison of probabilistic and deterministic liquefaction triggering models for hazard assessment in 23 global earthquakes.” *Geo-Risk 2017: Reliability-based design and code developments* (J. Huang, G.A. Fenton, L. Zhang, and D.V. Griffiths, eds.), ASCE Geotechnical Special Publication 283, 31-42.

Maurer, B.W., Green, R.A., van Ballegooy, S., and Wotherspoon, L. (2017b). “Assessing liquefaction susceptibility using the CPT Soil Behavior Type Index,” *Proc. 3rd Intern. Conf. on Performance-Based Design in Earthquake Geotechnical Engineering* (PBDIII), Vancouver, Canada, 16-19 July.

Maurer, B.W., Green, R.A., van Ballegooy, S., and Wotherspoon, L. (2019). “Development of region-specific soil behavior type index correlations for evaluating liquefaction hazard in Christchurch, New Zealand.” *Soil Dynamics and Earthquake Engineering*, 117:96-105.

Moss, R.E.S, Seed, R.B., Kayen, R.E., Stewart, J.P., Der Kiureghian, A., and Cetin, K.O. (2006). “CPT-based probabilistic and deterministic assessment of in situ seismic soil liquefaction potential.” *Journal of Geotechnical and Geoenvironmental Engineering*, 132(8):1032-1051.

Oommen, T., Baise, L. G., and Vogel, R. (2010). “Validation and application of empirical liquefaction models.” *Journal of Geotechnical and Geoenvironmental Engineering, 136*(12): 1618-1633.

Robertson, P.K. and Wride, C.E. (1998). “Evaluating cyclic liquefaction potential using cone penetration test.” *Canadian Geotechnical Journal*, 35(3): 442-459.

Seed, H.B. and Idriss, I.M. (1971). "Simplified procedure for evaluating soil liquefaction potential." *Journal of the Soil Mechanics and Foundations Division*, 97(SM9): 1249–1273.

Upadhyaya, S., Maurer, B.W., Green, R.A., and Rodriguez-Marek, A. (2018). "Effect of non-liquefiable high fines-content, high plasticity soils on liquefaction potential index (LPI) performance." *Geotechnical Earthquake Engineering and Soil Dynamics V: Liquefaction Triggering, Consequences, and Mitigation* (S.J. Brandenberg and M.T. Manzari, eds.), ASCE Geotechnical Special Publication 290, 191-198.

Upadhyaya, S., Green, R.A., Maurer, B.W., and Rodriguez-Marek, A. (2019). "Selecting factor of safety against liquefaction for design based on cost considerations." *7th International Conference on Earthquake Geotechnical Engineering*, June 17-20, Rome, Italy.

Whitman, R.V. (1971). "Resistance of soil to liquefaction and settlement." *Soils and Foundations*, 11: 59-68.

Zhu, J., Baise, L.G., and Thompson, E.M. (2017). "An updated geospatial liquefaction model for global application." *Bulletin of the Seismological Society of America*, 107(3): 1365-1385.

Zou, K.H. (2007). "Receiver operating characteristic (ROC) literature research." On-line bibliography available from: <http://www.spl.harvard.edu/archive/spl-pre2007/pages/ppl/zou/roc.html> accessed 10 March 2016.

Tables

Table 2.1 Factors of Safety (*FS*) for liquefaction hazard assessment (from Martin and Lew 1999).

Consequences of Liquefaction	$N_{1,60cs}$	*FS*
Settlement	≤15	1.1
	≥30	1.0
Surface Manifestation	≤15	1.2
	≥30	1.0
Lateral Spreading	≤15	1.3
	≥30	1.0

Table 2.2 Summary of number of "liquefaction," "no liquefaction," and "marginal" case histories in the databases used in developing different liquefaction triggering models.

Triggering model	Number of cases			
	liquefaction	no liquefaction	marginal	total
BI14 SPT	133	116	3	252
Cea18 SPT	113	95	2	210
BI14 CPT	180	71	2	253
Gea19 CPT	180	71	2	253
Kea13 Vs	287	124	4	415

Figures

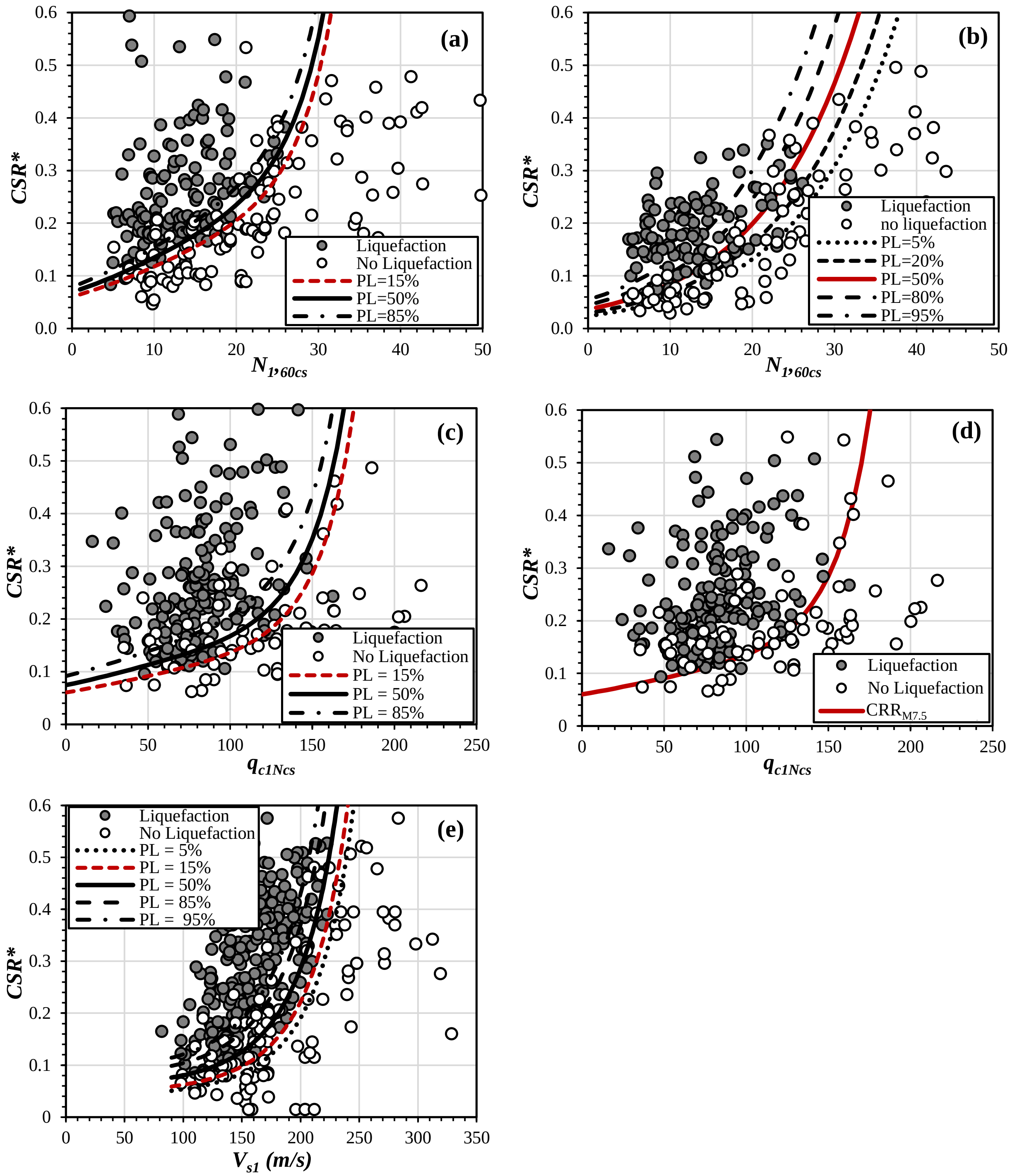

Figure 2.1 Case history data plotted together with the $CRR_{M7.5}$ curves for different probabilities of liquefaction: (a) BI14-SPT; (b) Cea18; (c) BI14-CPT; (d) Gea19 (deterministic); (e) Kea13. The deterministic $CRR_{M7.5}$ curves are shown in red.

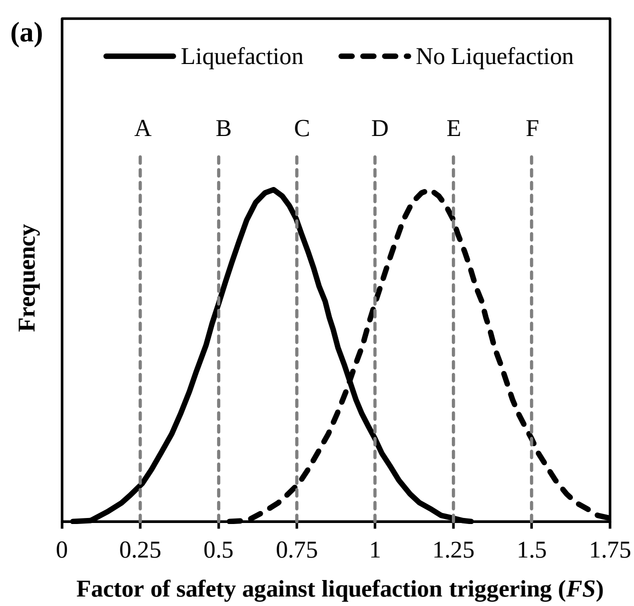

Figure 2.2 Conceptual illustration of ROC analyses: (a) frequency distributions of liquefaction and no liquefaction observations as a function of *FS*; (b) corresponding ROC curve.

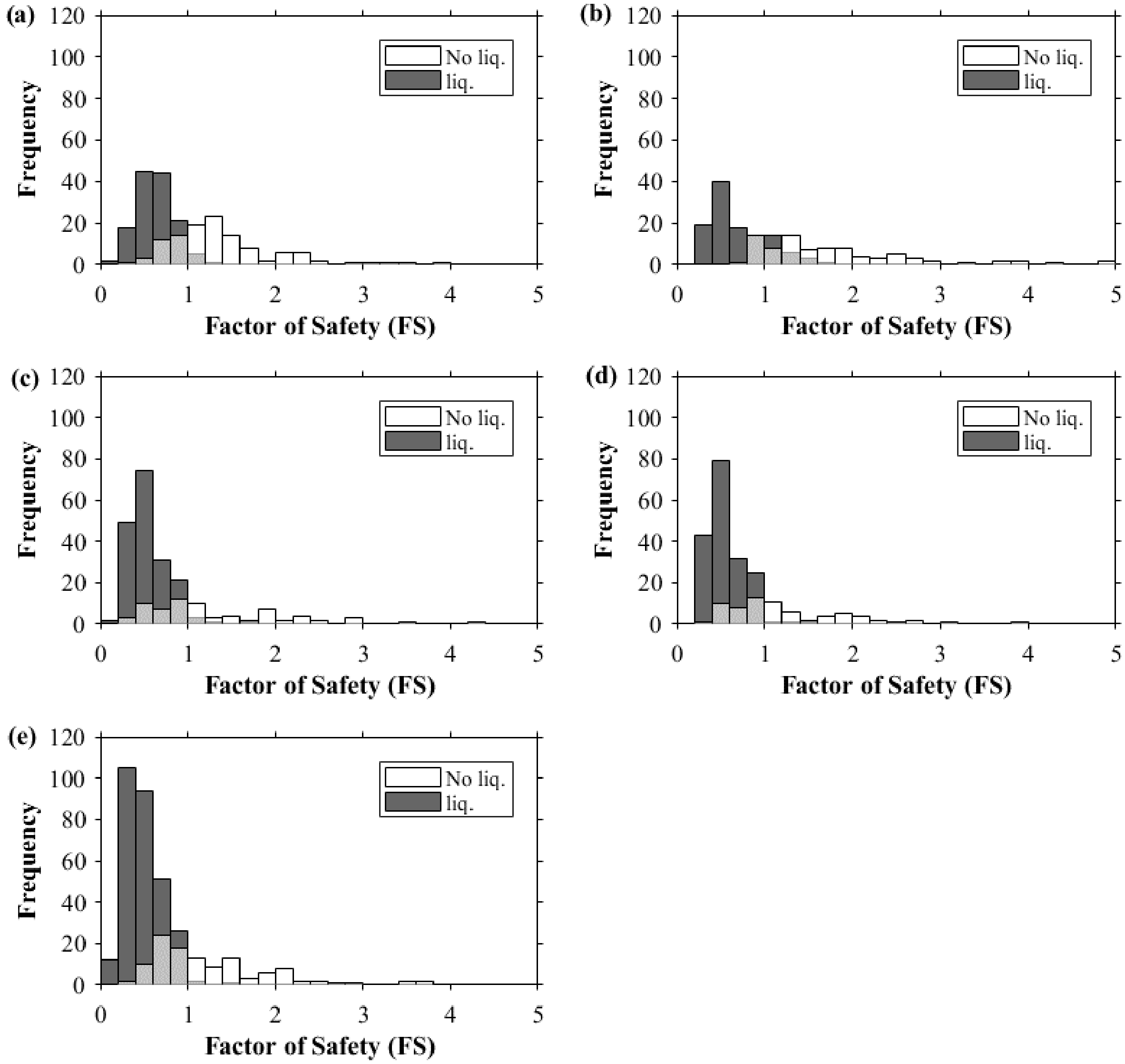

Figure 2.3 Histograms of *FS* for the case history databases used to develop: (a) BI14-SPT; (b) Cea18; (c) BI14-CPT; (d) Gea19; (e) Kea13. The light grey bars indicate the overlapping of the histograms of liquefaction and no liquefaction case histories.

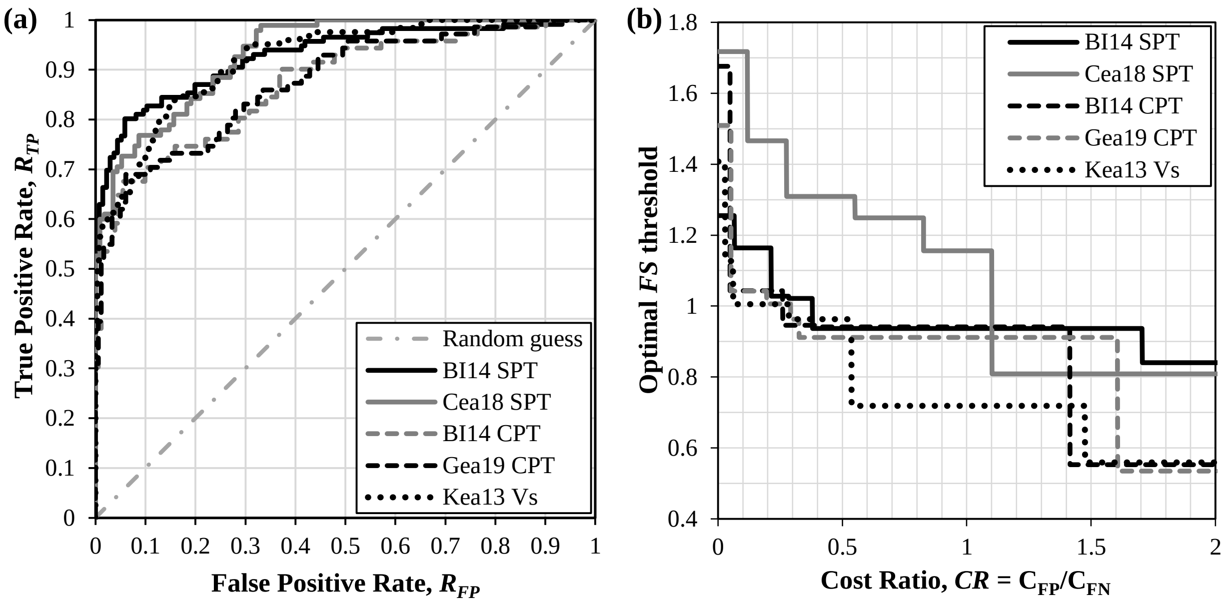

Figure 2.4 ROC analyses of *FS* data for BI14-SPT, Cea18, BI14-CPT, Gea19, and Kea13: (a) ROC curves; and (b) optimal *FS* decision threshold versus *CR* curves.

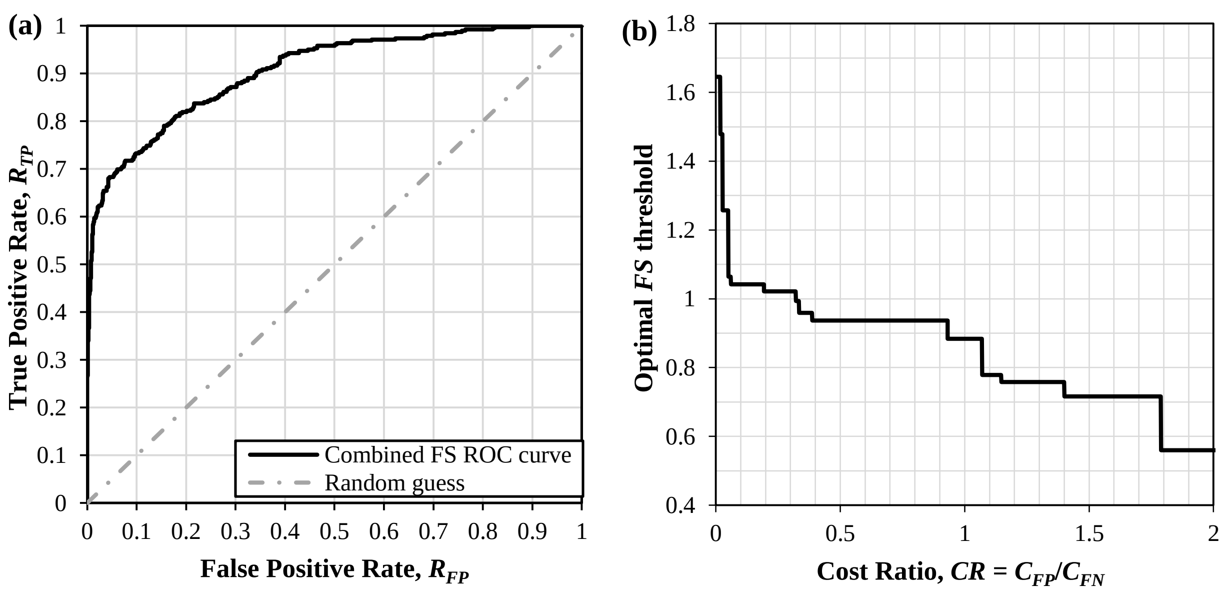

Figure 2.5 ROC analyses of *FS* data combined from BI14-SPT, BI14-CPT, Gea19, and Kea13: (a) ROC curve; and (b) optimal *FS* decision threshold versus *CR* curves.

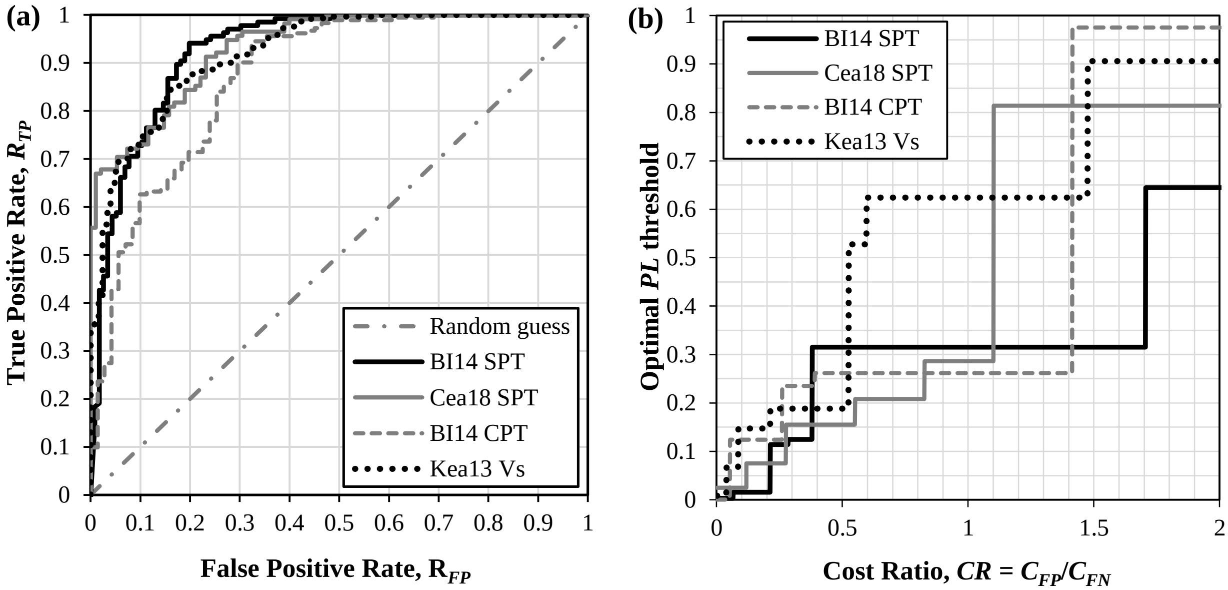

Figure 2.6 ROC analyses of *PL* data for BI14-SPT, Cea18, BI14-CPT, and Kea13: (a) ROC curves; and (b) optimal *PL* decision threshold versus *CR* curves.

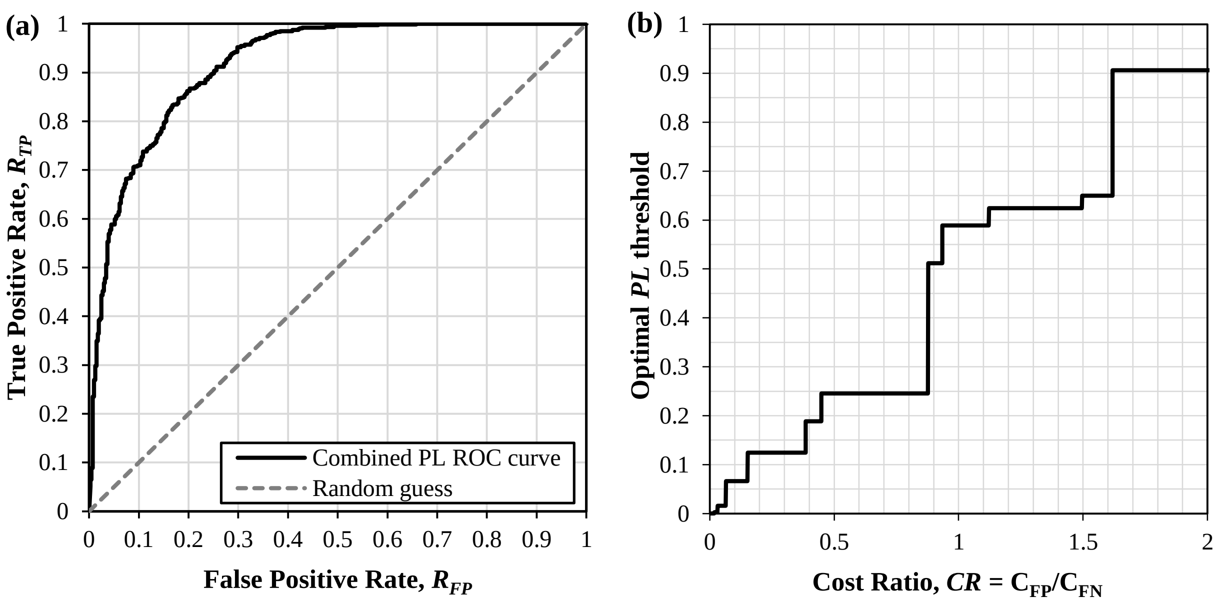

Figure 2.7 ROC analyses of *PL* data combined from BI14-SPT, Cea18, BI14-CPT, and Kea13: (a) ROC curve; and (b) optimal *PL* decision threshold versus *CR* curves.

Chapter 3: Surficial liquefaction manifestation severity thresholds for profiles having high fines-content, high plasticity soils

Sneha Upadhyaya[1]; Brett W. Maurer[2]; Russell A. Green[3]; Adrian Rodriguez-Marek[3]; and Sjoerd van Ballegooy[4]

[1]Graduate Student, Department of Civil and Environmental Engineering, Virginia Tech, Blacksburg, VA 24061.

[2]Assistant Professor, Department of Civil and Environmental Engineering, University of Washington, Seattle, WA 98195.

[3]Professor, Department of Civil and Environmental Engineering, Virginia Tech, Blacksburg, VA 24061.

[4]Technical Director, Geotechnical, Tonkin + Taylor Ltd., 105 Carlton Gore Rd., Newmarket, Auckland 1023, New Zealand.

3.1 Abstract

The occurrence and severity of surficial liquefaction manifestation was significantly over-predicted for a large subset of case histories from the 2010-2011 Canterbury Earthquake sequence in New Zealand. Such over-predicted case histories generally were comprised of profiles having predominantly high fines-content, high plasticity soil strata. Herein, receiver operating characteristic (ROC) analyses of the liquefaction case histories from the Canterbury earthquakes are used to investigate the performance of three different manifestation severity index (*MSI*) models as a function of the amount of high fines-content, high plasticity strata in a profile, which is quantified through the soil behavior type index (I_c) averaged over the upper 10 m of a profile (I_{c10}). It is shown that, for each *MSI* model: (1) the threshold *MSI* value for deterministically distinguishing cases with and without manifestation increases as I_{c10} increases; and (2) the ability of the *MSI* to segregate cases with and without manifestation decreases with increasing I_{c10}. Additionally, probabilistic models are proposed for evaluating the severity of surficial liquefaction manifestation as a function of *MSI* and I_{c10}. The approaches presented in this study allow for better interpretations of the predictions made by existing *MSI* models, given that their efficacy decreases at sites with high I_{c10}. An improved *MSI* model is ultimately needed such that the effects of high fines-content high plasticity soils are directly incorporated within the model itself.

3.2 Introduction

The objective of this study is to investigate the effect of high fines-content, high plasticity soils on the prediction of the occurrence and severity of surficial liquefaction manifestations. Towards this end, the predictive performance of three existing manifestation severity index (*MSI*) models [i.e., Liquefaction Potential Index (*LPI*); Ishihara-inspired *LPI* (*LPIish*); and Liquefaction Severity Number (*LSN*)] are investigated as a function of the Cone Penetration Test (CPT) soil behavior type index (I_c) averaged over upper 10 m of the soil profile (I_{c10}), wherein I_{c10} is used to infer the amount of high fines-content, high plasticity strata in the profile. Specifically, manifestation severity thresholds for distinguishing cases with different manifestation severities (e.g., cases with and without manifestation) for each *MSI* model considered herein are evaluated as a function of I_{c10}. Additionally, probabilistic models are proposed to evaluate the severity of surficial liquefaction manifestation as a function of computed *MSI* and I_{c10}.

The 2010-2011 Canterbury earthquake sequence (CES) in New Zealand resulted in widespread liquefaction causing extensive damage to infrastructure throughout the city of Christchurch and its surroundings (e.g., Cubrinovski and Green 2010; Cubrinovski et al. 2011; Green et al. 2014; Maurer et al. 2014; van Ballegooy et al. 2014b). While the CES included up to ten earthquake events that triggered liquefaction (Quigley et al. 2013), the M_w 7.1, 4 September 2010 Darfield and the M_w 6.2, 22 February 2011 Christchurch earthquakes were the most significant in terms of the spatial extent and the severity of liquefaction damage. The ground motions from these earthquakes were recorded by a large network of strong motion stations in the area (Bradley and Cubrinovski 2011; Bradley 2012). Following the CES, an extensive geotechnical site characterization program was initiated in Christchurch and its environs, the majority of which was funded by the New Zealand Earthquake Commission (EQC), resulting in more than 35,000 CPT soundings performed to date. Additionally, the ground surface observations were well-documented via post-earthquake ground reconnaissance and high-resolution aerial photos and satellite imagery. All of this data is stored in the New Zealand Geotechnical Database (NZGD 2016), an online repository available for use by researchers and practitioners. This unprecedented quantity of data has been utilized by various studies to investigate the accuracies of various models that predict liquefaction triggering and the resulting severity of surficial liquefaction manifestations (e.g., Green et al. 2014; 2015; Maurer et al. 2014; 2015b,c; van Ballegooy et al. 2012; 2014b; 2015).

These studies have shown that while existing models were generally effective in predicting the liquefaction response, the severity of manifestation was systematically over-predicted for a non-trivial number of sites.

Such over-predictions may be attributed to several factors associated with the uncertainties in site characterization and in the models that predict liquefaction triggering and the severity of manifestations (e.g., Boulanger et al. 2016). Predominant factors include the presence of a thick non-liquefiable crust and/or interbedded non-liquefiable soils high in fines-content and plasticity (e.g., Maurer et al. 2014; 2015a,b; Green et al. 2018). In particular, the presence of plastic soils with low permeability can affect the generation and redistribution of excess pore pressure within a soil profile, potentially suppressing surface manifestation of the liquefied soils (e.g., Ozutsumi et al. 2002; Juang et al. 2005; Jia and Wang 2012; Maurer et al. 2015b; Beyzaei et al. 2018; Cubrinovski et al. 2019). In this regard, proposed manifestation severity thresholds specific to different *MSI* models have been found to be less applicable at sites with predominantly silty or clayey soils. For example, Lee et al. (2003) used *LPI* to analyze case histories from the 1999 Chi-Chi (Taiwan) earthquake, mainly comprised of sites with silty sands and sandy silt strata, and proposed that a threshold *LPI* of 13 should be used to distinguish between sites with and without manifestations of liquefaction (in contrast with the $LPI = 5$ threshold originally proposed by Iwasaki et al. 1978). Similarly, Maurer et al. (2015b) analyzed the CES case histories and found the threshold *LPI* value to be significantly higher at sites with predominantly silty and clayey soil mixtures than at sites with predominantly clean sands or silty sands. Maurer et al. (2015b) made this distinction using the average CPT soil-behavior-type index (I_c) for the uppermost 10 m of each soil profile (I_{c10}) to parse sites into those comprised of predominantly clean sands or silty sands ($I_{c10} < 2.05$), and those comprised of predominantly silty or clayey soil mixtures ($I_{c10} \geq 2.05$). They found that sites with $I_{c10} < 2.05$ had an optimum threshold *LPI* for distinguishing sites with and without manifestation of 4.9 whereas sites with $I_{c10} \geq 2.05$ had an optimum threshold *LPI* of 13. The findings from these studies indicate that the relationship between the computed *MSI* and the severity of surficial liquefaction manifestation is dependent on the extent to which a soil profile contains high fines-content high plasticity soil strata.

This study rigorously investigates the effects of high fines-content, high plasticity soils on the predictive performance of three existing *MSI* models using empirical liquefaction case histories resulting from Canterbury, New Zealand earthquakes. In particular, this study utilizes case histories from the two earthquake events included in the CES (i.e., the M_w 7.1 September 2010 Darfield and the M_w 6.2 February 2011 Christchurch earthquakes), as well as from the more recent M_w 5.7 February 2016 Valentine's Day earthquake. Using an approach similar to Maurer et al. (2015b), this study uses I_{c10} to parse soil profiles by their average inferred soil-type, but considers multiple finer bins of I_{c10} to study the influence of I_{c10} on the predictive performance of *MSI* models with greater resolution. Specifically, receiver operating characteristic (ROC) analyses are performed to investigate the optimum *MSI* thresholds specific to *LPI*, *LPIish*, and *LSN* models as well as their predictive efficiencies, as a function of I_{c10}. Additionally, using logistic regression, probabilistic models are proposed for predicting the severity of manifestation as a function of *MSI* and I_{c10}. In the following, an overview of the *LPI*, *LPIish*, and *LSN* models is presented, which is followed by a summary of the liquefaction case-history dataset and the methodologies used to analyze them, to include an overview of ROC analysis. Finally, the results are presented and discussed in detail.

3.3 Overview of existing manifestation severity index (*MSI*) models

3.3.1 Liquefaction Potential Index (LPI)

The liquefaction potential index (*LPI*) proposed by Iwasaki et al. (1978) is commonly used to characterize the expected severity of the surficial liquefaction manifestation:

$$LPI = \int_0^{z_{max}} F(FS) \cdot w(z)\, dz \tag{3.1}$$

where *FS* is the factor of safety against liquefaction triggering, computed by a liquefaction triggering model; *z* is depth below the ground surface in meters; z_{max} is the maximum depth considered, generally taken as 20 m; and $F(FS)$ and $w(z)$ are functions that account for the weighted contributions of *FS* and *z* towards the severity of surficial liquefaction manifestation. Specifically, $F(FS) = 1 – FS$ for $FS \leq 1$ and $F(FS) = 0$ otherwise; and $w(z) = 10 – 0.5z$. Thus, *LPI* assumes that the severity of surface manifestation depends on the cumulative thickness of liquefied soil layers, the proximity of those layers to the ground surface, and the amount by which *FS* in each layer is less than 1.0. Given this definition, *LPI* can range from zero to 100. Analyzing the Standard Penetration Test (SPT) data from 55 sites in Japan, Iwasaki et al. (1978) proposed that severe liquefaction is expected for sites where *LPI* > 15 but not where *LPI* < 5. This criterion, defined by two threshold values of *LPI*, is commonly referred to as "Iwasaki Criterion." In today's practice, *LPI* = 5 is commonly used as a deterministic threshold for predicting surficial liquefaction manifestation, such that some degree of manifestation is expected where *LPI* > 5, but no manifestation is expected where *LPI* < 5.

3.3.2 Ishihara-inspired Liquefaction Potential Index (LPIish)

Maurer et al. (2015a) proposed modifications to *LPI* to account for the influence of non-liquefied crust thickness on the severity of surficial liquefaction manifestations using the relationship proposed by Ishihara (1985), that relates the thicknesses of the non-liquefied crust (H_1) and the liquefied stratum (H_2) to the occurrence of surficial liquefaction manifestation. The modified *LPI* was termed *LPIish* and is defined as (Maurer et al. 2015a):

$$LPIish = \int_{H_1}^{z_{max}} F(FS) \cdot \frac{25.56}{z} \cdot dz \tag{3.2a}$$

where

$$F(FS) = \begin{cases} 1 - FS \ if \ FS \leq 1 \cap H_1 \cdot m(FS) \leq 3 \\ 0 \qquad\qquad\qquad\qquad\qquad otherwise \end{cases} \tag{3.2b}$$

and

$$m(FS) = exp\left(\frac{5}{25.56(1-FS)}\right) - 1; \quad m(FS > 0.95) = 100 \tag{3.2c}$$

where z, *FS* and z_{max} are as defined previously for *LPI* (Eq. 3.1). As can be surmised from Eq. 3.2, the *LPIish* framework accounts for the relative thicknesses of H_1 and H_2 by imposing an additional constraint on *F*(*FS*). Additionally, *LPIish* uses a power-law depth weighting function, consistent with Ishihara's boundary curves, which allows *LPIish* to give a higher weight to shallower layers than *LPI* in predicting the severity of surficial manifestation.

3.3.3 Liquefaction Severity Number (LSN)

Liquefaction Severity Number (*LSN*) was proposed by van Ballegooy et al. (2012; 2014b) and uses post-liquefaction volumetric strain (ε_v) as an index to account for the influence of contractive and dilative tendencies of soils on the severity of surficial manifestation. *LSN* is given by:

$$LSN = \int_0^{z_{max}} 1000 \cdot \frac{\varepsilon_v}{z} dz \tag{3.3}$$

where z and z_{max} are as defined previously for *LPI* (Eq. 3.1). z_{max} is generally taken as 10 m for *LSN*, however this study considers 20 m. ε_v can be estimated as a function of soil density (D_r) and *FS* using the relationships originally proposed by Ishihara and Yoshimine (1992) and later modified by Zhang et al. (2002) to express ε_v as a function of normalized and fines-corrected cone tip resistance (q_{c1Ncs}) and *FS*. Similar to *LPIish*, *LSN* also uses a power-law depth weighting function.

3.4 Data and Methodology

3.4.1 Canterbury earthquakes liquefaction case histories

This study utilizes about 3500 CPT soundings from sites where the severity of surficial manifestation was well-documented after at least one of the following earthquakes: the M_w 7.1 September 2010 Darfield earthquake, the M_w 6.2 February 2011 Christchurch earthquake, and the M_w 5.7 February 2016 Valentine's Day earthquake, collectively referred to herein as the Canterbury earthquakes (CE). A detailed description of the quality control criteria used in compiling these CPT soundings is provided in Maurer et al. (2014; 2015b). Cases where the predominant form of manifestation was documented as lateral spreading were excluded from the analyses, since none of the *MSI* models considered in this study account for the factors governing the occurrence and severity of lateral spreading. For all other cases, the severity of manifestation was classified as either "marginal," "moderate," or "severe" following the Green et al. (2014) criteria. With all these considerations, 9631 high quality case histories were used in further analyses.

Peak ground accelerations (*PGAs*) are required to estimate the seismic demand at the case history sites. In prior CE studies (e.g., Green et al. 2014; Maurer et al. 2014; 2015b,c,d; 2017a,b; 2019; van Ballegooy et al. 2015; Upadhyaya et al. 2018; among others), *PGAs* were obtained using the Bradley (2013b) procedure, which combines the unconditional *PGA* distributions as estimated by the Bradley (2013a) ground motion prediction equation, the actual recorded *PGAs* at the strong motion stations (SMSs), and the spatial correlation model of Goda and Hong (2008), to compute the conditional *PGAs* at the sites of interest. However, the *PGAs* at four SMSs during the M_w 6.2

February 2011 Christchurch earthquake were inferred to be associated with high-frequency dilation spikes as a result of liquefaction triggering in the soil profiles at the stations and were higher than the pre-liquefaction *PGAs* (e.g., Wotherspoon et al. 2014; 2015). Such artificially high *PGAs* at the liquefied SMSs can result in over-estimated *PGAs* at the nearby case-history sites (hence, overly conservative seismic demand), which in turn can lead to over-predictions of the severity of surficial liquefaction manifestations (Upadhyaya et al. 2019a). Accordingly, in the present study, pre-liquefaction *PGAs* at the four liquefied SMSs were used to estimate *PGAs* at the case history locations for the 2011 Christchurch earthquake. Note that for the 2010 Darfield and 2016 Valentine's day earthquakes, previously estimated *PGAs* remain unchanged.

Accurate estimation of ground-water table (GWT) depth is critical to evaluating liquefaction triggering and the resulting severity of surficial manifestations (e.g., Chung and Rogers 2011; Maurer et al. 2014). The GWT depth at each case-history site immediately prior to the earthquake was estimated using the robust, event-specific regional ground water models of van Ballegooy et al. (2014a), as in prior CE studies (e.g., Maurer et al. 2014; 2015b,c,d; 2017a,b; 2019; van Ballegooy et al. 2015; Upadhyaya et al. 2018; among others).

3.4.2 Evaluation of liquefaction triggering and severity of surficial liquefaction manifestation

Factor of safety (*FS*) against liquefaction is used as a primary input in computing *LPI*, *LPIish*, and *LSN*. In this study, *FS* was computed using the deterministic liquefaction triggering model of Boulanger and Idriss (2014). Inherent to this process, an I_c cutoff value of 2.5 was used to distinguish between liquefiable and non-liquefiable soils, such that soils with $I_c > 2.5$ were considered to be non-liquefiable (Maurer et al. 2017b; 2019). Moreover, the fines-content (*FC*) was estimated using the Christchurch-specific I_c-*FC* correlation proposed by Maurer et al. (2019). Finally, for each of the 9631 case histories considered in this study, *LPI*, *LPIish*, and *LSN* values were computed using Eqs. 3.1, 3.2, and 3.3, respectively.

3.4.3 Receiver Operating Characteristic (ROC) analyses

To investigate the influence of high fines-content, high plasticity soils on the predictive performance of each *MSI* model considered in this study, the CE case histories were divided into multiple subsets on the basis of I_{c10}. As stated earlier, I_{c10} is used herein to infer the extent to which a profile contains high fines-content, high plasticity soils. The use of I_c for inferring soil type was first proposed by Jeffries and Davis (1993) and then modified and popularized by Robertson and Wride (1998). Using CPT data and lab tests on samples from parallel borings, Maurer et al. (2017b; 2019) confirmed the suitability of using I_c to infer fines-content and soil type within the CE study area. Receiver Operating Characteristics (ROC) analyses (e.g., Fawcett 2005) were then performed on each I_{c10} subset to evaluate: (1) the optimum threshold *MSI* values for distinguishing cases with and without manifestation; and (2) the predictive efficiency of the *MSI* model, as a function of I_{c10}. An overview of the ROC analysis is presented in the following section.

3.4.3.1 Overview of ROC analysis

Receiver Operating Characteristics (ROC) analysis has been widely used to evaluate the performance of diagnostic models, including extensive use in medical diagnostics (e.g., Zou 2007) and to a much lesser degree in geotechnical engineering (e.g., Oommen et al. 2010; Maurer et al. 2015b,c,d; 2017a,b; 2019; Green et al. 2017; Zhu et al. 2017; Upadhyaya et al. 2018; 2019b). In particular, in cases where the distribution of "positives" (e.g., cases of observed surficial liquefaction manifestation) and "negatives" (e.g., cases of no observed surficial liquefaction manifestations) overlap, ROC analyses can be used (1) to identify the optimum diagnostic threshold (e.g., *MSI* thresholds) for distinguishing between the positives and negatives; and (2) to evaluate the predictive efficiency of a diagnostic model (i.e., the ability to distinguish between positives and negatives using thresholds). The primary focus of this paper is on (1).

A ROC curve is a plot of the True Positive Rate (R_{TP}) (i.e., surficial liquefaction manifestation was observed, as predicted) versus the False Positive Rate (R_{FP}) (i.e., surficial liquefaction manifestation is predicted, but was not observed) for varying threshold values (e.g., *MSI* thresholds). Figure 3.1 shows a conceptual illustration of ROC analysis using *LPI* as an example. The distributions of *LPI* for positives and negatives is shown in Figure 3.1a, and the relationship among the distributions, the threshold values, and the ROC curve, is shown in Figure 3.1b.

In ROC curve space, a diagnostic test that has no predictive ability (i.e., a random guess) results in a ROC curve that plots as 1:1 line through the origin. In contrast, a diagnostic test that has a perfect predictive ability (i.e., a perfect model) plots along the left vertical and upper horizontal axes, connecting at the point (0,1) and indicates the existence of a threshold value that perfectly segregates the dataset (e.g., all cases with observed surficial manifestation will have *MSI* above the threshold and all cases with no observed surficial manifestation will have *MSI* below the threshold). The area under the ROC curve (*AUC*) is statistically equivalent to the probability that cases with observed surficial liquefaction manifestation have higher computed *MSI* values than cases without observed surficial liquefaction manifestations (e.g., Fawcett 2005). Therefore, a larger *AUC* indicates better predictive capabilities. To put this into perspective, a random guess returns an *AUC* of 0.5 whereas a perfect model returns an *AUC* of 1. The optimum operating point (*OOP*) in a ROC analysis is defined as the threshold value (e.g., threshold *LPI*) that minimizes the rate of misprediction [i.e., R_{FP} + (1-R_{TP})]. Contour of the quantity [R_{FP} + (1-R_{TP})] plots as a straight line in ROC space with slope of 1, also called an iso-performance line, as illustrated in Figure 3.1b. As such, an iso-performance line is tangent to the ROC curve at the *OOP*.

3.5 Results and Discussion

3.5.1 Relationship between MSI and severity of surficial liquefaction manifestation as a function of I_{c10}

For each *MSI* model, ROC analyses were performed on the entire dataset as well as on the subsets of the dataset formed by grouping the data into different bins of I_{c10}. Similar to Maurer et al. (2015b), the dataset was initially divided into two bins of I_{c10}: $I_{c10} < 2.05$ and $I_{c10} \geq 2.05$, where $I_c = 2.05$ is the I_c boundary between clean to silty sands and silty sands to sandy silts (Robertson and Wride 1998). Table 3.1 summarizes the ROC statistics (i.e., *AUC* and *OOP* values) for *LPI, LPIish*, and *LSN* models, considering the entire dataset as well as the two different subsets of I_{c10}. It can be observed that, for each *MSI* model, the *OOP* for the subset of cases with $I_{c10} \geq 2.05$ is significantly higher than that for the subset with $I_{c10} < 2.05$, indicating that the relationship between computed *MSI* and the severity of surficial liquefaction manifestation varies with I_{c10}. For example, for $I_{c10} < 2.05$, the threshold *LPI* for distinguishing cases with and without manifestation was found to be 3.7. In contrast, the threshold *LPI* for $I_{c10} \geq 2.05$ was found to be 7.5. Note that these threshold *LPI* values are found to differ from those computed by Maurer et al. (2015b), who found the threshold *LPI* values for $I_{c10} < 2.05$ and $I_{c10} \geq 2.05$ to be 4.9 and 13, respectively. Potential factors for this discrepancy may include the use of a significantly larger number of case histories in the present study due to addition of case histories from the 2016 Valentine's Day earthquake, updated estimates of *PGAs* for the 2011 Christchurch earthquake, and the I_c cutoff of 2.5 used herein versus the I_c cutoff of 2.6 used by Maurer et al 2015b. Moreover, it was observed that, while the *OOPs* for $I_{c10} < 2.05$ were very similar to those obtained using the entire dataset, the *OOPs* for $I_{c10} \geq 2.05$

were significantly higher. This is likely because the $I_{c10} < 2.05$ subset contains a significantly larger number of case histories than the $I_{c10} \geq 2.05$ subset (note that 75% of the CE case histories have $I_{c10} < 2.05$). Consequently, *MSI* thresholds that are derived using the entire dataset may accurately predict the manifestations severity for profiles having predominantly clean to silty sands, but may over-predict the manifestation severity for profiles having predominantly silty to clayey soil mixtures. Furthermore, it may be observed that, for each *MSI* model, the *AUC* values for $I_{c10} <$ 2.05 are higher than those for $I_{c10} \geq 2.05$, indicating that each *MSI* model performs better at predicting the severity of surficial liquefaction manifestation for sites with $I_{c10} < 2.05$.

Similar analyses were performed using multiple finer bins of I_{c10} to evaluate the influence of I_{c10} on the predictive performance of the *MSI* models in greater resolution. Example I_c versus depth profiles that have I_{c10} falling in five different ranges: $I_{c10} < 1.7$; $1.7 \leq I_{c10} < 1.9$; $1.9 \leq I_{c10} < 2.1$; $2.1 \leq I_{c10} < 2.3$; and $I_{c10} \geq 2.3$ are shown in Figure 3.2. Table 3.2 summarizes *AUC* and *OOP* values for these five different bins of I_{c10} for *LPI*, *LPIish*, and *LSN* models. In general, regardless of the *MSI* model used, the threshold *MSI* values were found to increase with increasing I_{c10}, which clearly indicates that, for each *MSI* model, the relationship between computed *MSI* and the severity of surficial liquefaction manifestation is I_{c10}-dependent. As such, for a given *MSI* value, the severity of manifestation decreases as I_{c10} increases. Therefore, I_{c10}-specific *MSI* thresholds may be employed to more-accurately estimate the severity of surficial liquefaction manifestation at a given site. Furthermore, it can be observed that *AUC* values generally decrease with increasing I_{c10}, indicating that the predictive efficiency of the *MSI* models decreases with increasing I_{c10}.

It should be noted that the I_{c10}-specific *MSI* thresholds determined herein, particularly for higher I_{c10} bins, may only apply to soil profiles that have stratigraphies similar to those in Christchurch, New Zealand (e.g., Figure 3.2). The high I_{c10} soil profiles in Christchurch are generally found to be non-uniform with multiple interbedded layers of high fines-content high plasticity soils. Different depositional environments from those in Christchurch could result in a profile having a given I_{c10}, but a very different liquefaction manifestation response.

3.5.2 Probabilistic assessment of the severity of surficial liquefaction manifestation as a function of MSI and I_{c10}

As may be inferred from the results shown in the previous section, for any computed *MSI*, the probability of surficial liquefaction manifestation decreases as I_{c10} increases. As such, the probability of manifestation may be empirically estimated as a function of *MSI* and I_{c10} using a logistic regression approach. Logistic regression is a tool that can be used to estimate the probability that an event occurs given one or more predictor variables. Multiple liquefaction studies in the literature (e.g., Li et al. 2006a,b; Papathanassiou 2008; Chung and Rogers 2017; among others) have used logistic regression to estimate the probability of surface manifestation as a function of independent predictor variables (e.g., *LPI*).

The following empirical model was adopted in this study to express the probability of surficial liquefaction manifestation as a function of *MSI* and I_{c10}:

$$P(S|MSI, I_{c10}) = \frac{1}{1 + e^{-[B_o + (B_1 + B_2 \cdot I_{c10}) \cdot MSI]}} \tag{3.4}$$

where, B_0, B_1, and B_2 are the model coefficients that can be determined through regression analyses.

For each *MSI* model, B_0, B_1, and B_2 were obtained by performing generalized linear model regression (*glmfit*) with a *logit* link function in matlab (The Mathworks 2018), which is based on the maximum likelihood estimation approach (Baker 2011; 2015). Table 3.3 summarizes these model coefficients obtained using *LPI*, *LPIish*, and *LSN*. Moreover, Figures 3.3, 3.4, and 3.5 show plots of Eq. 3.4 for different values of I_{c10}, using *LPI*, *LPIish*, and *LSN* models, respectively. As such, the curves shown in Figures 3.3 to 3.5 can be used to estimate the probability of surficial liquefaction manifestation for any computed *MSI* value as a function of I_{c10}. For example, using Figure 3.3, for computed *LPI* = 10, the probability of surficial liquefaction manifestation would be ~84% for a site with I_{c10} = 1.7 but only ~31% for a site with I_{c10} = 2.7.

Furthermore, using the CE dataset, the predictive performance of the $P(S|MSI,I_{c10})$ model was compared with that of a probabilistic model expressed solely as a function of *MSI* [i.e., $P(S|MSI)$], to investigate whether including I_{c10} as a supplementary predictor variable to *MSI* provides any added benefit. The $P(S|MSI)$ model is defined as:

$$P(S|MSI) = \frac{1}{1 + e^{-[C_o + C_1 \cdot MSI]}} \tag{3.5}$$

where, C_0 and C_1 are the model coefficients and were determined through the regression approach described earlier. The $P(S|MSI)$ coefficients obtained using *LPI*, *LPIish*, and *LSN* are summarized in Table 3.4.

Two different performance metrics were used to compare the predictive efficiencies of the $P(S|MSI,I_{c10})$ and $P(S|MSI)$ models: (a) *AUC* from ROC analysis; and (b) Akaike Information Criterion (*AIC*) (Akaike 1974). While the *AUC* from ROC analysis is already discussed in a previous section, a brief description of the Akaike Information Criterion (*AIC*) is provided herein. *AIC* is a likelihood-based metric that can be used to select a best performing model from a set of competing models fitted to the same data; the best fitted model is the one that has minimum *AIC*. *AIC* can be computed as:

$$AIC = -2 \cdot ln(L) + 2K \tag{3.6}$$

where, L is the likelihood of producing the observed data for a given model and K is the number of model parameters.

Table 3.5 compares the *AUC* and *AIC* values for the $P(S|MSI,I_{c10})$ and $P(S|MSI)$ models derived using *LPI*, *LPIish*, and *LSN*. It may be observed that, regardless of the *MSI* model being used, the $P(S|MSI,I_{c10})$ model has a slightly higher *AUC* and a lower *AIC* than the $P(S|MSI)$ model, which is indicative of the improved performance of the former over the latter. Also shown in Table 3.5 are the increase in *AUC* and decrease in *AIC* values, designated as ΔAUC and ΔAIC, respectively. It can be observed that, among the three *MSI* models considered in this study, ΔAUC and ΔAIC values follow the order: *LPI* > *LPIish* > *LSN*. This indicates that inclusion of I_{c10} as the supplementary predictive variable was most effective for *LPI* and least effective for *LSN*. It should be noted however that the increase in *AUC* for each *MSI* is very small, indicating that the improvement in the model due to the inclusion of I_{c10} may not be statistically significant. This is likely because the CE dataset is largely dominated by cases with lower I_{c10}. As mentioned earlier, 75% of the CE case histories have $I_{c10} < 2.05$. As a result, the improvements in prediction due to inclusion of I_{c10} is likely being averaged out among the different I_{c10} ranges.

Manifestation severity indices have been shown to correlate with the observed severity of surficial liquefaction manifestation, such that as *MSI* increases, the degree of manifestation severity increases. It is thus implied that the probability of surficial liquefaction manifestation would similarly correlate with the observed degree of manifestation severity. As such, criteria based on probability of surficial liquefaction manifestation may be established to assess the severity of manifestation as a function of *MSI* and I_{c10}. For each *MSI* model, using CE case histories, ROC analyses were performed on the $P(S|MSI,I_{c10})$ values computed using Eq. 3.4, to obtain optimum threshold probabilities distinguishing: (a) cases with no manifestation from cases with any manifestation severity; (b) cases with no manifestation from cases with marginal manifestation; (c) cases with marginal manifestation from cases with moderate manifestation; and (d) cases with moderate manifestation from cases with severe manifestation. The *MSI* model-specific threshold probabilities of manifestation for distinguishing cases with different severities of manifestation are summarized in Table 3.6. Thus, instead of using I_{c10}-specific threshold *MSI* values as determined previously (e.g., Table 3.2), one set of probability-based criteria as shown in Table 3.6 may be used to assess the severity of the surficial liquefaction manifestation at any site.

3.6 Conclusions

Utilizing 9631 high quality liquefaction case histories from the 2010-2016 Canterbury earthquakes, this study investigated the predictive performances of *LPI*, *LPIish*, and *LSN* models, as a function of the CPT soil behavior type index (I_c) averaged over the upper 10 m of a soil profile (I_{c10}), wherein I_{c10} is used to infer the extent to which a profile contains high fines-content, high plasticity soils. It was shown that, for each manifestation severity index (*MSI*) model: (1) the relationship between computed *MSI* and the severity of surficial liquefaction manifestation is I_{c10}-dependent, such that at any given *MSI* value, the severity of manifestation decreases as I_{c10} increases; and (2) the predictive efficiency of the *MSI* model (i.e., the ability to segregate cases based on observed manifestation severity using *MSI* thresholds) decreases as I_{c10} increases. These findings suggest that I_{c10}-specific severity thresholds may be needed to accurately estimate the severity of surficial liquefaction manifestations using an *MSI* model. However, even when I_{c10}-specific thresholds are employed, the *MSI* models are unlikely to efficiently predict the severity of manifestations.

Additionally, using logistic regression, probabilistic models were proposed for evaluating the severity of surficial liquefaction manifestation as a function of *MSI* and I_{c10}. It was shown that the predictive efficiencies of these models were higher than the models defined solely as a function of *MSI*, suggesting that including I_{c10} as an additional predictor variable may improve the predictions of the liquefaction manifestation severity. Furthermore, optimum threshold probabilities for different severities of surficial liquefaction manifestation were determined by performing ROC analyses on the CE dataset.

It should however be noted that the findings of this study are artifacts of the inherent limitations in the existing *MSI* models to account for the influence of high fines-content high plasticity soils on the occurrence and severity of surficial liquefaction manifestations. Given that the *MSI* models perform poorly in profiles having high fines-content high plasticity soils, the approaches presented herein are indirect ways to correct the predictions made by the existing *MSI* models. The ultimate goal of this research is to understand and incorporate the influence of high fines-content, high plasticity soils within the manifestation model itself. Finally, the findings from this study are entirely based on the case histories from Canterbury, New Zealand, earthquakes; their applicability outside the study area is unknown.

3.7 Acknowledgements

This research was funded by National Science Foundation (NSF) grants CMMI-1435494, CMMI-1724575, CMMI-1751216, and CMMI-1825189, as well as Pacific Earthquake Engineering Research Center (PEER) grant 1132-NCTRBM and U.S. Geological Survey (USGS) award G18AP-00006. This support is gratefully acknowledged. However, any opinions, findings, and conclusions or recommendations expressed in this paper are those of the authors and do not necessarily reflect the views of NSF, PEER, or the USGS.

References

Akaike, H. (1973). “Information theory and an extension of the maximum likelihood principle.” *Second International Symposium on Information Theory*, 267-281.

Baker, J. (2011). “Fitting fragility functions to structural analysis data using maximum likelihood estimation.” *Stanford University*.

Baker, J. (2015). “Efficient analytical fragility function fitting using dynamic structural analysis.” *Earthquake Spectra*, 31(1), 579-599.

Beyzaei, C.Z., Bray, J.D., Cubrinovski, M., Reimer, M. and Stringer, M. (2018). “Laboratory-based characterization of shallow silty soils in southwest Christchurch.” *Soil Dynamics and Earthquake Engineering*, 110: 93-109.

Boulanger, R.W. and Idriss, I.M. (2014). *CPT and SPT based liquefaction triggering procedures*. Report No. UCD/CGM.-14/01, Center for Geotechnical Modelling, Department of Civil and Environmental Engineering, UC Davis, CA, USA.

Boulanger, R.W., Moug, D.M., Munter, S.K., Price, A.B., and DeJong, J.T. (2016). "Evaluating liquefaction and lateral spreading in interbedded sand, silt, and clay deposits using the cone penetrometer." *Australian Geomechanics*, 51(4): 109-128.

Bradley, B.A. and Cubrinovski, M. (2011). "Near-source strong ground motions observed in the 22 February 2011 Christchurch earthquake." *Seismological Research Letters*, 82: 853-865.

Bradley, B. A. (2012). "Strong ground motion characteristics observed in the 4 September 2010 Darfield, New Zealand earthquake." *Soil Dynamics and Earthquake Engineering*, 42: 32-46.

Bradley, B.A. (2013a). "A New Zealand-specific pseudo-spectral acceleration ground-motion prediction equation for active shallow crustal earthquakes based on foreign models." *Bulletin of the Seismological Society of America,* 103(3): 1801-1822.

Bradley, B.A. (2013b). "Site-Specific and spatially-distributed ground motion intensity estimation in the 2010-2011 Christchurch earthquakes." *Soil Dynamics and Earthquake Engineering,* 48: 35-47.

Chung, J. and Rogers, J.D. (2011). "Simplified method for spatial evaluation of liquefaction potential in the St. Louis Area." *Journal of Geotechnical and Geoenvironmental Engineering*, 137(5): 505-515.

Chung, J. and Rogers, J.D. (2017). "Deterministic and probabilistic assessment of liquefaction hazards using the liquefaction potential index and liquefaction reduction number." *Journal of Geotechnical and Geoenvironmental Engineering*, 143(10): 0401703.

Cubrinovski, M. and Green, R.A. (eds.) (2010). "Geotechnical Reconnaissance of the 2010 Darfield (Canterbury) Earthquake." (contributing authors in alphabetical order: J. Allen, S. Ashford, E. Bowman, B. Bradley, B. Cox, M. Cubrinovski, R. Green, T. Hutchinson, E. Kavazanjian, R. Orense, M. Pender, M. Quigley, and L. Wotherspoon), *Bulletin of the New Zealand Society for Earthquake Engineering*, 43(4): 243-320.

Cubrinovski, M., Bray, J.D., Taylor, M., Giorgini, S., Bradley, B., Wotherspoon, L., and Zupan J. (2011). "Soil liquefaction effects in the central business district during the February 2011 Christchurch earthquake." *Seismological Research Letters*, 82(6): 893-904.

Cubrinovski, M., Rhodes, A., Ntritsos, N., and Van Ballegooy, S. (2019). "System response of liquefiable deposits." *Soil Dynamics and Earthquake Engineering*, 124: 212-229.

Fawcett, T. (2005). "An introduction to ROC analysis." *Pattern recognition letters*, *27*(8): 861-874.

Goda, K. and H. P. Hong (2008). "Spatial correlation of peak ground motions and response spectra." *Bulletin of the Seismological Society of America* 98 (1): 354–465.

Green, R.A., Cubrinovski, M., Cox, B., Wood, C., Wotherspoon, L., Bradley, B., and Maurer, B.W. (2014). "Select liquefaction case histories from the 2010-2011 Canterbury earthquake sequence." *Earthquake Spectra*, 30(1): 131-153.

Green, R.A., Maurer, B.W., Cubrinovski, M. and Bradley, B.A. (2015). "Assessment of the relative predictive capabilities of CPT-Based liquefaction evaluation procedures: Lessons learned from the 2010-2011 Canterbury earthquake sequence." *Proc. 6th Intern. Conf. on Earthquake Geotechnical Engineering* (6ICEGE), Christchurch, New Zealand, 2-4 November.

Green, R.A., Upadhyaya, S., Wood, C.M., Maurer, B.W., Cox, B.R., Wotherspoon, L., Bradley, B.A., and Cubrinovski M. (2017). "Relative efficacy of CPT- versus Vs-based simplified liquefaction evaluation procedures." *Proc. 19th Intern. Conf. on Soil Mechanics and Geotechnical Engineering*, Seoul, Korea, 17-22 September.

Green, R.A., Maurer, B.W., and van Ballegooy, S. (2018). "The Influence of the non-liquefied crust on the severity of surficial liquefaction manifestations: Case history from the 2016 Valentine's Day earthquake in New Zealand." *Proc. Geotechnical Earthquake Engineering and Soil Dynamics V* (GEESD V), *Liquefaction Triggering, Consequences, and Mitigation* (S.J. Brandenberg and M.T. Manzari, eds.), ASCE Geotechnical Special Publication (GSP) 290, 21-32.

Ishihara, K. (1985). "Stability of natural deposits during earthquakes." *Proceedings of the 11th International Conference on Soil Mechanics and Foundation Engineering,* San Francisco, CA, USA, 1: 321-376.

Ishihara, K., and Yoshimine, M. (1992). "Evaluation of settlements in sand deposits following liquefaction during earthquakes." *Soils and Foundations* 32(1): 173-88.

Iwasaki, T., Tatsuoka, F., Tokida, K., and Yasuda, S. (1978). "A practical method for assessing soil liquefaction potential based on case studies at various sites in Japan." *Proceedings of the*

2nd International Conference on Microzonation, Nov 26-Dec 1, San Francisco, CA, USA, 885-896.

Jeffries, M.G. and Davies, M.P. (1993). “Use of CPTu to estimate equivalent SPT N_{60}.” *Geotechnical Testing Journal*, 16(4): 458-468.

Jia, M.C. and Wang, B.Y. (2012). “Liquefaction testing of stratified sands interlayered with silt.” *Applied Mechanics and Materials*, 256, 116-119.

Juang, C. H., Yang, S. H., Yuan, H., and Fang, S. Y. (2005). “Liquefaction in the Chi-Chi earthquake-effect of fines and capping non-liquefiable layers.” *Soils and Foundations*, 45(6): 89-101.

Lee, D.H., Ku, C.S., and Yuan, H. (2003). “A study of liquefaction risk potential at Yuanlin, Taiwan.” *Engineering Geology*, 71(1), 97-117.

Li, D.K., Juang, C.H., and Andrus, R.D. (2006a). “Estimation of liquefaction effect by means of liquefaction potential index.” *GeoShanghai International Conference 2006: Ground Modification and Seismic Mitigation* (A. Porbaha, S. Shen, J. Wartman, and J. Chai eds.), ASCE Geotechnical Special Publication 152, 359-364.

Li, D.K., Juang, C.H., and Andrus, R.D. (2006b). “Liquefaction potential index: A critical assessment using probability concept.” *Journal of GeoEngineering*, 1(1): 11-24.

Maurer, B.W., Green, R.A., Cubrinovski, M., and Bradley, B.A. (2014). “Evaluation of the liquefaction potential index for assessing liquefaction hazard in Christchurch, New Zealand.” *Journal of Geotechnical and Geoenvironmental Engineering*, 140(7): 04014032.

Maurer, B.W., Green, R.A., and Taylor, O.S. (2015a). “Moving towards an improved index for assessing liquefaction hazard: lessons from historical data.” *Soils and Foundations*, 55(4): 778-787.

Maurer, B.W., Green, R.A., Cubrinovski, M., and Bradley, B. (2015b). “Fines-content effects on liquefaction hazard evaluation for infrastructure during the 2010-2011 Canterbury, New Zealand earthquake sequence.” *Soil Dynamics and Earthquake Engineering*, 76: 58-68.

Maurer, B.W., Green, R.A., Cubrinovski, M., and Bradley, B. (2015c). “Assessment of CPT-based methods for liquefaction evaluation in a liquefaction potential index framework.” *Géotechnique*, 65(5): 328-336.

Maurer, B.W., Green, R.A., Cubrinovski, M., and Bradley, B. (2015d). “Calibrating the Liquefaction Severity Number (LSN) for Varying Misprediction Economies: A Case Study in

Christchurch, New Zealand." *Proc. 6th International Conference on Earthquake Geotechnical Engineering*, Christchurch, New Zealand, 1-4 November 2015.

Maurer, B.W., Green, R.A., van Ballegooy, S., Bradley, B.A., and Upadhyaya, S. (2017a). "Performance comparison of probabilistic and deterministic liquefaction triggering models for hazard assessment in 23 global earthquakes." *Geo-Risk 2017: Reliability-based design and code developments* (J. Huang, G.A. Fenton, L. Zhang, and D.V. Griffiths, eds.), ASCE Geotechnical Special Publication 283, 31-42.

Maurer, B.W., Green, R.A., van Ballegooy, S., and Wotherspoon, L. (2017b). "Assessing liquefaction susceptibility using the CPT Soil Behavior Type Index," *Proc. 3rd Intern. Conf. on Performance-Based Design in Earthquake Geotechnical Engineering* (PBDIII), Vancouver, Canada, 16-19 July.

Maurer, B.W., Green, R.A., van Ballegooy, S., and Wotherspoon, L. (2019). "Development of region-specific soil behavior type index correlations for evaluating liquefaction hazard in Christchurch, New Zealand." *Soil Dynamics and Earthquake Engineering*, 117:96-105.

Oommen, T., Baise, L. G., and Vogel, R. (2010). "Validation and application of empirical liquefaction models." *Journal of Geotechnical and Geoenvironmental Engineering, 136*(12): 1618-1633.

Ozutsumi, O., Sawada, S., Iai, S., Takeshima, Y., Sugiyama, W., and Shimazu, T. (2002). "Effective stress analyses of liquefaction-induced deformation in river dikes." *Soil Dynamics and Earthquake Engineering*, 22(9): 1075-1082.

Papathanassiou, G. (2008). "LPI-based approach for calibrating the severity of liquefaction-induced failures and for assessing the probability of liquefaction surface evidence." *Engineering Geology*, 96(1-2): 94-104.

Quigley, M.C., Bastin, S., and Bradley, B.A. (2013). "Recurrent liquefaction in Christchurch, New Zealand, during the Canterbury earthquake sequence." *Geology*, 41(4): 419-422.

Robertson, P.K. and Wride, C.E. (1998). "Evaluating cyclic liquefaction potential using cone penetration test." *Canadian Geotechnical Journal*, 35(3): 442-459.

The Mathworks. (2018). "MATLAB and Statistics Toolbox Release 2018b," *The Mathworks*, Inc., Natick, Massachusetts, United States.

Upadhyaya, S., Maurer, B.W., Green, R.A., and Rodriguez-Marek, A. (2018). "Effect of non-liquefiable high fines-content, high plasticity soils on liquefaction potential index (LPI) performance." *Geotechnical Earthquake Engineering and Soil Dynamics V: Liquefaction Triggering, Consequences, and Mitigation* (S.J. Brandenberg and M.T. Manzari, eds.), ASCE Geotechnical Special Publication 290, 191-198.

Upadhyaya, S., Green, R.A., Rodriguez-Marek, A., Maurer, B.W., Wotherspoon, L., Bradley, B.A., and Cubrinovski, M. (2019a). "Influence of corrections to recorded peak ground accelerations due to liquefaction on predicted liquefaction response during the M_w 6.2, February 2011 Christchurch earthquake." *13th Australia New Zealand Conference on Geomechanics 2019*, April 1-3, Perth, Australia.

Upadhyaya, S., Green, R.A., Maurer, B.W., and Rodriguez-Marek, A. (2019b). "Selecting factor of safety against liquefaction for design based on cost considerations." *7th International Conference on Earthquake Geotechnical Engineering*, June 17-20, Rome, Italy.

van Ballegooy, S., Malan, P.J., Jacka, M.E., Lacrosse, V.I.M.F., Leeves, J.R., Lyth, J.E., and Cowan, H. (2012). "Methods for characterising effects of liquefaction in terms of damage severity." *Proc. 15th World Conference on Earthquake Engineering* (15 WCEE), Lisbon, Portugal, September 24-28.

van Ballegooy, S., Cox, S.C., Thurlow, C., Rutter, H.K., Reynolds T., Harrington, G., Fraser, J., and Smith, T. (2014a). *Median water table elevation in Christchurch and surrounding area after the 4 September 2010 Darfield earthquake: Version 2*. GNS Science Report 2014/18.

van Ballegooy, S., Malan, P., Lacrosse, V., Jacka, M.E., Cubrinovski, M., Bray, J.D., O'Rourke, T.D., Crawford, S.A., and Cowan, H. (2014b). "Assessment of liquefaction-induced land damage for residential Christchurch." *Earthquake Spectra*, 30(1): 31-55.

van Ballegooy, S., Green, R.A., Lees, J., Wentz, F., and Maurer, B.W. (2015). "Assessment of various CPT based liquefaction severity index frameworks relative to the Ishihara (1985) H_1-H_2 boundary curves." *Soil Dynamics and Earthquake Engineering*, 79(Part B): 347-364.

Wotherspoon, L.M, Orense, R.P, Bradley, B.A., Cox, B.R., Wood, C. and Green, R.A. (2014). *Geotechnical characterisation of Christchurch strong motion stations*, Earthquake Commission Biennial Grant Report; 2014, project no. 12/629.

Wotherspoon, L.M., Orense, R.P., Green, R.A., Bradley, B.A., Cox, B.R. and Wood, C.M. (2015). "Assessment of liquefaction evaluation procedures and severity index frameworks at Christchurch strong motion stations." *Soil Dynamics and Earthquake Engineering* 79(Part B): 335-346.

Zhang, G., Robertson, P.K., and Brachman, R.W.I. (2002). "Estimating liquefaction-induced ground settlements from CPT for level ground." *Canadian Geotechnical Journal,* 39(5): 1168-1180.

Zhu, J., Baise, L.G., and Thompson, E.M. (2017). "An updated geospatial liquefaction model for global application." *Bulletin of the Seismological Society of America,* 107(3): 1365-1385.

Zou, K.H. (2007). "Receiver operating characteristic (ROC) literature research." On-line bibliography available from: <http://www.spl.harvard.edu/archive/spl-pre2007/pages/ppl/zou/roc.html> accessed 10 March 2016.

Tables

Table 3.1 Summary of ROC statistics on two subsets of I_{c10} for different *MSI* models.

***MSI* model**	**All I_{c10}**		**$I_{c10} < 2.05$**		**$I_{c10} \geq 2.05$**	
	AUC	***OOP***	***AUC***	***OOP***	***AUC***	***OOP***
LPI	0.825	3.7	0.850	3.7	0.764	7.5
LPIish	0.828	1.7	0.847	1.7	0.776	4.4
LSN	0.775	10	0.798	11	0.695	15

Table 3.2 Summary of ROC statistics on multiple finer subsets of I_{c10} for different *MSI* models.

***MSI* model**	**$I_{c10} < 1.7$**		**$1.7 \leq I_{c10} < 1.9$**		**$1.9 \leq I_{c10} < 2.1$**		**$2.1 \leq I_{c10} < 2.3$**		**$I_{c10} \geq 2.3$**	
	AUC	***OOP***	***AUC***	***OOP***	***AUC***	***OOP***	***AUC***	***OOP***	***AUC***	***OOP***
LPI	0.860	2.3	0.855	3.9	0.808	7.5	0.798	7.1	0.791	8.8
LPIish	0.850	0.5	0.857	1.7	0.814	3.1	0.804	3.9	0.737	4.4
LSN	0.812	8	0.801	13	0.745	13	0.718	15	0.659	15

Table 3.3 P(S|MSI,I_{c10}) model coefficients.

***MSI* model**	**B_0**	**B_1**	**B_2**
LPI	-1.677	0.645	-0.206
LPIish	-1.408	0.747	-0.233
LSN	-1.580	0.147	-0.033

Table 3.4 P(S|MSI) model coefficients.

***MSI* model**	**C_0**	**C_1**
LPI	-1.567	0.208
LPIish	-1.358	0.259
LSN	-1.549	0.079

Table 3.5 Comparison of *AUC* and *AIC* values between P($S|MSI,I_{c10}$) and P($S|MSI$) models.

***MSI* model**	**AUC**		**ΔAUC**	**AIC**		**ΔAIC**
	P($S|MSI, I_{c10}$)	**P($S|MSI$)**		**P($S|MSI, I_{c10}$)**	**P($S|MSI$)**	
LPI	0.833	0.825	0.008	9741	10054	313
LPIish	0.834	0.828	0.006	10080	10275	195
LSN	0.777	0.775	0.002	11175	11222	47

Table 3.6 Optimum threshold probabilities for different severities of surficial liquefaction manifestation.

Manifestation severity	**Probability thresholds**		
	P($S|LPI, I_{c10}$)	**P($S|LPIish, I_{c10}$)**	**P($S|LSN, I_{c10}$)**
Any manifestation	0.37	0.31	0.35
Marginal manifestation	0.25	0.28	0.31
Moderate manifestation	0.59	0.49	0.48
Severe manifestation	0.82	0.78	0.60

Figures

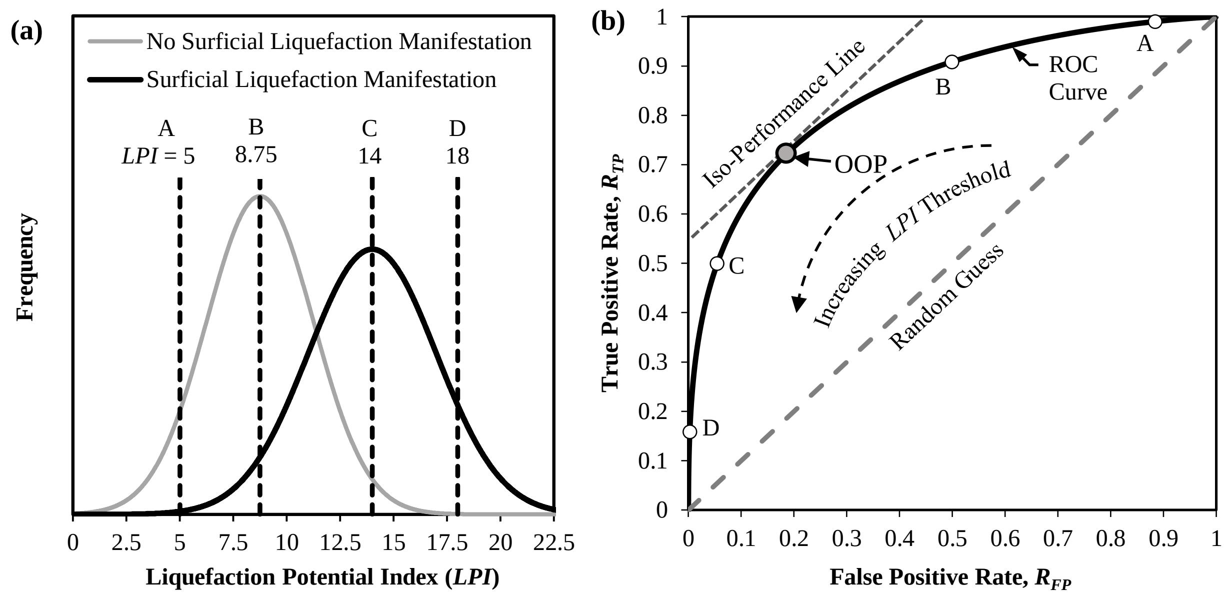

Figure 3.1 Conceptual illustration of ROC analyses: (a) frequency distributions of surficial liquefaction manifestation and no surficial liquefaction manifestation observations as a function of *LPI*; (b) corresponding ROC curve (after Maurer et al. 2015b,c,d).

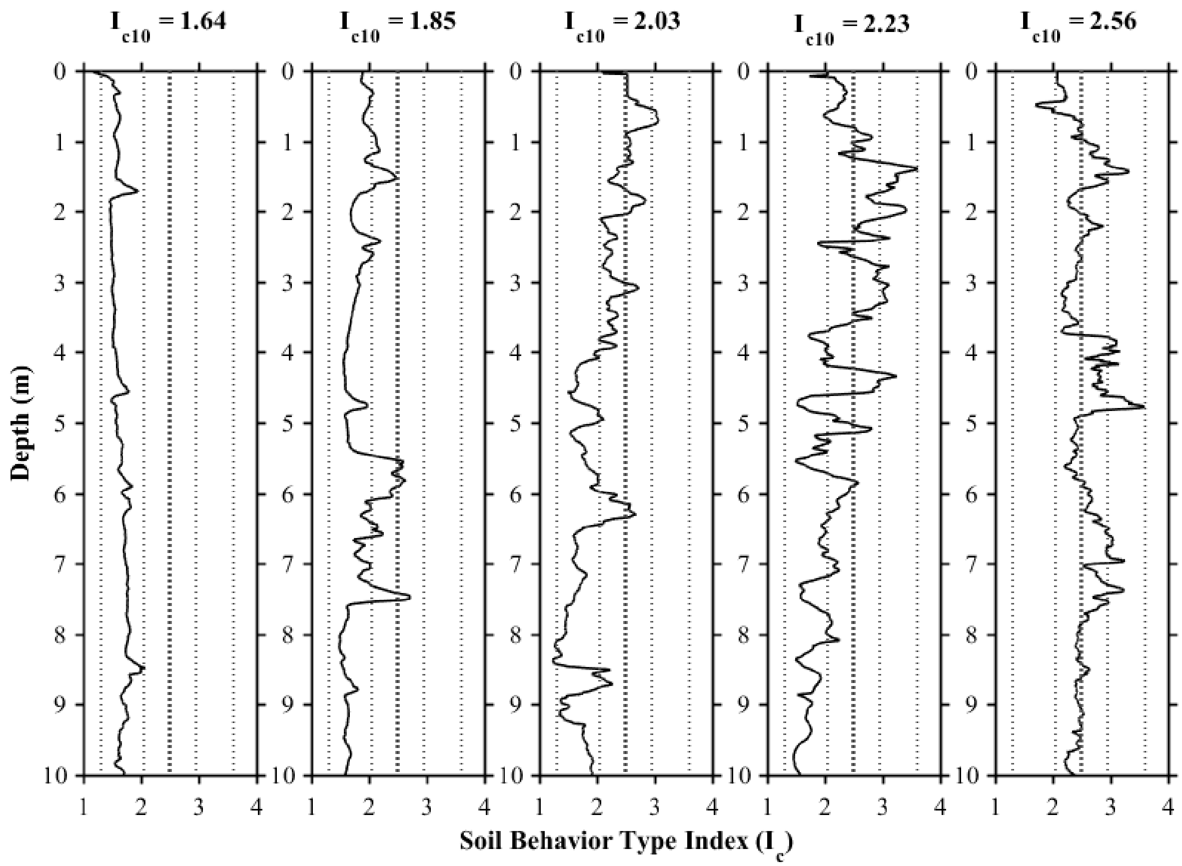

Figure 3.2 Example I_c versus depth profiles from the CE dataset that have I_{c10} falling in different ranges considered in this study: $I_{c10} < 1.7$; $1.7 \leq I_{c10} < 1.9$; $1.9 \leq I_{c10} < 2.1$; $2.1 \leq I_{c10} < 2.3$; and $I_{c10} \geq 2.3$.

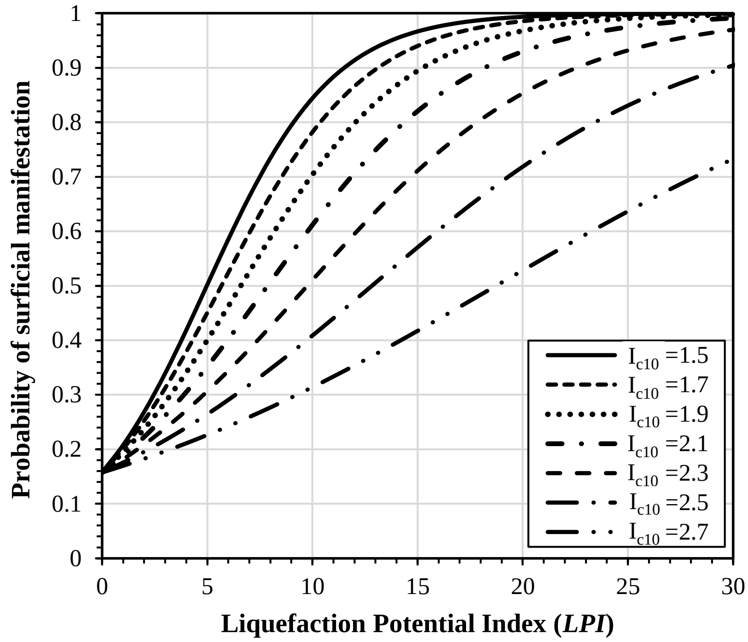

Figure 3.3 Probability of surficial liquefaction manifestation as a function of *LPI* and I_{c10}.

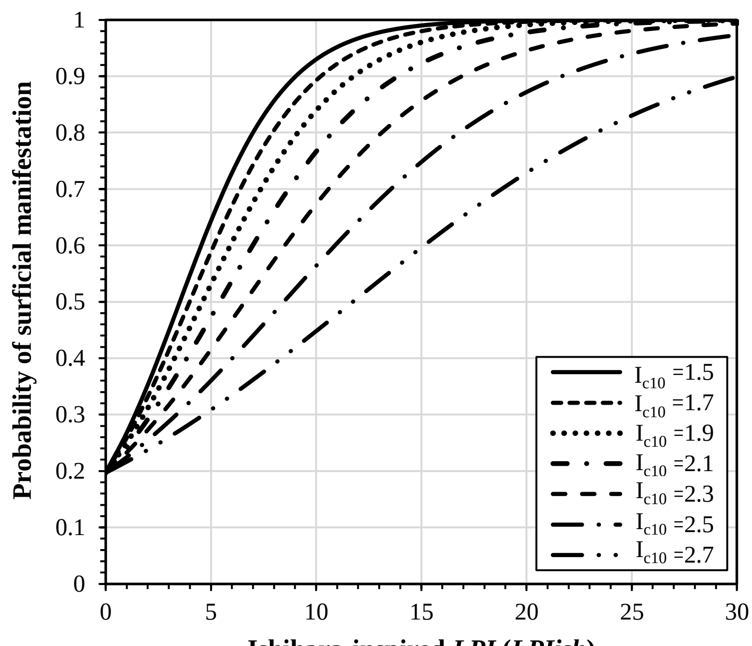

Figure 3.4 Probability of surficial liquefaction manifestation as a function of *LPIish* and I_{c10}.

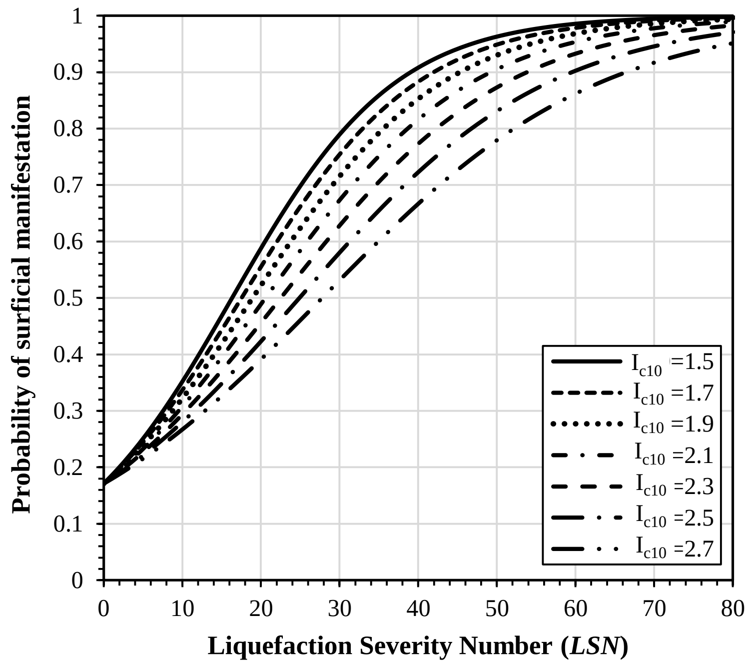

Figure 3.5 Probability of surficial liquefaction manifestation as a function of *LSN* and I_{c10}.

Chapter 4: Ishihara-inspired Liquefaction Severity Number (*LSNish*)

Sneha Upadhyaya[1]; Russell A. Green[2]; Brett W. Maurer[3]; Adrian Rodriguez-Marek[2]; and Sjoerd van Ballegooy[4]

[1]Graduate Student, Department of Civil and Environmental Engineering, Virginia Tech, Blacksburg, VA 24061.

[2]Professor, Department of Civil and Environmental Engineering, Virginia Tech, Blacksburg, VA 24061.

[3]Assistant Professor, Department of Civil and Environmental Engineering, University of Washington, Seattle, WA 98195.

[4]Technical Director, Geotechnical, Tonkin + Taylor Ltd., 105 Carlton Gore Rd., Newmarket, Auckland 1023, New Zealand.

4.1 Abstract

The severity of surface manifestation of liquefaction is commonly used as a proxy for liquefaction damage potential. However, the existing models used in predicting the severity of manifestation may not fully account for factors controlling manifestation. Herein, a new model is derived using insights from the existing models and the understanding of the mechanics of manifestation from the literature. The new manifestation model is termed *LSNish* since it is a merger of the Liquefaction Severity Number (*LSN*) formulation and Ishihara's relationship for predicting surface manifestation based on the relative thicknesses of the non-liquefied crust and the underlying liquefied layer. As such, *LSNish* accounts for the post-liquefaction volumetric strain potential as well as the crust thickness in predicting the severity of surficial liquefaction manifestations. *LSNish* was evaluated using compiled Canterbury, New Zealand, liquefaction case histories and its predictive efficiency was compared to those of existing models. It was found that despite more fully accounting for factors that influence surficial liquefaction manifestations, *LSNish* did not demonstrate improved performance over the existing models. Several possible causes for such findings are discussed; a likely reason is the double counting of the dilative tendencies of dense soils by *LSNish*, since the liquefaction triggering model inherently accounts for such effects. This same issue is a shortcoming of *LSN*. A proper accounting and clear separation of distinct factors influencing triggering and manifestation in future would improve the performance of *LSNish*.

4.2 Introduction

The main objective of this study is to develop a new model for predicting the occurrence and the severity of surficial liquefaction manifestation that accounts for the influences of non-liquefied crust/capping layer thickness as well as contractive/dilative tendencies of soil. The manifestation model developed herein is named as Ishihara inspired Liquefaction Severity Number (*LSNish*) since it is a conceptual and mathematical merger of Ishihara's H_1-H_2 boundary curves (Ishihara 1985) for predicting the occurrence of surficial liquefaction manifestations and the Liquefaction Severity Number (*LSN*) formulation by van Ballegooy et al. (2012; 2014b).

The severity of surficial liquefaction manifestation is often used as a proxy for liquefaction-induced damage potential for near-surface infrastructure. As such, accurate prediction of the severity of surficial liquefaction manifestation is critical for reliably assessing the risk due to liquefaction. This requires a proper understanding of the mechanics of surficial manifestation and the factors controlling it. Past studies have shown that surficial liquefaction manifestation is governed by several factors, including: (1) properties of the liquefied strata such as the depth, thickness, density, fines-content, and post-triggering strain potential; (2) properties of the non-liquefied soil strata (either in the form of a thick crust/capping layer or interbedded within a soil profile) such as fines-content, plasticity, permeability, and thickness; and (3) the stratification/sequencing of the liquefied and non-liquefied strata and the cross-interaction between these layers within a soil profile (e.g., Iwasaki et al. 1978; Ishihara and Ogawa 1978; Ishihara 1985; van Ballegooy et al. 2012; 2014b; Maurer et al. 2015a,b; Upadhyaya et al. 2018; Beyzaei et al. 2018; Cubrinovski et al. 2019; among others).

Different models have been proposed in the literature to predict the occurrence/severity of surficial liquefaction manifestation, usually in the form of a numerical index, referred to herein as a manifestation severity index (MSI). These models use the results from a liquefaction triggering model and tie the cumulative response of the soil profile to the occurrence/severity of surficial liquefaction manifestation. However, not all the factors influential to surficial liquefaction manifestation, as discussed above, are adequately accounted for by the existing MSI models. One of the earliest models is the Liquefaction Potential Index (*LPI*), proposed by Iwasaki et al. (1978), which considers the influence of depth, thickness, and soil density (D_r) through factor of safety (*FS*) of the liquefied layers (e.g., for a given level of seismic demand, *FS* increases as D_r increases) to predict the severity of manifestation. While *LPI* has been widely used to characterize the damage potential of liquefaction throughout the world (e.g., Sonmez 2003; Papathanassiou et al. 2005; 2008; Baise et al. 2006; Cramer et al. 2008; Hayati and Andrus 2008; Holzer et al. 2006; 2008; 2009; Yalcin et al. 2008; Chung and Rogers 2011; Dixit et al. 2012; Sana and Nath, 2016; among others), it was found to perform inconsistently during some recent earthquakes (e.g., the 2010-2011 Canterbury earthquakes in New Zealand) (e.g., Maurer et al 2014; 2015b,c). This inconsistency can be attributed to limitations in the *LPI* formulation to appropriately account for all the factors influencing surficial manifestation of liquefaction. Specifically, the *LPI* formulation may not adequately account for the contractive/dilative tendencies of the soil on the potential consequences of liquefaction. For example, a dense and a loose sand stratum both having $FS = 0.8$ could result in the same *LPI* value but their consequences will likely be very different. Moreover, the *LPI* formulation assumes that surface manifestations will not occur unless $FS < 1$. However, surficial manifestations related to liquefaction may occur due to elevated excess pore pressures during shaking even when $FS \geq 1$. Additionally, the *LPI* formulation does not account for the influence of thick non-liquefied crust and/or the effects of non-liquefiable high fines-content (*FC*), high plasticity soils on the severity of surficial liquefaction manifestations. Although the influence of these effects could be accounted for by using different *LPI* manifestation severity thresholds (i.e., *LPI* values distinguishing between different manifestation severity classes, e.g., cases with and without manifestation) for these conditions (e.g., Maurer et al. 2015b; Upadhyaya et al. 2019c), it is preferred to have a model that can directly account for these conditions in a less ad hoc manner.

In efforts to address some of the shortcomings of the *LPI* formulation, alternative MSI models were proposed, such as the Ishihara-inspired *LPI* (*LPIish*) by Maurer et al. (2015a) and Liquefaction Severity Number (*LSN*) by van Ballegooy et al. (2012; 2014b). A major improvement of *LPIish* over *LPI* is that it accounts for the effect of the non-liquefiable crust/capping layer thickness using Ishihara's (1985) relationship that relates the thicknesses of the non-liquefied crust (H_1) and of the liquefied stratum (H_2) to the occurrence of surficial liquefaction manifestations. However, as with *LPI*, *LPIish* may not fully account for the contractive/dilative tendencies of the soil on the severity of manifestations. The *LSN* formulation conceptually improves upon *LPI*, as well as *LPIish*, in that it accounts for the additional influence of contractive/dilative tendencies of the soil via the inclusion of a relationship between D_r and the post-liquefaction volumetric strain potential (ε_v). However, *LSN* does not account for the effects of non-liquefied crust thickness on the occurrence/severity of surficial liquefaction manifestations.

The motivation of this paper is to develop an MSI that more fully accounts for the effects of non-liquefiable crust thickness and the effects of contractive/dilative tendencies of the soil on the severity of surficial liquefaction manifestations. This is achieved by combining the positive aspects of *LPIish* and *LSN* in a single formulation, resulting in a novel MSI model, termed *LSNish*, that more fully accounts for the effects of non-liquefiable crust thickness using Ishihara's H_1-H_2 boundary curves and the contractive/dilative tendencies of the soil on the severity of surficial liquefaction manifestation via inclusion of ε_v. Similar to the derivation of *LPIish* by Maurer et al. (2015a), the new index is derived as a conceptual and mathematical merger of the Ishihara (1985) H_1-H_2 relationships and the *LSN* formulation. In the following, overviews of *LPI*, *LPIish*, and *LSN* models are presented first, which are then followed by the derivation of the new index, *LSNish*. Next, *LSNish* is evaluated using a large dataset of liquefaction case histories from the 2010-2016 Canterbury, New Zealand, earthquakes (CE) and its predictive efficiency is compared with that of existing MSI models (i.e., *LPI*, *LPIish*, and *LSN*).

4.3 Overview of existing manifestation severity index (MSI) models

4.3.1 Liquefaction Potential Index (LPI)

The liquefaction potential index (*LPI*) is defined as (Iwasaki et al. 1978):

$$LPI = \int_0^{z_{max}} F(FS) \cdot w(z)\, \mathrm{dz} \tag{4.1}$$

where: *FS* is the factor of safety against liquefaction triggering, computed by a liquefaction triggering model; z is depth below the ground surface in meters; z_{max} is the maximum depth considered, generally 20 m; and $F(FS)$ and $w(z)$ are functions that account for the weighted contributions of *FS* and z on surface manifestation. Specifically, $F(FS) = 1 - FS$ for $FS \leq 1$ and $F(FS) = 0$ otherwise; and $w(z) = 10 - 0.5z$. Thus, *LPI* assumes that the severity of surface manifestation depends on the cumulative thickness of liquefied soil layers, the proximity of those layers to the ground surface, and the amount by which *FS* in each layer is less than 1.0. Given this definition, *LPI* can range from zero to 100.

4.3.2 Ishihara-inspired Liquefaction Potential Index (LPIish)

Using the data from the 1983, M_w7.7 Nihonkai-chubu and the 1976, M_w7.8 Tangshan earthquakes, Ishihara (1985) proposed generalized relationship relating the thicknesses of the non-liquefiable crust (H_1) and of the underlying liquefied strata (H_2) to the occurrence of liquefaction induced damage at the ground surface. This relationship was developed in the form of boundary curves, that separate cases with and without surficial liquefaction manifestation as a function of peak ground acceleration (*PGA*), as shown in Figure 4.1. Moreover, the H_1-H_2 boundary curves indicate that, for a given *PGA*, there exists a limiting H_1, thicker than which no surficial liquefaction manifestations occur regardless of the value of H_2. While Ishihara's H_1-H_2 curves have been shown to perform well in some studies (e.g., Youd and Garris 1995), other studies have shown that the curves are not easily implementable for non-uniform soil profiles that have multiple interbedded non-liquefying soil strata, such as those in Christchurch, New Zealand. This is mainly due to difficulty in defining H_2 for these profiles (e.g., van Ballegooy et al. 2014b; 2015).

To account for the influence of non-liquefied crust thickness on the severity of surficial liquefaction manifestations using a more quantitative approach, Maurer et al. (2015a) utilized Ishihara's boundary curves to derive an alternative liquefaction damage index, *LPIish*, which is given by:

$$LPIish = \int_{H_1}^{z_{max}} F(FS) \cdot \frac{25.56}{z} dz \tag{4.2a}$$

where

$$F(FS) = \begin{cases} 1 - FS \; if \; FS \leq 1 \cap H_1 \cdot m(FS) \leq 3 \\ 0 \qquad\qquad\qquad\qquad\qquad otherwise \end{cases} \tag{4.2b}$$

and

$$m(FS) = exp\left(\frac{5}{25.56 \cdot (1 - FS)}\right) - 1; \quad m(FS > 0.95) = 100 \tag{4.2c}$$

where *FS* and z_{max} are defined the same as they are for *LPI*. As can be surmised from Eq. 4.2, the *LPIish* framework accounts for the limiting thickness of non-liquefied crust by imposing an additional constraint on *F*(*FS*) and uses a power-law depth weighting function, consistent with Ishihara's H_1-H_2 boundary curves. The power law depth weighting function results in *LPIish* giving a higher weight to shallower layers than *LPI* in predicting the severity of surficial liquefaction manifestations.

4.3.3 Liquefaction Severity Number (LSN)

As stated in the Introduction, *LSN* was proposed by van Ballegooy et al. (2012; 2014b) and uses a relationship between D_r and ε_v to account for the contractive/dilative tendencies of the soil on the severity of surficial liquefaction manifestations. *LSN* is given by:

$$LSN = \int_0^{z_{max}} 1000 \cdot \frac{\varepsilon_v}{z} dz \tag{4.3}$$

where z_{max} is the maximum depth considered, generally 10 m, and ε_v is estimated by using the relationship proposed by Zhang et al. (2002) (entered as a decimal in Eq. 4.3), which is based on the ε_v-D_r-FS relationship proposed by Ishihara and Yoshimine (1992). Thus, unlike *LPI* and *LPIish* which only consider the influence of soil strata with $FS < 1$ on the severity of surficial liquefaction manifestations, *LSN* considers the contribution of layers with $FS \leq 2$ via the ε_v-D_r-FS relationship proposed by Ishihara and Yoshimine (1992).

4.4 Derivation of Ishihara-inspired *LSN* (*LSNish*)

As mentioned earlier, *LSNish* merges the positive aspects of the *LPIish* and *LSN* models. The derivation of *LSNish* follows a procedure similar to the derivation of *LPIish* (Maurer et al. 2015a) (i.e., derived using Ishihara's boundary curves) and is detailed in the following sub-sections:

4.4.1 Assumptions

1. It is assumed that the penetration resistance corresponding to each of Ishihara's boundary curves is the same. In any stress-based "simplified" liquefaction triggering model, *FS* is computed as the ratio of normalized cyclic resistance ratio ($CRR_{M7.5}$) to normalized cyclic stress ratio (CSR^*) (i.e., $FS = CRR_{M7.5}/CSR^*$). Since $CRR_{M7.5}$ is correlated to normalized penetration resistance, it is also assumed that $CRR_{M7.5}$ corresponding to each of Ishihara's boundary curves is the same. Moreover, because CSR^* is directly proportional to *PGA*, it follows that *FS* for the liquefiable strata will be inversely proportional to *PGA*.

2. It is assumed that each of Ishihara's H_1-H_2 boundary curves represent the same value of *LSNish* (i.e., the threshold *LSNish* value for the occurrence of surficial liquefaction manifestation).

3. It is assumed that each of Ishihara's H_1-H_2 boundary curves can be approximated by two straight lines, wherein the initial portion of the curve is assumed to have a slope *m* and the latter portion is approximated as a vertical line having slope ∞, as shown in Figure 4.2. As such, the thickness of the liquefiable strata (H_2), and the thickness of the non-liquefiable curst (H_1) may be related through the slope (m) that is unique to each boundary curve (i.e., $H_2 = H_1 \times m$).

4. It is assumed that the *FS* is constant with depth within the liquefiable strata (H_2).

4.4.2 Functional Form of LSNish

The functional form for *LSNish* is defined as:

$$LSNish = \int_{H_1}^{H_1+H_2} F(\varepsilon_v) \cdot w(z) \cdot dz \quad (4.4)$$

In Eq. 4.4, the $F(\varepsilon_v)$ function accounts for the contribution of *FS* and D_r on the severity of surficial liquefaction manifestations via ε_v, and $w(z)$ is the depth weighting function.

Per Assumption (4), *FS* for the liquefiable strata is constant with depth. Also, per Assumption (1), the normalized penetration resistance of the liquefiable strata is constant with depth. From these two assumptions, it is implied that ε_v for the liquefiable strata is also constant with depth. As a result, $F(\varepsilon_v)$ can be taken out of the integral, as shown in Eq. 4.5.

$$LSNish = F(\varepsilon_v) \int_{H_1}^{H_1+H_2} w(z) \cdot dz \quad (4.5)$$

Per Assumption (2), *LSNish* is constant for each boundary curve and thus the integral in Eq. 4.5 must be constant and independent of the values of H_1 and H_2. This condition is satisfied by assuming a power-law functional form of $w(z)$, given by:

$$w(z) = \frac{k}{z} \quad (4.6)$$

where k is a constant and will be determined subsequently. Per Assumption (3), $H_2 = H_1 \times m$. Thus, Eq. 4.5 can be modified as:

$$LSNish = F(\varepsilon_v) \int_{H_1}^{H_1(m+1)} \frac{k}{z} \cdot dz = F(\varepsilon_v) \cdot k \cdot \ln\left(\frac{H_1(1+m)}{H_1}\right) = F(\varepsilon_v) \cdot k \cdot \ln(m+1) \\ = c \tag{4.7}$$

where: c is a constant equal to threshold value of *LSNish* for surficial liquefaction manifestation.

Rearranging the terms in Eq. 4.7, the slope (m) can be expressed as:

$$m = exp\left(\frac{c}{k \cdot F(\varepsilon_v)}\right) - 1 \tag{4.8}$$

4.4.3 Determining constants

As shown in Eq. 4.8, a relationship can be established between m and ε_v. Also, from Assumption (1), the *FS* for the boundary curves associated with *PGA*s of 0.2g and 0.4-0.5g (~0.45g) may be related as:

$$\frac{FS_{0.4-0.5g}}{FS_{0.2g}} \approx \frac{0.2g}{0.45g} \quad \Rightarrow \quad FS_{0.45g} = 0.45\, FS_{0.2g} \tag{4.9}$$

Moreover, from Figure 4.2, the slopes of the initial portion of the boundary curves associated with *PGA* of 0.2g and 0.4-0.5g can be approximated as 1 and 0.33, respectively. Accordingly, from Eq. 4.8, the slopes of these two boundary curves can be expressed as:

$$m_{0.2g} = \; exp\left(\frac{c}{k \cdot F(\varepsilon_v)_{0.2g}}\right) - 1 \; \approx 1 \tag{4.10}$$

and

$$m_{0.45g} = exp\left(\frac{c}{k \cdot F(\varepsilon_v)_{0.45g}}\right) - 1 \; \approx 0.33 \tag{4.11}$$

As stated earlier, c represents the threshold *LSNish* value (i.e., the *LSNish* value that is expected to segregate cases with and without manifestations). Herein, it is assumed that c = 5, similar to the threshold *LPI* proposed by Iwasaki et al. (1978). However, it should be noted that this choice of c

is arbitrary and could be any number that is expected to serve as a threshold for distinguishing cases with and without manifestations in forward analyses.

$F(\varepsilon_v)$ is defined herein as a linear function of ε_v, wherein ε_v can be estimated using the Zhang et al. (2002) procedure. The Zhang et al. (2002) procedure estimates ε_v as a function of FS and the normalized and fines-corrected Cone Penetration Test (CPT) tip resistance (q_{c1Ncs}) and is based on the ε_v-D_r-FS relationship proposed by Ishihara and Yoshimine (1992). The maximum value of ε_v per Ishihara and Yoshimine (1992) is 5.5%. Since it is desired that $F(\varepsilon_v)$ ranges from 0 to 1 (to be consistent with the ranges of F parameter in the *LPI* and *LPIish* formulations), $F(\varepsilon_v)$ is expressed as:

$$F(\varepsilon_v) = \frac{\varepsilon_v}{5.5} \tag{4.12}$$

where ε_v is expressed in percent. To determine the value of k that satisfies Eqs. 4.10 and 4.11, representative values of FS and q_{c1Ncs} need to be estimated. From reviewing the liquefaction case histories from the 1983 M_w7.7 Nihonkai-Chube earthquake in Japan, Ishihara (1985) determined that the representative normalized SPT penetration resistance (i.e., $N_{1,60}$) for liquefaction triggering was approximately 12 blows/30 cm, which is approximately equal to $q_{c1Ncs} \approx 90$ atm. For this value of q_{c1Ncs}, $FS_{0.2g}$ has to be equal to 0.99 and k = 36.929 for Eqs. 4.10 and 4.11 to be satisfied.

4.4.4 Final Form

As mentioned previously, Ishihara's H_1-H_2 boundary curves indicate that, for a given *PGA*, there exists a limiting crust thickness, thicker than which no surficial liquefaction manifestations occur regardless of the thickness of underlying liquefiable strata. This limiting crust thickness is also integrated in the *LSNish* formulation. As indicated by Ishihara's boundary curves (e.g., Figure 4.2), when the quantity H_1 x m exceeds ~3, surficial manifestations are not expected regardless of the value of H_2. Since m is a function of ε_v, it is implied that as ε_v increases, the thickness of the non-liquefiable crust required to suppress manifestation increases.

The final form of *LSNish* is given below:

$$LSNish = \int_{H_1}^{z_{max}} F(\varepsilon_v) \cdot \frac{36.929}{z} \cdot dz \tag{4.13a}$$

where z_{max} is defined the same as it is for *LPI* (i.e., 20 m), and:

$$F(\varepsilon_v) = \begin{cases} \dfrac{\varepsilon_v}{5.5} & if\ FS\ \leq 2\ and\ H_1 \cdot m(\varepsilon_v) \leq 3 \\ 0 & otherwise \end{cases} \tag{4.13b}$$

$$m(\varepsilon_v) = \exp\left(\frac{0.7447}{\varepsilon_v}\right) - 1; \quad m(\varepsilon_v < 0.16) = 100 \tag{4.13c}$$

where ε_v is expressed in percent. As can be surmised from Eq. 4.13, *LSNish* accounts for: (1) the influence of ε_v on the severity of surficial liquefaction manifestation; (2) the concept of limiting thickness of the non-liquefied crust; and (3) the contribution of layers with $FS \leq 2$ in contributing to the severity of surficial liquefaction manifestations.

4.5 Evaluation of *LSNish*

4.5.1 Canterbury earthquakes liquefaction case-history dataset

LSNish was evaluated using 7167 Cone Penetration Test (CPT) liquefaction case histories from the 2010-2016 CE. These 7167 CPT liquefaction case histories were derived as a subset of approximately 10,000 high quality case histories resulting from the M_w 7.1 September 2010 Darfield, the M_w 6.2 February 2011 Christchurch, and the M_w 5.7 February 2016 Valentine's Day earthquakes in Canterbury, New Zealand, largely assembled by Maurer et al. (2014; 2015b,c,d; 2017a,b; 2019). It should be noted that the *LSNish* formulation still does not account for the influence of non-liquefiable, high *FC*, high plasticity soil strata on the occurrence/severity of surficial liquefaction manifestation. Therefore, *LSNish* can be best evaluated using case histories comprised of predominantly clean to silty sand profiles. Maurer et al. (2015b) found that sites in the region that have an average CPT soil-behavior-type index (I_c) (Robertson and Wride 1998) for the upper 10 m of the soil profile (I_{c10}) less than 2.05 generally correspond to sites having predominantly clean to silty sands. Accordingly, the 7167 liquefaction case histories used in this study are only comprised of CPT soundings that have $I_{c10} < 2.05$. Of the 7167 case histories, 2574 cases are from the 2010 Darfield earthquake, 2582 cases are from the 2011 Christchurch earthquake, and 2011 cases are from the 2016 Valentine's day earthquake. Furthermore, 38% of the case histories were categorized as "no manifestation" and the remaining 62% were categorized as either "marginal," "moderate," or "severe" manifestation following the Green et al. (2014) classification.

PGAs are needed to estimate the seismic demand at the case history sites. In prior CE studies (e.g., Green et al. 2011; 2014; Maurer et al. 2014; 2015a,b,c,d; 2017a,b; 2019; van Ballegooy et al. 2015; among others), *PGAs* were obtained using the Bradley (2013b) procedure, which combines the unconditional *PGA* distributions as estimated by the Bradley (2013a) ground motion prediction equation, the actual recorded *PGAs* at the strong motion stations (SMSs), and the spatial correlation model of Goda and Hong (2008), to compute the conditional *PGAs* at the sites of interest. However, the *PGAs* at four SMSs during the M_w 6.2 February 2011 Christchurch earthquake were inferred to be associated with high-frequency dilation spikes as a result of liquefaction triggering and were higher than the pre-liquefaction *PGAs* (e.g., Wotherspoon et al. 2014, 2015). Such artificially high *PGAs* at the liquefied SMSs can potentially result in over-estimated *PGAs* at the nearby case-history sites (hence, overly conservative seismic demand), which in turn can lead to over-predictions of the severity of surficial liquefaction manifestations (Upadhyaya et al. 2019a). Accordingly, in the present study, pre-liquefaction *PGAs* at the four liquefied SMSs were used to estimate *PGAs* at the case history locations for the 2011 Christchurch earthquake. Note that for the 2010 Darfield and 2016 Valentine's day earthquakes, previously estimated *PGAs* remain unchanged.

Accurate estimation of ground-water table (GWT) depth is critical to liquefaction triggering evaluations. The GWT depth at each case-history site immediately prior to the earthquake was estimated using the robust, event-specific regional ground water models of van Ballegooy et al. (2014a), as in prior CE studies (e.g., Maurer et al. 2014; 2015b,c,d; 2017a,b; 2019; van Ballegooy et al. 2015; Upadhyaya et al. 2018; among others).

4.5.2 Evaluation of liquefaction triggering and severity of surficial liquefaction manifestation

In evaluating *LSNish*, *FS* is used as an input to estimate ε_v. *FS* for field case histories has been traditionally defined using deterministic normalized cyclic resistance ratio ($CRR_{M7.5}$) curves. However, the deterministic $CRR_{M7.5}$ are almost always conservatively positioned to minimize the number of false negatives (i.e., "liquefaction" cases that fall below or to the right of the $CRR_{M7.5}$ curve). As a result, *FS* computed using the deterministic $CRR_{M7.5}$ curve may lead to conservative predictions of the occurrence/severity of surficial liquefaction manifestations (i.e., conservative estimates of *LSNish*) for some cases. For unbiased estimates of *FS* and subsequent unbiased predictions of the severity of surficial liquefaction manifestations, use of median $CRR_{M7.5}$ may seem more appropriate. In the present study, *FS* was computed using the liquefaction triggering model of Boulanger and Idriss (2014) [BI14] using both their deterministic and median $CRR_{M7.5}$ curves, to investigate which among the two curves would result in better predictions of surficial manifestations, when operating within the *LSNish* formulation. Inherent to this process, soils with I_c > 2.5 were considered to be non-liquefiable (Maurer et al. 2017b, 2019). Additionally, the *FC* required to compute q_{c1Ncs} was estimated using the Christchurch-specific I_c - *FC* correlation proposed by Maurer et al. (2019).

For each CE case history, *LSNish* was computed using Eq. 4.13. The predictive efficiency of the *LSNish* model was compared to that of the existing MSI models (i.e., *LPI*, *LPIish*, and *LSN*) by performing receiver operating characteristic (ROC) analyses on the CE dataset. An overview of ROC analysis is presented in the following section.

4.5.3 Overview of ROC analysis

ROC analysis is widely used to evaluate the performance of diagnostic models, including extensive use in medical diagnostics (e.g., Zou 2007) and to a much lesser degree in geotechnical engineering (e.g., Oommen et al. 2010; Maurer et al. 2015b,c,d; 2017a,b; 2019; Green et al. 2017; Zhu et al. 2017; Upadhyaya et al. 2018; 2019b). In particular, in cases where the distribution of "positives" (e.g., cases of observed surficial liquefaction manifestations) and "negatives" (e.g., cases of no observed surficial liquefaction manifestations) overlap (e.g., Figure 4.3a), ROC analyses can be used (1) to identify the optimum diagnostic threshold (e.g., *LSNish* threshold); and (2) to assess the relative efficacy of competing diagnostic models, independent of the thresholds used. A ROC curve is a plot of the True Positive Rate (R_{TP}) (i.e., surficial liquefaction manifestations were observed, as predicted) versus the False Positive Rate (R_{FP}) (i.e., surficial liquefaction manifestations are predicted, but were not observed) for varying threshold values (e.g., *LSNish*). A conceptual illustration of ROC analysis, including the relationship among the distributions for positives and negatives, the threshold value, and the ROC curve, is shown in Figure 4.3.

In ROC curve space, a diagnostic test that has no predictive ability (i.e., a random guess) results in a ROC curve that plots as 1:1 line through the origin. In contrast, a diagnostic test that has a perfect predictive ability (i.e., a perfect model) plots along the left vertical and upper horizontal axes, connecting at the point (0,1) and indicates the existence of a threshold value that perfectly segregates the dataset (e.g., all cases with observed surficial manifestation will have *LSNish* above the threshold and all cases with no observed surficial manifestation will have *LSNish* below the threshold). The area under the ROC curve (*AUC*) can be used as a metric to evaluate the predictive performance of a diagnostic model (e.g., *LSNish*), whereby a higher *AUC* value indicates better predictive capabilities (e.g., Fawcett 2005). As such, a random guess returns an *AUC* of 0.5, whereas a perfect model returns an *AUC* of 1. The optimum operating point (*OOP*) in a ROC analysis is defined as the threshold value (i.e., threshold *LSNish*) that minimizes the rate of misprediction [i.e., R_{FP} + (1-R_{TP})]. Contours of the quantity [R_{FP} + (1-R_{TP})] are iso-performance lines joining points of equivalent performance in ROC space, as illustrated in Figure 4.3b.

4.5.4 Results and Discussion

ROC analyses were performed on the CE dataset using the *LSNish* model, as well as the three other existing MSI models (i.e., *LPI*, *LPIish*, and *LSN*). Additionally, each MSI model was evaluated using both the deterministic and median BI14 $CRR_{M7.5}$ curves. ROC statistics (i.e., *AUC* and *OOP*) were obtained to evaluate the performance of each MSI model in distinguishing (a) cases with no manifestations from cases with any manifestation severity; (b) cases with no manifestations from cases with marginal manifestations; (c) cases with marginal manifestations from cases with moderate manifestations; and (d) cases with moderate manifestations from cases with severe manifestations. Tables 4.1 and 4.2 summarize the ROC statistics (i.e., *AUC* and *OOP*) for each MSI model, evaluated using the BI14 deterministic and median $CRR_{M7.5}$ curves, respectively, for different severities of surficial liquefaction manifestations as described above. Figures 4.4a and 4.4b show the ROC curves for the four different MSI models, considering only the binomial predictive ability [i.e., case (a): cases with no manifestation from cases with any manifestation severity], evaluated in conjunction with the BI14 deterministic and median $CRR_{M7.5}$ curves, respectively. Also shown on Figures 4.4a and 4.4b are the optimum threshold values associated with each MSI model. Moreover, Figures 4.5a and 4.5b compare the *AUC*s associated with these four different MSI models, evaluated in conjunction with the BI14 deterministic and median $CRR_{M7.5}$ curves, respectively.

It can be seen that the *AUC*s for *LPI* and *LPIish* models are generally slightly higher when evaluated in conjunction with the deterministic $CRR_{M7.5}$ curve than with the median $CRR_{M7.5}$ curve. In contrast, the *AUC*s for *LSN* and *LSNish* models are generally slightly lower when evaluated using the deterministic $CRR_{M7.5}$ curve than using the median $CRR_{M7.5}$ curve. Since the changes in

AUC are not very significant between the deterministic and median $CRR_{M7.5}$ curves, it can be inferred that the MSI models perform equally efficiently using either variant of the $CRR_{M7.5}$ curves. However, it should be noted that the optimal threshold MSI values are quite different between the deterministic and median $CRR_{M7.5}$ curves, with the median $CRR_{M7.5}$ curve resulting in lower threshold values than the deterministic $CRR_{M7.5}$ curve. For example, the optimal threshold *LSNish* values distinguishing cases of no manifestations from cases with any manifestation severity when evaluated using the deterministic and median $CRR_{M7.5}$ curves are 5.4 and 3.6, respectively.

Most importantly, the results from ROC analyses show that, the *AUC* values returned by the four different MSI models follow the order: $LPI \approx LPIish > LSN \approx LSNish$, regardless of the $CRR_{M7.5}$ curve used in evaluating the models. As such, two main observations can be made. *First*, despite accounting for non-liquefied crust thickness, *LPIish* and *LSNish* did not show improvements over *LPI* and *LSN*, respectively. This is likely due to the fact that the case histories used in this study are only comprised of CPT soundings that have $I_{c10} < 2.05$, the majority of which are located in eastern Christchurch where the ground water table is shallow (usually ranging between 1~2m). As a result, the non-liquefied crust thickness may not have much of an influence on the severity of surficial liquefaction manifestations. Another possible reason could be that Ishihara's H_1-H_2 curves may not sufficiently account for the influence of non-liquefied crust thickness on the occurrence and severity of manifestations, although the authors believe that the general trends exhibited by Ishihara's H_1-H_2 curves are correct. *Second*, the higher *AUC*s for *LPI* and *LPIish* than the *LSN* and *LSNish* models indicate that the latter group performs more poorly despite accounting for the influence of soil density on the occurrence/severity of surficial liquefaction manifestation via the ε_v-D_r-FS relationship, which is contrary to what would be expected. Several factors may explain the cause of the less accurate predictions. For example, the ε_v model of Zhang et al. (2002) is based on the ε_v-D_r-FS relationship proposed by Ishihara and Yoshimine (1992) developed using laboratory test data on reconstituted clean sand samples. In contrast to the *FS* determined from laboratory tests for a specific soil that has a specific fabric, the field-based triggering curves are developed from a range of soils having a range of fabrics. As a result, there may be inconsistencies in how the Ishihara and Yoshimine (1992) ε_v-D_r-FS relationship is being applied in conjunction with *FS* determined from $CRR_{M7.5}$ curves determined from field case histories.

However, in the authors' opinion, the most likely reason for the poorer performance of *LSN* and *LSNish* is that the influence of post-triggering volumetric strain potential of dense soils on the severity of surficial liquefaction manifestation is being double-counted by these models. This is because *FS*, which is used as an input to compute ε_v, inherently accounts for such effects via the shape of the $CRR_{M7.5}$ curve. Specifically, the $CRR_{M7.5}$ curves likely tend towards vertical at medium to high penetration resistance due to dilative tendencies of dense soils that inhibits the surficial liquefaction manifestation, even if liquefaction is triggered at depth (e.g., Dobry 1989). While the existing triggering curves are treated as "actual" or "true" triggering curves in current practice, in reality, they are very likely combined "triggering" and "manifestation" curves. This is mainly because the $CRR_{M7.5}$ curves are based on the liquefaction response of profiles inferred from post-earthquake surface observations at sites. Sites without surficial evidence of liquefaction are classified, by default, as "no liquefaction," despite the possibility of liquefaction having triggered at depth, but not manifesting at the ground surface. Consequently, embedded in the resulting triggering curve are factors which relate not only to triggering, but also to post-triggering surface manifestation. These findings suggest that the current models for predicting liquefaction response may not account for the mechanics of liquefaction triggering and surface manifestation in a consistent and sufficient manner. The liquefaction triggering and manifestation models need to be developed simultaneously within a consistent framework that provides a clear separation and proper accounting of mechanics controlling each phenomenon. Given that *LSNish* accounts for the factors controlling manifestation in a more appropriate manner, it is hypothesized that *LSNish* would result in better predictions of the severity of surficial liquefaction manifestation than the existing MSI models, if used in conjunction with a "true" liquefaction triggering curve (i.e., free of factors influencing surficial liquefaction manifestation) (Upadhyaya et al. 2019d).

4.6 Conclusion

This paper presented a new manifestation severity index model, termed *LSNish*, that was derived as conceptual merger of the *LSN* formulation and Ishihara's H_1-H_2 boundary curves. As such, *LSNish* conceptually accounts for: (1) the influence of post-liquefaction volumetric strain potential on the severity of surficial liquefaction manifestation; (2) the limiting thickness of the non-liquefied crust, thicker than which no surficial manifestation can occur regardless of the thickness of the underlying liquefiable strata; and (3) the contribution of layers where liquefaction did not trigger (i.e., *FS* >1) but the excess pore pressures due to shaking reached high enough to cause surficial manifestations.

LSNish was evaluated using 7167 CPT liquefaction case histories from the 2010-2016 Canterbury earthquakes, comprised of predominantly clean to silty sand profiles and its predictive efficiency was compared with that of *LPI*, *LPIish*, and *LSN* models. These models were evaluated in conjunction with the BI14 triggering model, wherein both the deterministic and median $CRR_{M7.5}$ curves were used to compute *FS*. It was found that both the deterministic and median $CRR_{M7.5}$ curves were equally efficient when used within the *LSNish* formulation, but, the optimal threshold *LSNish* values associated with each curve were different. Most importantly, it was observed that the predictive efficiency of *LSNish* and *LSN* models were lower than those of *LPI* and *LPIish*, despite accounting for the additional influence of soil density on the severity of surficial liquefaction manifestation via the ε_v-D_r-*FS* relationship. One likely reason for this is that the influence of post-triggering volumetric strain potential on the severity of surficial liquefaction manifestation is being "double counted" by *LSN* and *LSNish* models, since the shape of the $CRR_{M7.5}$ curve inherently accounts for the dilative tendencies of dense soils, which inhibits surficial liquefaction manifestations even when liquefaction is triggered at depth. These findings suggest that the current framework for predicting the occurrence/severity of surficial liquefaction manifestation do not account for the mechanics of triggering and manifestation in a proper and sufficient manner. While the triggering curves are assumed to be "true" (i.e., free of factors influencing manifestation), in reality it is likely that they inherently account for some of the factors controlling surficial manifestation of liquefaction. Thus, there is a need to develop a framework that consistently and appropriately accounts for the mechanics behind liquefaction triggering and surficial liquefaction manifestation.

4.7 Acknowledgements

This research was funded by National Science Foundation (NSF) grants CMMI-1435494, CMMI-1724575, CMMI-1751216, and CMMI-1825189, as well as Pacific Earthquake Engineering Research Center (PEER) grant 1132-NCTRBM and U.S. Geological Survey (USGS) award G18AP-00006. This support is gratefully acknowledged. However, any opinions, findings, and conclusions or recommendations expressed in this paper are those of the authors and do not necessarily reflect the views of NSF, PEER, or the USGS.

References

Baise, L.G., Higgins, R.B., and Brankman, C.M. (2006). "Liquefaction hazard mapping-statistical and spatial characterization of susceptible units." *Journal of Geotechnical and Geoenvironmental Engineering* 132(6): 705-715.

Beyzaei, C.Z., Bray, J.D., van Ballegooy, S., Cubrinovski, M., and Bastin, S. (2018). "Depositional environment effects on observed liquefaction performance in silt swamps during the Canterbury earthquake sequence." *Soil Dynamics and Earthquake Engineering*, 107: 303-321.

Boulanger, R.W. and Idriss, I.M. (2014). *CPT and SPT based liquefaction triggering procedures*. Report No. UCD/CGM.-14/01, Center for Geotechnical Modelling, Department of Civil and Environmental Engineering, UC Davis, CA, USA.

Bradley, B.A. (2013a). "A New Zealand-specific pseudo-spectral acceleration ground-motion prediction equation for active shallow crustal earthquakes based on foreign models." *Bulletin of the Seismological Society of America*, 103(3): 1801-1822.

Bradley, B.A. (2013b). "Site-Specific and spatially-distributed ground motion intensity estimation in the 2010-2011 Christchurch earthquakes." *Soil Dynamics and Earthquake Engineering*, 48: 35-47.

Cramer, C.H., Rix, G.J., and Tucker, K. (2008). "Probabilistic liquefaction hazard maps for Memphis, Tennessee." *Seismological Research Letters* 79(3): 416-423.

Cubrinovski, M., Rhodes, A., Ntritsos, N., and Van Ballegooy, S. (2019). "System response of liquefiable deposits." *Soil Dynamics and Earthquake Engineering*, 124: 212-229.

Dixit, J., Dewaikar, D. M., and Jangid, R. S. (2012). "Assessment of liquefaction potential index for Mumbai City." *Natural Hazards and Earth Systems Sciences*, 12(9): 2759–2768.

Dobry, R. (1989). "Some basic aspects of soil liquefaction during earthquakes." *Earthquake Hazards and the Design of Constructed Facilities in the Eastern United States*. Annals of the New York Academy of Sciences, Volume 558, New York, NY: 172-183.

Fawcett, T. (2005). "An introduction to ROC analysis." *Pattern recognition letters*, *27*(8): 861-874.

Goda, K. and H. P. Hong (2008). "Spatial correlation of peak ground motions and response spectra." *Bulletin of the Seismological Society of America* 98 (1): 354–465.

Green, R.A., Cubrinovski, M., Cox, B., Wood, C., Wotherspoon, L., Bradley, B., and Maurer, B.W. (2014). "Select liquefaction case histories from the 2010-2011 Canterbury earthquake sequence." *Earthquake Spectra*, 30(1): 131-153.

Green, R.A., Upadhyaya, S., Wood, C.M., Maurer, B.W., Cox, B.R., Wotherspoon, L., Bradley, B.A., and Cubrinovski M. (2017). "Relative efficacy of CPT- versus Vs-based simplified liquefaction evaluation procedures," *Proc. 19th Intern. Conf. on Soil Mechanics and Geotechnical Engineering*, Seoul, Korea, 17-22 September.

Hayati, H. and Andrus, R.D. (2008). "Liquefaction potential map of Charleston, South Carolina based on the 1986 earthquake." *Journal of Geotechnical and Geoenvironmental Engineering* 134(6): 815-828.

Holzer, T.L., Bennett, M.J., Noce, T.E., Padovani, A.C., Tinsley III, J.C. (2006). "Liquefaction hazard mapping with LPI in the greater Oakland, California, area." *Earthquake Spectra*, 22(3): 693-708.

Holzer, T.L. (2008). "Probabilistic liquefaction hazard mapping." In Zeng, D., Manzari, M.T., and Hiltunen, D.R., *Geotechnical Earthquake Engineering and Soil Dynamics IV*: Sacramento, CA, ASCE Geotechnical Special Publication 181.

Holzer, T.L., Noce, T.E., and Bennett, M.J. (2009). "Scenario liquefaction hazard maps of Santa Clara Valley, Northern California." *Bulletin of the Seismological Society of America, 99(1): 367-381.*

Ishihara, K. and Ogawa, K. (1978). "Liquefaction susceptibility map of downtown Tokyo." *Proceedings of the 2nd International Conference on Microzonation,* Nov 26-Dec 1, San Francisco, CA, USA, 897–910.

Ishihara, K. (1985). "Stability of natural deposits during earthquakes." *Proceedings of the 11th International Conference on Soil Mechanics and Foundation Engineering,* San Francisco, CA, USA, 1: 321-376.

Ishihara, K., and Yoshimine, M. (1992). "Evaluation of settlements in sand deposits following liquefaction during earthquakes." *Soils and Foundations* 32(1): 173-88.

Iwasaki, T., Tatsuoka, F., Tokida, K., and Yasuda, S. (1978). "A practical method for assessing soil liquefaction potential based on case studies at various sites in Japan." *Proceedings of the 2nd International Conference on Microzonation*, Nov 26-Dec 1, San Francisco, CA, USA, 885-896.

Maurer, B.W., Green, R.A., Cubrinovski, M., and Bradley, B.A. (2014). "Evaluation of the liquefaction potential index for assessing liquefaction hazard in Christchurch, New Zealand." *Journal of Geotechnical and Geoenvironmental Engineering,* 140(7): 04014032.

Maurer, B.W., Green, R.A., and Taylor, O.S. (2015a). "Moving towards an improved index for assessing liquefaction hazard: lessons from historical data." *Soils and Foundations,* 55(4): 778-787.

Maurer, B.W., Green, R.A., Cubrinovski, M., and Bradley, B. (2015b). "Fines-content effects on liquefaction hazard evaluation for infrastructure during the 2010-2011 Canterbury, New Zealand earthquake sequence." *Soil Dynamics and Earthquake Engineering*, 76: 58-68.

Maurer, B.W., Green, R.A., Cubrinovski, M., and Bradley, B. (2015c). "Assessment of CPT-based methods for liquefaction evaluation in a liquefaction potential index framework." *Géotechnique*, 65(5): 328-336.

Maurer, B.W., Green, R.A., Cubrinovski, M., and Bradley, B. (2015d). "Calibrating the Liquefaction Severity Number (LSN) for Varying Misprediction Economies: A Case Study in Christchurch, New Zealand." *Proc. 6th International Conference on Earthquake Geotechnical Engineering,* Christchurch, New Zealand, 1-4 November 2015.

Maurer, B.W., Green, R.A., van Ballegooy, S., Bradley, B.A., and Upadhyaya, S. (2017a). "Performance comparison of probabilistic and deterministic liquefaction triggering models for hazard assessment in 23 global earthquakes." *Geo-Risk 2017: Reliability-based design and code developments* (J. Huang, G.A. Fenton, L. Zhang, and D.V. Griffiths, eds.), ASCE Geotechnical Special Publication 283, 31-42.

Maurer, B.W., Green, R.A., van Ballegooy, S., and Wotherspoon, L. (2017b). "Assessing liquefaction susceptibility using the CPT Soil Behavior Type Index," *Proc. 3rd Intern. Conf. on Performance-Based Design in Earthquake Geotechnical Engineering* (PBDIII), Vancouver, Canada, 16-19 July.

Maurer, B.W., Green, R.A., van Ballegooy, S., and Wotherspoon, L. (2019). "Development of region-specific soil behavior type index correlations for evaluating liquefaction hazard in Christchurch, New Zealand." *Soil Dynamics and Earthquake Engineering*, 117:96-105.

Oommen, T., Baise, L. G., and Vogel, R. (2010). "Validation and application of empirical liquefaction models." *Journal of Geotechnical and Geoenvironmental Engineering*, *136*(12): 1618-1633.

Papathanassiou, G., Pavlides, S., and Ganas, A. (2005). "The 2003 Lefkada earthquake: Field observation and preliminary microzonation map based on liquefaction potential index for the town of Lefkada." *Engineering Geology*, 82(1): 12-31.

Papathanassiou, G. (2008). "LPI-based approach for calibrating the severity of liquefaction-induced failures and for assessing the probability of liquefaction surface evidence." *Engineering Geology*, 96(1-2): 94-104.

Robertson, P.K. and Wride, C.E. (1998). "Evaluating cyclic liquefaction potential using cone penetration test." *Canadian Geotechnical Journal*, 35(3): 442-459.

Sana, H. and Nath, S.K. (2016). "Liquefaction potential analysis of the Kashmire valley alluvium, NW Himalaya." *Soil Dynamics and Earthquake Engineering*, 85: 11-18.

Sönmez, H. (2003). "Modification of the liquefaction potential index and liquefaction severity mapping for a liquefaction-prone area (Inegol, Turkey)." *Engineering Geology*, 44(7): 862–871.

Upadhyaya, S., Maurer, B.W., Green, R.A., and Rodriguez-Marek, A. (2018). "Effect of non-liquefiable high fines-content, high plasticity soils on liquefaction potential index (LPI) performance." *Geotechnical Earthquake Engineering and Soil Dynamics V: Liquefaction Triggering, Consequences, and Mitigation* (S.J. Brandenberg and M.T. Manzari, eds.), ASCE Geotechnical Special Publication 290, 191-198.

Upadhyaya, S., Green, R.A., Rodriguez-Marek, A., Maurer, B.W., Wotherspoon, L., Bradley, B.A., and Cubrinovski, M. (2019a). "Influence of corrections to recorded peak ground accelerations due to liquefaction on predicted liquefaction response during the M_w 6.2, February 2011 Christchurch earthquake." *13th Australia New Zealand Conference on Geomechanics 2019,* April 1-3, Perth, Australia.

Upadhyaya, S., Green, R.A., Maurer, B.W., and Rodriguez-Marek, A. (2019b). "Selecting factor of safety against liquefaction for design based on cost considerations." *7th International Conference on Earthquake Geotechnical Engineering,* June 17-20, Rome, Italy.

Upadhyaya, S., Maurer, B.W., Green, R.A., and Rodriguez-Marek, A. (2019c). "Surficial liquefaction manifestation severity thresholds for profiles having high fines-content, high plasticity soils." Unpublished manuscript (included in this dissertation).

Upadhyaya, S., Green, R.A., Rodriguez-Marek, A., and Maurer, B.W. (2019d). "Development of a "true" liquefaction triggering curve." Unpublished manuscript (included in this dissertation).

van Ballegooy, S., Malan, P.J., Jacka, M.E., Lacrosse, V.I.M.F., Leeves, J.R., Lyth, J.E., and Cowan, H. (2012). "Methods for characterising effects of liquefaction in terms of damage severity." *Proc. 15th World Conference on Earthquake Engineering* (15 WCEE), Lisbon, Portugal, September 24-28.

van Ballegooy, S., Cox, S.C., Thurlow, C., Rutter, H.K., Reynolds T., Harrington, G., Fraser, J., and Smith, T. (2014a). *Median water table elevation in Christchurch and surrounding area after the 4 September 2010 Darfield earthquake: Version 2*. GNS Science Report 2014/18.

van Ballegooy, S., Malan, P., Lacrosse, V., Jacka, M.E., Cubrinovski, M., Bray, J.D., O'Rourke, T.D., Crawford, S.A., and Cowan, H. (2014b). "Assessment of liquefaction-induced land damage for residential Christchurch." *Earthquake Spectra*, 30(1): 31-55.

van Ballegooy, S., Green, R.A., Lees, J., Wentz, F., and Maurer, B.W. (2015). "Assessment of various CPT based liquefaction severity index frameworks relative to the Ishihara (1985) H_1-H_2 boundary curves." *Soil Dynamics and Earthquake Engineering*, 79(Part B): 347-364.

Wotherspoon, L.M, Orense, R.P, Bradley, B.A., Cox, B.R., Wood, C. and Green, R.A. (2014). *Geotechnical characterisation of Christchurch strong motion stations*, Earthquake Commission Biennial Grant Report; 2014, project no. 12/629.

Wotherspoon, L.M., Orense, R.P., Green, R.A., Bradley, B.A., Cox, B.R. and Wood, C.M. (2015). "Assessment of liquefaction evaluation procedures and severity index frameworks at Christchurch strong motion stations." *Soil Dynamics and Earthquake Engineering* 79(Part B): 335-346.

Yalcin, A., Gokceoglu, C., and Sönmez, H. (2008). "Liquefaction severity map for Aksaray city center (Central Anatolia, Turkey)." *Natural Hazards and Earth Systems Sciences*, 8(4): 641–649.

Youd, T.L. and Garris, C.T. (1995). "Liquefaction-induced ground surface disruption." *Journal of Geotechnical Engineering*, ASCE, 121(11): 805-809.

Zhang, G., Robertson, P.K., and Brachman, R.W.I. (2002). "Estimating liquefaction-induced ground settlements from CPT for level ground." *Canadian Geotechnical Journal*, 39(5): 1168-1180.

Zhu, J., Baise, L.G., and Thompson, E.M. (2017). "An updated geospatial liquefaction model for global application." *Bulletin of the Seismological Society of America*, 107(3): 1365-1385.

Zou, K.H. (2007). “Receiver operating characteristic (ROC) literature research.” On-line bibliography available from: <http://www.spl.harvard.edu/archive/spl-pre2007/pages/ppl/zou/roc.html> accessed 10 March 2016.

Tables

Table 4.1 Summary of ROC statistics for different MSI models evaluated using the BI14 deterministic $CRR_{M7.5}$ curve, considering different severities of surficial liquefaction manifestation.

MSI model	**Any manifestation**		**Marginal**		**Moderate**		**Severe**	
	AUC	***OOP***	***AUC***	***OOP***	***AUC***	***OOP***	***AUC***	***OOP***
LPI	0.8500	3.7	0.7893	2.0	0.6852	5.6	0.6839	14.1
LPIish	0.8473	1.7	0.7868	1.1	0.6821	3.6	0.6926	9.7
LSN	0.7975	10.5	0.7417	9.1	0.6484	15.5	0.6726	24.7
LSNish	0.8007	5.4	0.7437	5.4	0.6508	7.9	0.6776	16.4

Table 4.2 Summary of ROC statistics for different MSI models evaluated using the BI14 median $CRR_{M7.5}$ curve, considering different severities of surficial liquefaction manifestation.

MSI model	**Any manifestation**		**Marginal**		**Moderate**		**Severe**	
	AUC	***OOP***	***AUC***	***OOP***	***AUC***	***OOP***	***AUC***	***OOP***
LPI	0.8496	1.5	0.7873	1.0	0.6872	3.4	0.6840	7.4
LPIish	0.8354	0.6	0.7688	0.3	0.6811	1.2	0.6880	4.6
LSN	0.8100	7.1	0.7525	7.5	0.6596	10.3	0.6809	23.2
LSNish	0.8031	3.6	0.7421	2.6	0.6607	5.3	0.6853	13.3

Figures

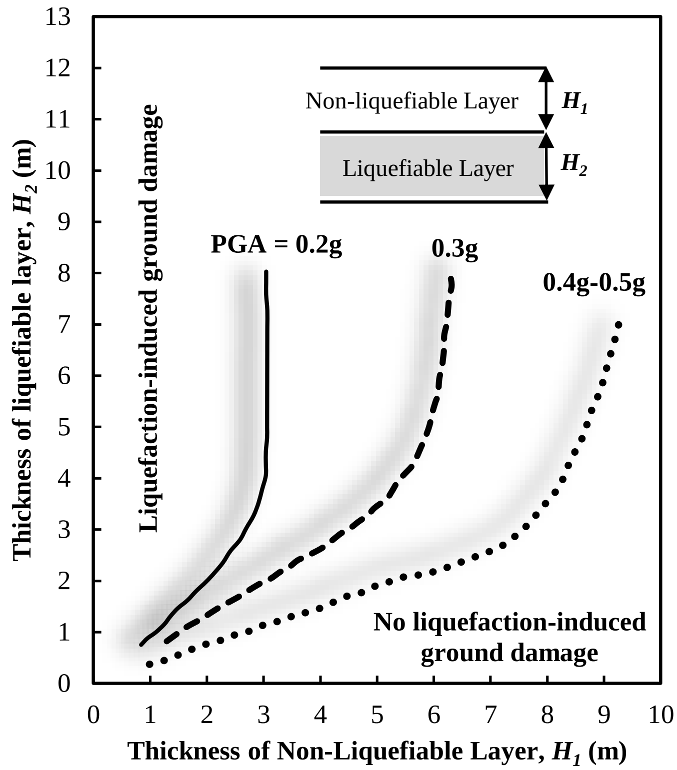

Figure 4.1 Chart showing the relationship between the thicknesses of the non-liquefiable capping layer (H_1) and the underlying liquefiable layer (H_2) for identifying liquefaction induced damage as a function of *PGA* (modified after Ishihara 1985).

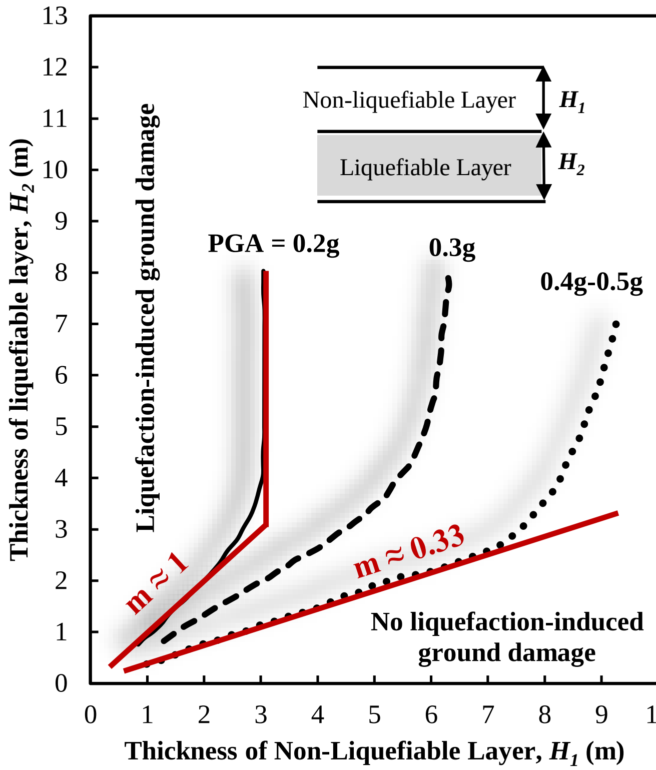

Figure 4.2 Ishihara H_1-H_2 boundary curves and approximation of the boundary curves by two straight lines (modified after Ishihara 1985).

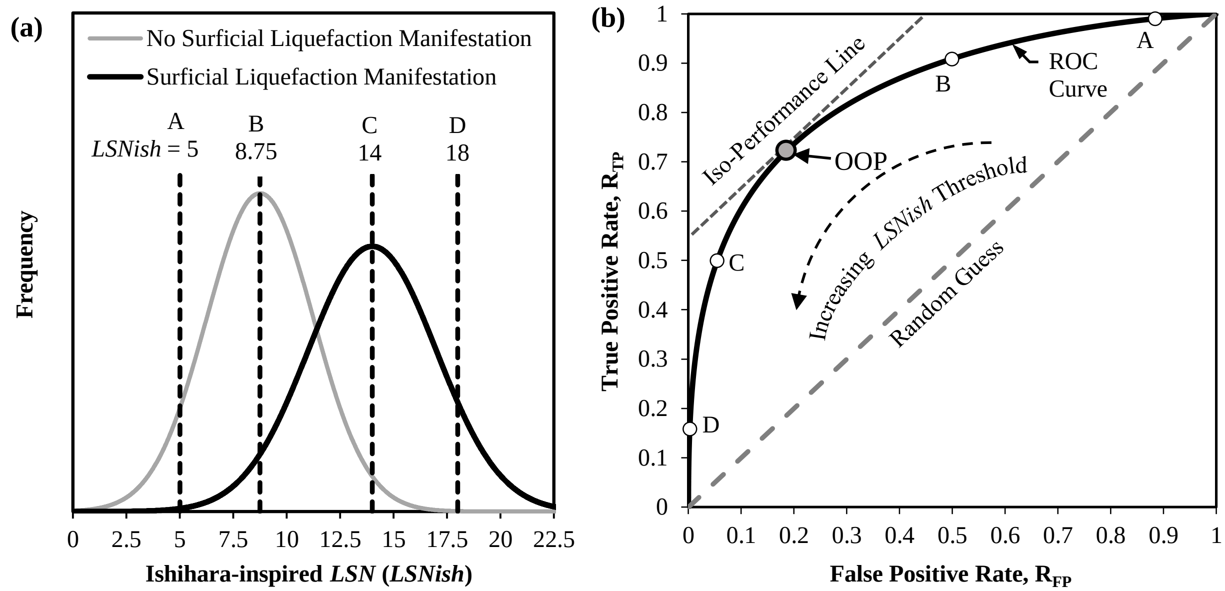

Figure 4.3 Conceptual illustration of ROC analyses: (a) frequency distributions of surficial liquefaction manifestation and no surficial liquefaction manifestation observations as a function of *LSNish*; (b) corresponding ROC curve (after Maurer et al. 2015b,c,d).

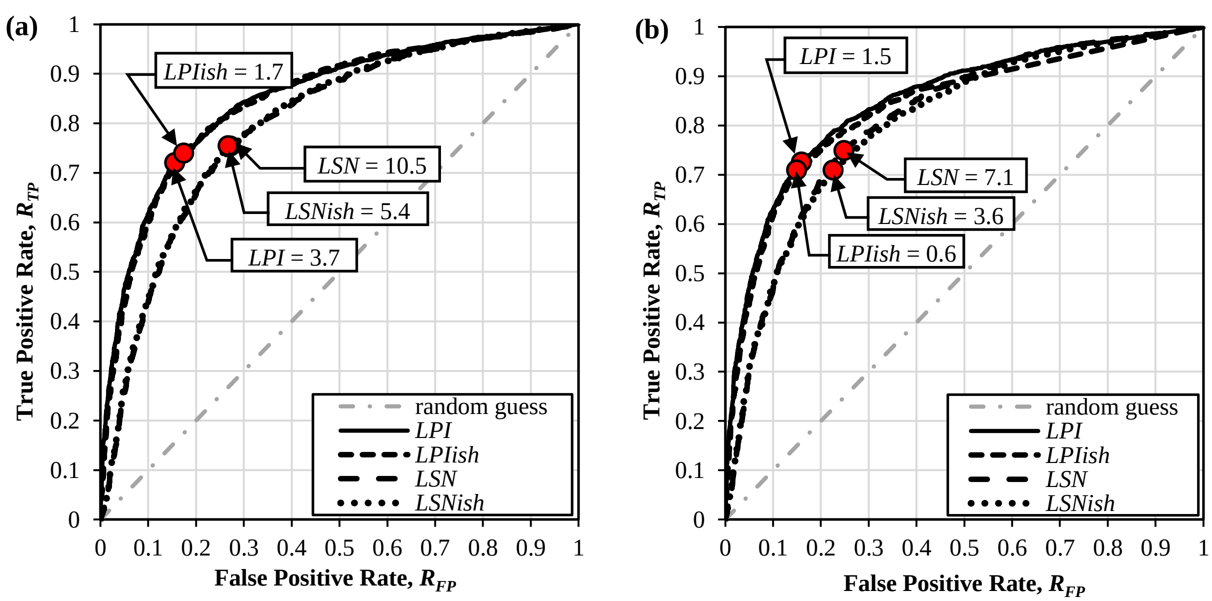

Figure 4.4 ROC curves for *LPI*, *LPIish*, *LSN*, and *LSNish* models, evaluated using: (a) BI14 deterministic $CRR_{M7.5}$; (b) BI14 median $CRR_{M7.5}$. Also shown are the optimal thresholds for each model.

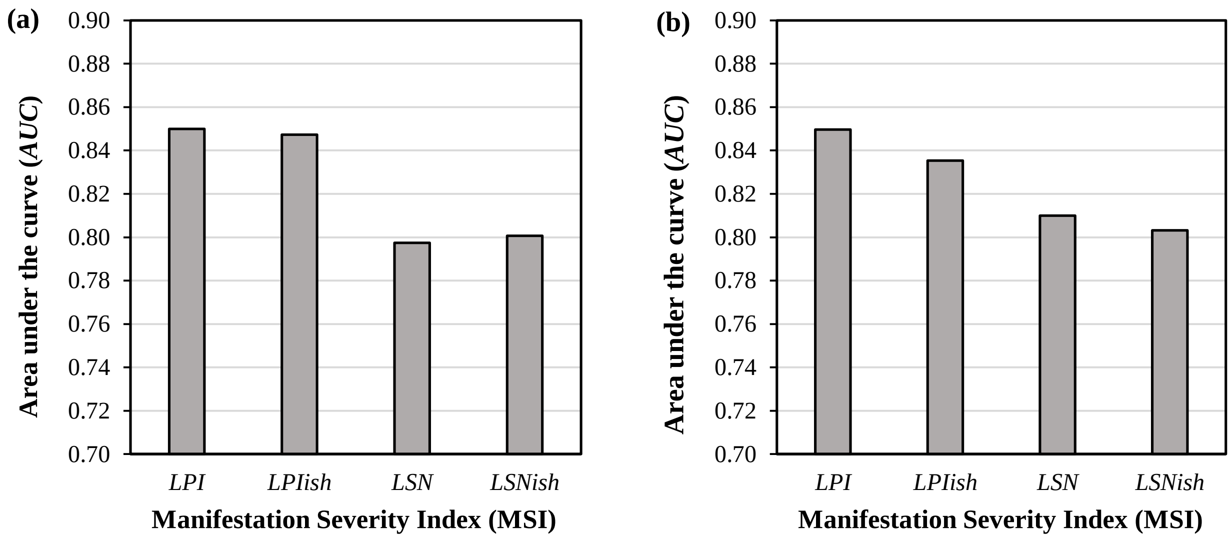

Figure 4.5 Comparison of *AUC* values for the *LPI*, *LPIish*, *LSN*, and *LSNish* models evaluated using: (a) BI14 deterministic $CRR_{M7.5}$; (b) BI14 median $CRR_{M7.5}$.

Chapter 5: Development of a "true" liquefaction triggering curve

Sneha Upadhyaya[1]; Russell A. Green[2]; Adrian Rodriguez-Marek[2]; and Brett W. Maurer[3]

[1]Graduate Student, Department of Civil and Environmental Engineering, Virginia Tech, Blacksburg, VA 24061.

[2]Professor, Department of Civil and Environmental Engineering, Virginia Tech, Blacksburg, VA 24061.

[3]Assistant Professor, Department of Civil and Environmental Engineering, University of Washington, Seattle, WA 98195.

5.1 Abstract

This paper presents an internally-consistent approach for predicting triggering and surface manifestation of liquefaction. It is shown that current models for predicting liquefaction triggering and surface manifestation may not account for the mechanics controlling each phenomenon in a consistent and sufficient manner. The manifestation models often assume that the triggering curves are "true" curves (i.e., free of factors influencing manifestation). However, as an artifact of the way triggering models are developed, they may inherently account for some of the factors influencing surface manifestations (e.g., dilative tendencies of dense soils). As a result, using the triggering curves in conjunction with the manifestation models likely results in the double-counting, omission, or general mismanagement of distinct factors that influence triggering and manifestation. Accordingly, an approach is presented to derive a "true" liquefaction triggering curve consistent with a manifestation model (e.g., Ishihara-inspired Liquefaction Severity Number, *LSNish*). Using a large database of case histories from the 2010-2016 Canterbury earthquakes (CE), deterministic and probabilistic variants of a "true" triggering curve are derived for predominantly clean to silty sand profiles. Operating in conjunction with the *LSNish* framework, the performance of the "true" triggering curve is compared to those of existing, popular triggering curves using a set of 50 global case histories.

5.2 Introduction

Soil liquefaction continues to be one of the leading causes of ground failure during earthquakes, resulting in significant damage to infrastructure around the world (e.g., the 2010-2016 Canterbury earthquakes (CE) in New Zealand, 2010 Maule earthquake in Chile, and 2011 Tohoku earthquake in Japan, etc). The strong ground shaking produced during the Canterbury earthquakes, in particular during the M_w 7.1 2010 Darfield earthquake and the M_w 6.2 2011 Christchurch earthquakes, induced widespread liquefaction causing extensive damage to infrastructure and residential buildings throughout the city of Christchurch and its surroundings (e.g., Cubrinovski and Green 2010; Cubrinovski et al. 2011; Green et al. 2014; Maurer et al. 2014; van Ballegooy et al. 2014b). Thus, there is a need to predict the occurrence and consequence of liquefaction. However, the existing models for predicting liquefaction triggering and consequent damage potential have limitations in that they may not account for the mechanics of liquefaction triggering and surface manifestation in a consistent and sufficient manner. The objective of this paper is to develop an internally-consistent framework for predicting liquefaction response such that factors influential to triggering and manifestation are handled more rationally and consistently.

The stress based "simplified" model is the most widely used approach for predicting liquefaction triggering. This model was first proposed by Whitman (1971) and Seed and Idriss (1971) and has continually evolved as additional field case histories have been compiled and laboratory results improved our understanding of the liquefaction phenomenon. However, the fundamental approach to developing the simplified models has remained the same. In this model, the normalized cyclic stress ratio (CSR^*) or seismic demand, and the normalized cyclic resistant ratio ($CRR_{M7.5}$) or soil capacity, are used to compute a factor of safety against liquefaction (FS) at a given depth:

$$FS = \frac{CRR_{M7.5}}{CSR^*} \tag{5.1}$$

where CSR^* is the cyclic stress ratio normalized to a magnitude 7.5 event and corrected to an effective overburden stress of 1 atm and level-ground conditions and $CRR_{M7.5}$ is the cyclic resistant ratio normalized to the same conditions as CSR^* and is computed using the semi-empirical relationships that are a function of in-situ test metrics, which have been normalized to overburden pressure and corrected for fines-content (e.g., Whitman 1971; Seed and Idriss 1971; Robertson and Wride 1998; Cetin et al. 2004; 2018; Moss et al. 2006; Idriss and Boulanger 2008; Kayen et al. 2013; Boulanger and Idriss 2014; Green et al. 2019a; among others). These normalized in-situ metrics include Standard Penetration Test (SPT) blow count (N_{160cs}); Cone Penetration Test (CPT) tip resistance (q_{c1Ncs}); and small strain shear-wave velocity (V_{s1}).

Although the "simplified" model predicts the occurrence of liquefaction at a specific depth, it does not predict the potential for damage to infrastructure, which has been shown to correlate with the severity of surficial liquefaction manifestations. Manifestation models have been proposed to relate liquefaction triggering to the damage potential via the prediction of occurrence/severity of surficial liquefaction manifestation, often in the form of a numerical index, referred to herein as a manifestation severity index (*MSI*). One of earliest such models is the Liquefaction Potential Index (*LPI*) proposed by Iwasaki et al. (1978), which has been widely used in liquefaction hazard assessments around the world (e.g., Sonmez 2003; Papathanassiou et al. 2005; 2008; 2015; Baise et al. 2006; Cramer et al. 2008; Hayati and Andrus 2008; Holzer et al. 2006; 2008; 2009; Yalcin et al. 2008; Chung and Rogers 2011; Dixit et al. 2012; Sana and Nath, 2016; among others). However, retrospective evaluations of *LPI* in some recent earthquakes (e.g., the 2010-2011 Canterbury earthquakes in New Zealand) have shown that it performs inconsistently (Maurer et al. 2014; 2015a,b,c). While there may be several factors leading to such inconsistency, such findings nonetheless suggest that *LPI* has inherent limitations. Some limitations of *LPI* include, but are not limited to, the following: (1) it may not account for the contractive/dilative tendency of the soil on the potential consequences of liquefaction, illustrated by the fact that the resulting consequences for loose and dense sand deposits having $FS = 0.8$, for example, would be likely very different, but would have the same *LPI* value; (2) it assumes that a soil stratum does not contribute to surface manifestations unless $FS \leq 1$, ignoring that surficial liquefaction manifestations can occur due to elevated excess pore pressures during shaking even when $FS > 1$ in a stratum; and (3) it does not account for the effects of thick non-liquefiable crusts and/or interbedded high fines-content, high plasticity soil strata on the severity of manifestations. In efforts to address some of the short-comings of *LPI*, alternative MSI models have been proposed, such as the "Ishihara inspired *LPI*" (*LPIish*) by Maurer et al. (2015a), the Liquefaction Severity Number (*LSN*) by van Ballegooy et al. (2012; 2014b) and more recently, the "Ishihara-inspired *LSN*" (*LSNish*) by Upadhyaya et al. (2019c).

LPIish improves on *LPI* in that: (1) it accounts for the influence of a thick non-liquefiable crust on the severity of surficial liquefaction manifestation using the Ishihara (1985) H_1-H_2 relationships, that relate the thickness of a liquefied layer (H_2) to the thickness of the overlying non-liquefied capping layer (H_1) required for surface manifestation; and (2) weighs more the contribution of shallower layers in predicting the severity of surficial liquefaction manifestations using a power law depth weighting function (i.e., 1/z), as opposed to the linear depth weighting function that *LPI* uses. As with *LPIish*, *LSN* also uses a power law depth weighting function, but conceptually improves on *LPI* in that: (1) it additionally accounts for the influence of contractive/dilative tendency of the soil on the severity of liquefaction surface manifestation via the ε_v-D_r-FS relationship, such that for a given *FS*, as relative density (D_r) increases, volumetric strain (ε_v) decreases (e.g., Ishihara and Yoshimine 1992); and (2) it considers the contribution of strata with *FS* up to 2 in computing the severity of surficial liquefaction manifestation. The more recently proposed *LSNish* is a merger of the Ishihara (1985) H_1-H_2 relationship and *LSN* model, in that it accounts for the effects of thick non-liquefiable crust as well as the influence of the contractive/dilative tendency of the soil on the severity of surficial liquefaction. Upadhyaya et al. (2019c) compared the predictive efficiencies of the four MSI models discussed above (e.g., *LPI*, *LPIish*, *LSN*, and *LSNish*) using the 2010-2016 CE liquefaction case-history dataset and found that the models that account for ε_v-D_r-FS relationship (i.e., *LSNish* and *LSN*) performed more poorly than the models that do not account for the ε_v-D_r-FS relationship (i.e., *LPI* and *LPIish*). As discussed in Upadhyaya et al. (2019c), this is likely due to the influence of ε_v on the severity of surficial liquefaction manifestation being "double counted" by *LSN* and *LSNish*. Relationships for estimating ε_v are expressed a function of *FS*, which inherently accounts for the dilative tendencies of dense soil minimizing surficial liquefaction manifestations, even when liquefaction is triggered.

The above findings by Upadhyaya et al. (2019c) highlight the fact that the existing methodology for developing liquefaction triggering curves is inconsistent with how these curves are used by the *MSI* models to predict the severity of surficial liquefaction manifestation. The inconsistency arises mainly because the triggering curves have been developed from field case histories where the determination of whether liquefaction triggered at a depth in the soil profile is primarily based on the presence or absence of surficial liquefaction manifestations. Inherent to this process, the observed manifestations (or lack thereof) are tied to a single critical layer within the soil profile having determined representative properties. However, in reality, the occurrence/severity of surficial liquefaction manifestation is a consequence of the overall response of the entire soil profile (e.g., Cubrinovski et al. 2019). Moreover, the critical layer must be selected such that its thickness, depth, density, fines content, plasticity, and strain-potential, considering also all properties of all overlying strata, is consistent with the surface observation. If this is not achieved, then embedded in the derivative triggering curve will be factors which relate not only to triggering, but also to the post-triggering manifestation of liquefaction (e.g., the dilative tendencies of dense soils). This may be reflected in the shape of the $CRR_{M7.5}$ curve which deviates from a straight line towards vertical at higher penetration values likely due to dilative tendencies of dense soils minimizing surface manifestations and not because liquefaction cannot be triggered in dense soils (e.g., Dobry 1989). Thus, using the triggering curves in conjunction with *MSI* models likely double-count some of the factors that influence surface manifestations.

Another issue with the methodology for developing liquefaction triggering curves lies in the interpretation of case histories used to develop the $CRR_{M7.5}$ curves, which involves considerable subjectivity. Since the $CRR_{M7.5}$ curves are almost exclusively based on post-liquefaction surface observations, biases in the curves due to alternative interpretations (or even misinterpretations) of case histories are inevitable. For example, a site that actually liquefied at a certain depth but did not have any evidence of liquefaction at the ground surface would generally be classified as "no liquefaction" due to the lack of surficial manifestations. Additionally, since the triggering models tie the observed response to a single "critical" layer having determined representative properties, varying judgements and assumptions involved in the selection of critical layers and their representative properties can influence the position of the triggering curve and associated uncertainties (Green et al. 2014; Green and Olson 2015). Furthermore, since the selection of a critical layer is done using judgement, it is unclear what factors are embedded in the triggering curve and it is unlikely that consistent judgement is used by the developers of different liquefaction triggering curves. As a result, the triggering curves cannot be used to predict the occurrence/severity of surface manifestation in a manner consistent with how they were developed.

The main objective of this study is to develop an internally-consistent framework for predicting liquefaction triggering and the resulting severity of surficial liquefaction manifestation. Utilizing a large liquefaction case-history database from the 2010-2016 Canterbury, New Zealand earthquakes (CE), this paper demonstrates a procedure to derive a "true" liquefaction triggering curve for predominantly clean sand to silty sand profiles consistent with a defined manifestation model (e.g., *LSNish*). In deriving the true triggering curve in this manner, there is no need to select a single "critical" layer as the response of the entire soil profile will be considered, which removes the subjectivity associated with selection of critical layers and their representative properties. Furthermore, both deterministic and probabilistic variants of the "true" triggering curves are developed, where the latter reflects the uncertainties in the field observations and in the parameters that control liquefaction triggering and surface manifestation.

In the following, a summary of the CE liquefaction case-history database in presented, followed by a detailed description of the approaches used in deriving the deterministic and probabilistic variants of the "true" triggering curve. Threshold *LSNish* values (in conjunction with the "true" triggering curve derived herein) are then proposed for different severities of surficial liquefaction manifestation using the CE dataset. Finally, a set of 50 world-wide case histories comprising of predominantly clean sand to silty sand profiles are used to evaluate and validate the efficacy of the proposed framework (i.e., *LSNish* in conjunction with the "true" triggering curve).

5.3 Canterbury earthquakes liquefaction case-history database

This study utilizes the CPT-based liquefaction case-history database from the 2010-2016 Canterbury earthquakes (CE) in New Zealand that was largely assembled by Maurer et al. (2014; 2015b,c,d; 2017a,b; 2019). This database contains about 10,000 high quality case histories resulting from 3834 CPT soundings from sites where the severity of liquefaction was well-documented after at least one of the following earthquakes: the M_w 7.1 September 2010 Darfield earthquake, the M_w 6.2 February 2011 Christchurch earthquake, and the M_w 5.7 February 2016 Valentine's Day earthquake. A detailed description of the quality control criteria used in compiling the case histories is provided in Maurer et al. (2014; 2015b). The severity of surficial liquefaction manifestation at each of these CPT soundings was obtained via post-earthquake ground reconnaissance and using high-resolution satellite imagery and categorized into 5 different classes following Green et al. (2014): no manifestation, marginal manifestation, moderate manifestation, severe manifestation, lateral spreading, and severe lateral spreading. All CPT soundings and imagery were extracted from the New Zealand Geotechnical Database (NZGD 2016).

The "marginal," "moderate," and "severe" categories of manifestation refer to the extent to which the ground surface is covered by liquefaction ejecta (e.g., Green et al. 2014; Maurer et al. 2014; 2015b). Since the severity of lateral spreading is a function of topography, among other factors, which is not accounted for by any of the MSI models discussed herein, case histories having lateral spreading and severe lateral spreading as the predominant form of manifestation were excluded from this study. Similarly, since the effect of non-liquefiable soil strata that have high fines content and/or plasticity on the severity of surficial liquefaction manifestation is a complex phenomenon that is not accounted for by any of the MSI models discussed herein, to include *LSNish*, only case histories having predominantly clean sand to silty sand profiles were considered. Maurer et al. (2015) found that sites in Christchurch with an average CPT soil-behavior-type index (I_c) for the upper 10 m of the soil profile (I_{c10}) less than 2.05 generally correspond to sites having predominantly clean sands to silty sands. Accordingly, only CPT soundings that have $I_{c10} < 2.05$ were considered in this study. With these considerations, 7167 CE case histories were used in the analyses presented herein.

5.3.1 Estimation of peak ground acceleration (PGA)

Peak ground accelerations (*PGAs*) are needed to estimate the seismic demand at the case history sites. In prior CE studies (e.g., Green et al. 2011; 2014; Maurer et al. 2014; 2015a,b,c,d; 2017a,b; 2019; van Ballegooy et al. 2015; among others) *PGAs* were obtained using the Bradley (2013b) procedure, which combines the unconditional *PGA* distributions as estimated by the Bradley (2013a) ground motion prediction equation, the recorded *PGAs* at the strong motion stations (SMSs), and the spatial correlation of intra-event residuals to compute the conditional *PGAs* at the sites of interest. However, some of the soil profiles on which these SMSs were installed experienced severe liquefaction, especially during the M_w 6.2 February 2011 Christchurch earthquake and the recorded *PGAs* are inferred to be associated with high-frequency dilation spikes after liquefaction was triggered. Such *PGAs* are often higher than the *PGAs* of the pre-liquefaction portion of the ground motions and likely higher than the *PGAs* that would have been experienced at the sites if liquefaction had not been triggered. Since the estimation of *PGA* is central to liquefaction triggering evaluations, such artificially high *PGAs* at the liquefied SMSs can result in over-estimated *PGAs* at the nearby case-history sites (hence, overly conservative seismic demand), which in turn can lead to over-predictions of the severity of surficial liquefaction manifestations. Wotherspoon et al. (2014, 2015) identified four such SMSs where the recorded *PGAs* were higher than the pre-liquefaction *PGAs* for the 2011 Christchurch earthquake and suggested revised *PGAs* for those stations. Upadhyaya et al. (2019a) investigated the influence of using these revised *PGAs* at the liquefied SMSs on the predicted severity of surficial liquefaction at select case histories and found that using the new *PGAs* estimated by revising the *PGAs* at the SMSs correctly predicted a significant number of case histories that were previously being over-predicted due to over-estimated *PGAs*. Accordingly, this study uses the revised pre-liquefaction *PGAs* at the liquefied SMSs to estimate *PGAs* at the CPT locations.

5.3.2 Estimation of ground-water table (GWT) depth

Accurate estimation of ground-water table (GWT) depth is critical to liquefaction triggering evaluations. The GWT depth at each case-history site immediately prior to the earthquake was estimated using the robust, event-specific regional ground water models of van Ballegooy et al. (2014a), similar to prior CE studies.

5.4 Derivation of "true" liquefaction triggering curve within the *LSNish* formulation

5.4.1 Deterministic approach

Utilizing 7167 CE liquefaction case histories, a "true" triggering curve was back-calculated in conjunction with the *LSNish* model such that its predictive efficiency was maximized. The approach used in deriving the "true" triggering curve is summarized in Figure 5.1 and discussed in detail in the subsequent sections.

5.4.1.1 Functional form of the "true" triggering curve

As discussed in the Introduction, the shape of the existing triggering curves deviates from a straight line at low to moderate penetration values towards vertical at higher penetration values likely due to the dilative tendencies of dense soils minimizing surficial liquefaction manifestations even when liquefaction is triggered. Several functional forms of triggering curves were considered in this study. However, the selected form was, in large part, based on laboratory test data from a detailed study by Ulmer (2019). Ulmer (2019) performed stress-controlled constant-volume cyclic direct simple shear tests on air-pluviated Monterey No. 0/30 sand having D_r ranging from 25% to 80% and an initial vertical effective confining stress (σ'_{vo}) equal to 100 kPa. Liquefaction triggering was defined as residual excess pore water pressure ratio (r_u) equal to 0.98. The *CSR* corresponding to number of cycles to liquefaction (N_L) = 14 (assuming that a M_w 7.5 earthquake contains 14 uniform loading cycles for bidirectional shaking; Green et al. 2019a) was obtained for each D_r group, which was then plotted against the equivalent q_{c1Ncs} values estimated from the q_{c1ncs}-D_r correlation of Idriss and Boulanger (2003), as shown in Figure 5.2. Based on trend shown in Figure 5.2 and given that *LSNish* already accounts for the influence of the contractive/dilative tendencies of the soil on the severity of surficial liquefaction manifestations via the ε_v-D_r-FS relationship, it was deemed reasonable to assume that the "true" triggering curve plots as a straight line. For comparison purposes, the Boulanger and Idriss (2014) [BI14] median $CRR_{M7.5}$ curve is also plotted in Figure 5.2.

Thus, assuming that the "true" triggering curve plots as a straight line, the functional form of the "true" $CRR_{M7.5}$ curve was defined as:

$$CRR_{M7.5} = \frac{q_{c1Ncs}}{a_1} + a_2 \tag{5.2}$$

where: a_1 and a_2 *are* the parameters that define the slope (where: slope = $1/a_1$) and the y-intercept of the "true" triggering curve, respectively, and are derived within an optimization algorithm such that the predictive efficiency of *LSNish* is maximized for the CE dataset considered in this study. The predictive efficiency of *LSNish* was assessed using Receiver Operating Characteristic (ROC) analyses, an overview of which is presented in the following section. *LSNish* can be computed as:

$$LSNish = \int_{H_1}^{20m} F(\varepsilon_v) \cdot \frac{36.929}{z} \cdot dz \tag{5.3}$$

where:

$$F(\varepsilon_v) = \begin{cases} \dfrac{\varepsilon_v}{5.5} & if\ FS\ \leq 2\ and\ H_1 \cdot m(\varepsilon_v) \leq 3 \\ 0 & otherwise \end{cases} \tag{5.4a}$$

$$m(\varepsilon_v) = \exp\left(\frac{0.7447}{\varepsilon_v}\right) - 1; \quad m(\varepsilon_v < 0.16) = 100 \tag{5.4b}$$

In Eq. 5.3, z is the depth below the ground surface in meters; ε_v is expressed in percent and is estimated as a function of FS and q_{c1Ncs} using the Zhang et al. (2002) procedure, which is based on the ε_v-D_r-FS relationship proposed by Ishihara and Yoshimine (1992); FS is computed using Eq. 5.1 wherein CSR^* is computed following the Green et al. (2019a) procedure in conjunction with the modified overburden correction factor (K_γ) formulation recently proposed by Green et al. (2019b) [Gea19b]. Inherent to this process, soils having $I_c > 2.5$ were considered non-liquefiable (e.g., Maurer et al. 2017; 2019). Note that this is a Christchurch-specific criteria proposed by Maurer et al. (2019), which is slightly different than the commonly used $I_c > 2.6$. Moreover, fines content (FC) was estimated using the Christchurch-specific I_c - FC correlation proposed by Maurer et al. (2019).

5.4.1.2 Overview of ROC analyses

Receiver Operating Characteristics (ROC) analysis has been widely used to evaluate the performance of diagnostic models, including extensive use in medical diagnostics (e.g., Zou 2007) and to a much lesser degree in geotechnical engineering (e.g., Oommen et al. 2010; Maurer et al. 2015b,c,d; 2017a,b; 2019; Green et al. 2017; Zhu et al. 2017; Upadhyaya et al. 2018;2019b). In particular, in cases where the distribution of "positives" (e.g., cases of observed surficial liquefaction manifestation) and "negatives" (e.g., cases of no observed surficial liquefaction manifestations) overlap (e.g., Figure 5.3a), ROC analyses can be used (1) to identify the optimum diagnostic threshold (e.g., *LSNish* threshold) for distinguishing between positives and negatives; and (2) to assess the relative efficacy of competing diagnostic models, independent of the thresholds used. A ROC curve is a plot of the True Positive Rate (R_{TP}) (i.e., surficial liquefaction manifestation was observed, as predicted) versus the False Positive Rate (R_{FP}) (i.e., surficial liquefaction manifestation is predicted, but was not observed) for varying threshold values (e.g., *LSNish*). A conceptual illustration of ROC analysis, including the relationship among the distributions for positives and negatives, the threshold value, and the ROC curve, is shown in Figure 5.3.

In ROC curve space, a diagnostic test that has no predictive ability (i.e., a random guess) results in a ROC curve that plots as 1:1 line through the origin. In contrast, a diagnostic test that has a perfect predictive ability (i.e., a perfect model) plots along the left vertical and upper horizontal axes, connecting at the point (0,1) and indicates the existence of a threshold value that perfectly segregates the dataset (e.g., all cases with observed surficial manifestation will have *LSNish* above the threshold and all cases with no observed surficial manifestation will have *LSNish* below the threshold). The area under the ROC curve (AUC) can be used as a metric to evaluate the predictive performance of a diagnostic model (e.g., *LSNish*), whereby higher AUC indicates better predictive capabilities (e.g., Fawcett 2005). As such, a random guess returns an AUC of 0.5, whereas a perfect model returns an AUC of 1. The optimum operating point (OOP) in a ROC analyses is defined as the threshold value (e.g., threshold *LSNish*) that minimizes the rate of misprediction [i.e., R_{FP} +

(1-R_{TP})]. Contours of the quantity [R_{FP} + (1-R_{TP})] are iso-performance lines joining points of equivalent performance in ROC space, as illustrated in Figure 5.3b.

Initially, ROC analyses were performed iteratively within an optimization function to obtain regression parameters a_1 and a_2 that maximized the *AUC* for the CE dataset. However, it was observed that the case history data itself could not constrain both parameters at the same time. Thus, the slope of the "true" triggering parameter was constrained such that it is equal to the slope of the laboratory-based $CRR_{M7.5}$ curve (i.e., a_1 = 1919.2) and the only parameter that was regressed using the case-history data was the y-intercept, which was found to be equal to 0.09 (i.e., a_2 = 0.09). Figure 5.4 contains the "true" triggering curve derived within *LSNish* formulation. Note that the "true" triggering curve derived herein optimizes the separation of cases with and without surficial liquefaction manifestations, therefore it is analogous to the median $CRR_{M7.5}$ curve. Thus, it is logical to compare the "true" triggering curve derived herein with the BI14 median $CRR_{M7.5}$ curve, also shown in Figure 5.4. To compare the predictive efficiencies of the "true" triggering curve derived herein with that of the BI14 median $CRR_{M7.5}$ curve, used in conjunction with the *LSNish* formulation for the CE dataset, the associated ROC curves are plotted in Figure 5.5. Note that the CSR^* required to compute *FS* was estimated using Gea19b procedure when the "true" triggering curve was used and BI14 procedure when the BI14 median $CRR_{M7.5}$ curve was used. It can be seen that the *AUC* associated with the "true" triggering curve derived herein is 6.8% higher than the BI14 median $CRR_{M7.5}$ curve. These findings suggest that for the dataset assessed, the "true" triggering curve is more efficacious than the BI14 median $CRR_{M7.5}$ curve in distinguishing sites with and without surficial liquefaction manifestation, when used within the *LSNish* formulation.

Threshold *MSI* values are commonly used to perform deterministic assessments of liquefaction damage potential at a site using any MSI model. However, these threshold values are specific to the MSI model and the liquefaction triggering model used (e.g., Maurer et al., 2015c). Accordingly, ROC analyses were performed on the CE dataset to compute optimum threshold *LSNish* values (in conjunction with the "true" triggering curve derived herein) considering: (1) only the occurrence of surficial manifestation (i.e., "yes" or "no"); and (2) different severities of surficial liquefaction manifestation (i.e., "minor," "moderate," or "severe"). These optimum threshold *LSNish* values are summarized in Table 5.1. It should be noted that these threshold values were determined using case histories having predominantly clean sand to silty sand profiles and are not recommended for use at sites having predominantly silty and clayey soil mixtures (i.e., soils with high FC and/or high plasticity).

5.4.2 Probabilistic approach

The deterministic approach presented in the previous section was expanded into a probabilistic framework, such that the "true" triggering curve reflects the uncertainties in field observations and in the parameters that control liquefaction triggering and surface manifestation. Probabilistic triggering relationships for SPT-, CPT-, and V_s-based in-situ testing methods have been proposed by a number of researchers (e.g., Juang et al. 2002; Cetin et al. 2002; 2004; 2018; Moss et al. 2006; Idriss and Boulanger 2010; Boulanger and Idriss 2012; 2014; among others). The limit state function, which represents the boundary between "liquefaction" and "no liquefaction" regions in the space of predictor variables, is generally expressed as (Cetin et al. 2002; 2004):

$$\mathrm{g}(X;\Theta,\varepsilon) = \hat{\mathrm{g}}(X;\Theta) + \varepsilon \tag{5.5}$$

where $\hat{\mathrm{g}}(\cdot)$ represents an approximation to the true limit function g; X denotes a vector of predictor variables that quantify the soil capacity (e.g., q_{c1Ncs}) and the seismic demand (e.g., CSR^*); Θ denotes the parameters of the limit state function; ε is an error term which is traditionally assumed to be normally distributed with a mean of zero and a standard deviation σ_ε.

By definition, $\mathrm{g}(X;\ \Theta,\ \varepsilon)$ takes zero or negative values when liquefaction is predicted to trigger and positive values when liquefaction is not predicted to trigger. Assuming that the predictive variables and the parameters of the limit state function are known, the probability of liquefaction triggering (P_L) can be expressed as (Cetin et al. 2002):

$$P_L = \Phi\left(-\frac{\hat{\mathrm{g}}(X;\Theta)}{\sigma_\varepsilon}\right) \tag{5.6}$$

where: $\Phi(\cdot)$ is the standard normal cumulative distribution function.

In past studies, the parameter set Θ has been determined using "liquefaction" and "no liquefaction" case histories. However, as discussed previously, this designation of "liquefaction" and "no liquefaction" is mostly based on the observations of surficial liquefaction manifestations, not on whether or not liquefaction was triggered at a depth in the soil profile. In this study, the parameters of the liquefaction triggering relationship are determined using a probabilistic framework that includes a surface manifestation model, therefore allowing for the development of a "true" liquefaction triggering curve. The proposed approach is detailed in the following section.

5.4.2.1 Limit state function for liquefaction triggering

As in past probabilistic studies, the following form of the limit-state function for liquefaction triggering was used:

$$g(q_{c1Ncs}, CSR^{*}; \Theta, \varepsilon) = \ln(CRR_{M7.5}) - \ln(CSR^{*}) + \varepsilon \tag{5.7}$$

As mentioned earlier, the $CRR_{M7.5}$ curve derived using the deterministic approach is analogous to a median $CRR_{M7.5}$ curve. To maintain consistency between the shape and position of the $CRR_{M7.5}$ curve from the deterministic and probabilistic approaches, the probabilistic relationship for $CRR_{M7.5}$ was expressed as:

$$CRR_{M7.5} = exp\left[ln\left(\frac{q_{c1Ncs}}{a_1} + a_2\right) + \sigma_{\varepsilon} \cdot \Phi^{-1}(P_L)\right] \tag{5.8}$$

where, a_1 = 1919.2 and a_2 = 0.09; σ_{ε} is treated as an unknown model parameter which is estimated using regression analyses; $\Phi^{-1}(\cdot)$ is the inverse of the standard cumulative normal distribution; and P_L is the probability of liquefaction triggering. Note that the implicit assumption is that the median "true" liquefaction curve is given by the deterministic curve obtained previously, and only the uncertainty around the median curve (σ_{ε}) is obtained from the probabilistic analysis. This choice is justified later in the paper when discussing the regression approach.

5.4.2.2 Probabilistic definition of surficial liquefaction manifestation

For a given soil profile, the probability of surficial liquefaction manifestation, $P(S)$, is defined as:

$$P(S) = \int P(S|LSNish) \cdot f_{LSNish}(l|\Theta; X) \cdot dl \tag{5.9}$$

where: S is a binary random variable that denotes surficial liquefaction manifestation; $P(S|LSNish)$ is the conditional probability of surficial liquefaction manifestation given an *LSNish* value and is akin to defining *LSNish* thresholds in the deterministic approach; $f_{LSNish}(l|\Theta;X)$ is the probability density function (PDF) of *LSNish* which is obtained from the probabilistic model in Eq. 5.8.

The conditional probability of surficial liquefaction manifestation, $P(S|LSNish)$, was defined using a logistic regression type model (e.g., Papathanassiou 2008; Juang et al. 2011; Chung and Rogers 2017) given by:

$$P(S|LSNish) = \frac{1}{1 + e^{-(B_0 + B_1 \cdot LSNish)}} \quad (5.10)$$

where: B_0 and B_1 are the model parameters which will be determined using regression. Thus, in addition to σ_ε, B_o and B_1 are two more parameters that will be obtained through regression.

The PDF of *LSNish* (i.e., f_{LSNish}) was obtained by mapping the uncertainties in the liquefaction triggering relationship (i.e., σ_ε) to the uncertainties in the *LSNish* model. In this process, random samples of ε were generated from a normal distribution with mean zero and standard deviation σ_ε. However, instead of using blind sampling which is computationally expensive, a reduced sampling approach was adopted. In this approach, probabilities between 0 and 1 are divided into N number of equally spaced bins and samples of ε are obtained as the inverse of the normal cumulative distribution function (CDF) at the middle of each bin. For each sample (ε_i), $LSNish_i$ is computed which results in a distribution of *LSNish* for each case history. It is assumed that *LSNish* generally follows a log normal distribution. However, since *LSNish* can take zero values, f_{LSNish} was defined using a combination of a Dirac Delta function at $LSNish = 0$ [i.e., $\delta(LSNish)$] and a lognormal distribution for $LSNish > 0$ with parameters $\mu_{ln(LSNish)}$ and $\sigma_{ln(LSNish)}$ that define the mean and standard deviation of natural logarithm of *LSNish*, respectively:

$$f_{LSNish} = P(LSNish = 0) \cdot \delta(LSNish) + w \cdot f_{LSNish|LSNish>0} \quad (5.11)$$

where:

$$w = 1 - P(LSNish = 0) \quad (5.12a)$$

$$\delta(LSNish) = \begin{cases} 0 & for\ LSNish \neq 0 \\ \infty & for\ LSNish = 0 \end{cases} \quad (5.12b)$$

and

$$\int_{-\infty}^{\infty} \delta(LSNish)dl = 1 \tag{5.12c}$$

In Eq. 5.11, $P(LSNish{=}0)$ is the probability of *LSNish* being zero and can be obtained as the ratio of number of samples of ε that result in $LSNish = 0$ to the total number of samples (N).

To determine the number of probability bins (N) needed to obtain estimates of $P(LSNish{=}0)$, $\mu_{ln(LSNish)}$, and $\sigma_{ln(LSNish)}$ that are comparable to those obtained from blind sampling, a sensitivity analyses was performed on a few randomly selected case histories from the CE dataset, wherein N was varied between 25 and 1000. It was found that $N = 100$ resulted in reasonable estimates of the above mentioned parameters.

5.4.2.3 Regression approach

The unknown parameters of the liquefaction triggering relationship (i.e., σ_ε) and the $P(S|LSNish)$ model parameters (i.e., B_o and B_1) were estimated simultaneously using maximum likelihood estimation, where the likelihood function is defined as:

$$L(\Theta) = \prod_{manifestation} P(S) \times \prod_{no\ manifestation} [1 - P(S)] \tag{5.13}$$

In performing the regression analyses, it was assumed that the input parameters are exact (i.e., the uncertainties in the input parameters were not incorporated in the regression analyses). The solution obtained by maximizing the likelihood function (e.g., Eq. 5.13) indicated that that the case history data itself was not sufficient to simultaneously constrain all the parameters of the triggering relationship (a_1, a_2, σ_ε) and the surface manifestation model parameters (B_0 and B_1). When an attempt was made to constrain all parameters simultaneously, the regression resulted in all the uncertainty assigned to the manifestation model, with the resulting uncertainty in the triggering model being negligible. One way to partition the uncertainty among the triggering and manifestation models is to constrain the $P(S|LSNish)$ curve such that it is made steeper, which results in some reasonable uncertainty in the triggering relationship. The $P(S|LSNish)$ curve was constrained such that $P(S|LSNish) \geq 0.99$ for $LSNish \geq 23$. Note that $LSNish = 23$ is the deterministic threshold for severe liquefaction manifestation and thus it is reasonable to assume that the probability of surficial liquefaction manifestation is close to 1 if this threshold is exceeded. From the maximum likelihood regression analyses, it was found that $\sigma_\varepsilon = 0.243$, $B_0 = -2.77$, and

B_1 = 0.37. The resulting "true" probabilistic liquefaction triggering relationships are presented in Eqs. 5.14 and 5.15.

$$CRR_{M7.5} = exp\left[ln\left(\frac{q_{c1Ncs}}{1919.2} + 0.09\right) + 0.243 \cdot \Phi^{-1}(P_L)\right] \tag{5.14}$$

$$P_L = \Phi\left[-\frac{ln\left(\frac{q_{c1Ncs}}{1919.2} + 0.09\right) - ln(CSR^*)}{0.243}\right] \tag{5.15}$$

The "true" triggering curves corresponding to P_L = 15%, 50%, and 85% are shown in Figure 5.6 and the regressed $P(S|LSNish)$ curve is shown in Figure 5.7. Also shown in Figure 5.7 are the observed probabilities of surficial manifestations computed by grouping the *LSNish* values into multiple equally spaced bins. For each bin, the observed probability of manifestation was computed as the ratio of cases with observed manifestation to the total number of cases in each bin. It can be seen that there is a good agreement between the regressed $P(S|LSNish)$ curve and the observed binned data for $P(S|LSNish) < 0.8$. An implication of this observation is that when $P(S|LSNish) > 0.8$, it is assumed that it is almost certain that surface manifestation occurs which is a reasonable conservative outcome. As mentioned earlier, in deriving the probabilistic triggering relationship it was assumed that the input parameters to the model are exact. As a result, the uncertainty in the triggering curve indirectly reflects the uncertainties in both the input parameters and the model uncertainty (i.e., total uncertainty). Since the existing triggering relationships have been generally presented in terms of model uncertainty alone, a direct comparison of the "true" triggering curves regressed herein and the existing probabilistic triggering curves cannot be made. However, Green et al. (2016) used the case history data of BI14 and regressed probabilistic triggering relationships for clean sands (i.e., FC ≤ 5%) in terms of total uncertainty, which are also shown in Figure 5.6. It can be seen that the uncertainty in the "true" triggering curves regressed herein is smaller than the total uncertainty computed by Green et al. (2016) for the BI14 triggering relationship. This is likely because the $P(S|LSNish)$ model (Figure 5.7) accounts for the uncertainties associated with factors influencing the surficial liquefaction manifestation, hence reducing the uncertainty in the triggering relationship.

Similar to the defining optimum *LSNish* thresholds in the deterministic approach, optimum threshold $P(S)$ values were also assessed by performing ROC analyses on the CE dataset, considering: (1) only the occurrence of surficial manifestation (i.e., "yes" or "no"); and (2) different severities of surficial liquefaction manifestation (i.e., "minor," "moderate," or "severe"). These threshold $P(S)$ values are summarized in Table 5.2.

5.5 Evaluation of 50 world-wide liquefaction case histories

The "true" triggering curve presented in this study has been developed solely based on the CE dataset, which contains case histories resulting from only three earthquakes and from a limited geological and seismological environment. To evaluate the efficacy of *LSNish* in conjunction with the "true" triggering curve for non-CE settings, 50 world-wide case histories having profiles comprising of predominantly clean sand to silty sand (i.e., I_{c10} < 2.05) were compiled from the existing literature. A summary of these 50 world-wide case histories is presented in Table S1 as a supplemental material. These 50 case histories comprise of 29 "liquefaction" and 21 "no liquefaction" cases from 6 different earthquake events from around the world.

For each of these 50 case histories, *LSNish* values were computed using both the deterministic "true" triggering model derived herein as well as the BI14 median triggering model, where soils having I_c > 2.6 were considered non-liquefiable. Using the optimum threshold values of *LSNish* for distinguishing cases with and without manifestation, evaluated using: (a) the "true" triggering model (e.g., Table 5.1); and (b) BI14 median triggering model (e.g., *LSNish* threshold of 3.6 as computed by Upadhyaya et al. 2019c), the overall accuracies (i.e., the ratio of number of accurately predicted cases to the total number of cases) were computed for each case. Note that the liquefaction manifestation severity for the world-wide case histories is only categorized as either "yes" or "no" and thus the threshold *LSNish* distinguishing "any manifestation" from "no manifestation" were used in computing the overall accuracy. It was found that the overall accuracies of *LSNish* used in conjunction with the "true" triggering model and the BI14 median triggering model were both found to be 66% (i.e., both the "true" triggering and the BI14 median triggering models used in conjunction with *LSNish* accurately predicted 33 out of 50 case histories). These findings suggest that for the world-wide dataset, the "true" triggering relationship is equally efficient as the BI14 triggering relationship in predicting the occurrence of surficial liquefaction manifestation when operating in conjunction with *LSNish*. Note that the BI14 triggering model was trained on almost all of the 50 world-wide case histories that are being used to test the "true" triggering curve. While the BI14 model did not perform well on the CE dataset on which the "true" triggering model was trained, the "true" triggering model derived herein is completely unbiased when tested on these 50 world-wide case histories.

Furthermore, following the probabilistic approach for evaluating the severity of surficial liquefaction manifestation (or, liquefaction damage potential) proposed herein, the probability of surficial liquefaction manifestation, $P(S)$, was computed in conjunction with the "true" triggering relationship for each of the 50 case histories (e.g., Eq. 5.9). Using the optimum threshold $P(S)$ that distinguishes "any manifestation" from "no manifestation" determined in the previous section (e.g., Table 5.2), overall accuracy of $P(S)$ in predicting the occurrence of surficial liquefaction manifestation was assessed for the world-wide dataset. The overall accuracy of $P(S)$ was found to be 66% which is the exact same as that obtained using the deterministic threshold *LSNish*.

5.6 Discussion and conclusion

This paper presented an internally-consistent framework for predicting liquefaction triggering and the resulting severity of surficial manifestation. Specifically, this paper presented a methodology to derive a "true" liquefaction triggering curve consistent with a defined manifestation model (i.e., *LSNish*) such that factors influential to triggering and manifestation are handled more rationally and consistently. Moreover, the methodology presented herein removes the subjectivity associated with the selection of critical layers and their representative properties as the cumulative response of the entire soil profile is tied to the observed surficial liquefaction manifestation. Utilizing 7167 CPT liquefaction case histories from the 2010-2016 Canterbury Earthquakes, deterministic and probabilistic variants of the "true" triggering curve were developed within the recently proposed *LSNish* model for predominantly clean sand to silty sand profiles. It was shown that the prediction efficiency of the *LSNish* model in conjunction with the "true" triggering curve derived herein was ~7% higher than in conjunction with the BI14 median triggering curve for the CE dataset. Additionally, by analyzing a second smaller subset comprised of 50 world-wide CPT liquefaction case histories, it was found that the overall accuracies of the "true" triggering curve and the BI14 median triggering curve were exactly the same (i.e., 66%) when operating within the *LSNish* model suggesting that the "true" triggering curve is equally efficacious if not better than the BI14 median triggering curve.

The case history data was not sufficient to constrain all the parameters of the triggering and manifestation relationships. This is largely because the CE dataset used in this study is comprised of case histories resulting from only three earthquakes in the same region. As a result, the case histories represent limited seismological and geological variability. Thus, it was necessary to use several assumptions to constrain some of the parameters of the triggering and manifestation relationships, which was largely guided by laboratory data and the authors' judgement. For example: the slope of the "true" triggering curve was constrained to be consistent with trends shown by the laboratory data since the field case history data itself was not robust enough to constrain both the shape/slope and the position of the curve. Additionally, since the "true" triggering curve was derived using the CE case histories, the results may be biased to Christchurch data. Although the resulting model derived herein was shown to be equally efficient as existing models when applied to 50 global case histories, more high quality case histories representing a more diverse range of seismological and geological settings will be needed for true validation of the framework presented in this paper.

Furthermore, the methodology for deriving a "true" triggering curve shown in this paper was demonstrated using the *LSNish* manifestation model since it accounts for the factors affecting surficial liquefaction manifestation in a more appropriate manner compared to other existing *MSI* models. However, there are uncertainties as to what factors influence surface manifestation and how exactly these factors control the manifestation mechanism. Thus, even the soundest and the most efficient of the existing *MSI* models do not account for all the factors influencing liquefaction response. For example, past studies have shown that the occurrence/severity of surficial liquefaction manifestation is influenced by the presence of non-liquefiable, high fines-content, high plasticity soils (e.g., Maurer et al. 2015b; Upadhyaya et al. 2018); however, such effects are not accounted for by any of the existing *MSI* models, to include *LSNish*. Accordingly, the "true" triggering curve was derived by only using case histories having predominantly clean sand to silty sand profiles. In the future, further research into the mechanics of liquefaction triggering as well as surficial liquefaction manifestation will be required to further improve and constrain the framework presented herein. Regardless, this paper presents an internally consistent framework for predicting liquefaction triggering and the resulting damage potential, thereby conceptually advancing the state-of-the-art in liquefaction risk assessment.

5.7 Acknowledgements

The authors greatly acknowledge the funding support through the National Science Foundation (NSF) grants CMMI-1435494, CMMI-1724575, CMMI-1751216, and CMMI-1825189, as well as Pacific Earthquake Engineering Research Center (PEER) grant 1132-NCTRBM and U.S. Geological Survey (USGS) award G18AP-00006. However, any opinions, findings, and conclusions or recommendations expressed in this paper are those of the authors and do not necessarily reflect the views of NSF, PEER, or USGS.

References

Baise, L.G., Higgins, R.B., and Brankman, C.M. (2006). "Liquefaction hazard mapping-statistical and spatial characterization of susceptible units." *Journal of Geotechnical and Geoenvironmental Engineering* 132(6): 705-715.

Boulanger, R.W. and Idriss, I.M. (2012). "Probabilistic standard penetration test-based liquefaction-triggering procedure." *Journal of Geotechnical and Geoenvironmental Engineering*, 138(10): 1185-1195.

Boulanger, R.W. and Idriss, I.M. (2014). *CPT and SPT based liquefaction triggering procedures*. Report No. UCD/CGM.-14/01, Center for Geotechnical Modelling, Department of Civil and Environmental Engineering, UC Davis, CA, USA.

Bradley, B.A. (2013a). "A New Zealand-specific pseudo-spectral acceleration ground-motion prediction equation for active shallow crustal earthquakes based on foreign models." *Bulletin of the Seismological Society of America*, 103(3): 1801-1822.

Bradley, B.A. (2013b). "Site-Specific and spatially-distributed ground motion intensity estimation in the 2010-2011 Christchurch earthquakes." *Soil Dynamics and Earthquake Engineering*, 48: 35-47.

Cetin, K. O., Der Kiureghian, A., and Seed, R. B. (2002). "Probabilistic models for the initiation of seismic soil liquefaction." *Structural safety*, *24*(1): 67-82.

Cetin, K. O., Seed, R. B., Der Kiureghian, A., Tokimatsu, K., Harder, L.F., Jr., Kayen, R. E., and Moss, R. E. S. (2004). "Standard penetration test-based probabilistic and deterministic assessment of seismic soil liquefaction potential." *Journal of Geotechnical and Geoenvironmental Engineering*, 130(12): 1314–1340.

Cetin, K.O., Seed, R.B., Kayen, R.E., Moss, R.E.S., Bilge, H.T., Ilgac, M., and Chowdhury, K. (2018). “SPT-based probabilistic and deterministic assessment of seismic soil liquefaction triggering hazard.” *Soil Dynamics and Earthquake Engineering*, 115: 698-709.

Chung, J., and Rogers, J.D. (2017). “Deterministic and probabilistic assessment of liquefaction hazards using the liquefaction potential index and liquefaction reduction number.” *Journal of Geotechnical and Geoenvironmental Engineering*, 143(10): 0401703.

Cramer, C.H., Rix, G.J., and Tucker, K. (2008). “Probabilistic liquefaction hazard maps for Memphis, Tennessee.” *Seismological Research Letters* 79(3): 416-423.

Cubrinovski, M. and Green, R.A. (eds.) (2010). “Geotechnical Reconnaissance of the 2010 Darfield (Canterbury) Earthquake”, (contributing authors in alphabetical order: J. Allen, S. Ashford, E. Bowman, B. Bradley, B. Cox, M. Cubrinovski, R. Green, T. Hutchinson, E. Kavazanjian, R. Orense, M. Pender, M. Quigley, and L. Wotherspoon), *Bulletin of the New Zealand Society for Earthquake Engineering*, 43(4): 243-320.

Cubrinovski, M., Bray, J.D., Taylor, M., Giorgini, S., Bradley, B., Wotherspoon, L., and Zupan J. (2011). “Soil liquefaction effects in the central business district during the February 2011 Christchurch earthquake.” *Seismological Research Letters*, 82(6): 893-904.

Cubrinovski, M., Rhodes, A., Ntritsos, N., and Van Ballegooy, S. (2019). “System response of liquefiable deposits.” *Soil Dynamics and Earthquake Engineering*, 124: 212-229.

Dixit, J., Dewaikar, D. M., and Jangid, R. S. (2012). “Assessment of liquefaction potential index for Mumbai City.” *Natural Hazards and Earth Systems Sciences*, 12(9): 2759–2768.

Dobry, R. (1989). “Some basic aspects of soil liquefaction during earthquakes.” *Earthquake Hazards and the Design of Constructed Facilities in the Eastern United States* (K.H. Jacob and C.J. Turkstra, eds.), Annals of the New York Academy of Sciences, Vol. 558, 172-182.

Fawcett, T. (2005). “An introduction to ROC analysis.” *Pattern recognition letters*, *27*(8): 861-874.

Green, R.A., Cubrinovski, M., Cox, B., Wood, C., Wotherspoon, L., Bradley, B., and Maurer, B.W. (2014). “Select liquefaction case histories from the 2010-2011 Canterbury earthquake sequence.” *Earthquake Spectra*, 30(1): 131-153.

Green, R.A. and Olson, S.M. (2015). “Interpretation of Liquefaction Field Case Histories for Use in Developing Liquefaction Triggering Curves,” *Proc. 6th Intern. Conf. on Earthquake Geotechnical Engineering* (6ICEGE), Christchurch, New Zealand, 2-4 November.

Green, R.A., Bommer, J.J., Rodriguez-Marek, A., and Stafford, P.J. (2016). *Unbiased cyclic resistance ratio relationships for evaluating liquefaction potential in Groningen* (J. van Elk and D. Doornhof, eds.). Nederlandse Aardolie Maatschappij B.V. (NAM), Netherlands, 61 pp.

Green, R.A., Upadhyaya, S., Wood, C.M., Maurer, B.W., Cox, B.R., Wotherspoon, L., Bradley, B.A., and Cubrinovski M. (2017). "Relative efficacy of CPT- versus Vs-based simplified liquefaction evaluation procedures," *Proc. 19th Intern. Conf. on Soil Mechanics and Geotechnical Engineering*, Seoul, Korea, 17-22 September.

Green, R.A., Bommer, J.J., Rodriguez-Marek, A., Maurer, B.W., Stafford, P., Edwards, B., Kruiver, P.P., de Lange, G., and van Elk, J. (2019). "Addressing limitations in existing 'simplified' liquefaction triggering evaluation procedures: application to induced seismicity in the Groningen gas field." *Bulletin of Earthquake Engineering*, 17: 4539-4557.

Green et al. (2019b). "Influence of effective confining stress on liquefaction triggering." Unpublished manuscript (in preparation).

Hayati, H. and Andrus, R.D. (2008). "Liquefaction potential map of Charleston, South Carolina based on the 1986 earthquake." *Journal of Geotechnical and Geoenvironmental Engineering* 134(6): 815-828.

Holzer, T.L., Bennett, M.J., Noce, T.E., Padovani, A.C., Tinsley III, J.C. (2006). "Liquefaction hazard mapping with LPI in the greater Oakland, California, area." *Earthquake Spectra*, 22(3): 693-708.

Holzer, T.L. (2008). "Probabilistic liquefaction hazard mapping." In Zeng, D., Manzari, M.T., and Hiltunen, D.R., *Geotechnical Earthquake Engineering and Soil Dynamics IV*: Sacramento, CA, ASCE Geotechnical Special Publication 181.

Holzer, T.L., Noce, T.E., and Bennett, M.J. (2009). "Scenario liquefaction hazard maps of Santa Clara Valley, Northern California." *Bulletin of the Seismological Society of America, 99(1): 367-381*.

Idriss, I.M. and Boulanger, R.W. (2008). *Soil liquefaction during earthquakes*. Monograph MNO-12, Earthquake Engineering Research Institute, Oakland, CA, 261 pp.

Idriss, I.M. and Boulanger, R.W. (2010). *SPT-based liquefaction triggering procedures*. Rep. UCD/CGM-10, 2.

Ishihara, K. (1985). “Stability of natural deposits during earthquakes.” *Proceedings of the 11th International Conference on Soil Mechanics and Foundation Engineering,* San Francisco, CA, USA, Aug. 1985, A.A. Balkema, Rotterdam, 1: 321-376.

Ishihara, K., and Yoshimine, M. (1992). “Evaluation of settlements in sand deposits following liquefaction during earthquakes.” *Soils and Foundations* 32(1): 173-88.

Iwasaki, T., Tatsuoka, F., Tokida, K., and Yasuda, S. (1978). “A practical method for assessing soil liquefaction potential based on case studies at various sites in Japan.” *Proceedings of the 2nd International Conference on Microzonation,* Nov 26-Dec 1, San Francisco, CA, USA, 885-896.

Juang, C.H., Jiang, T., and Andrus, R.D. (2002). “Assessing probability-based methods for liquefaction potential evaluation.” *Journal of Geotechnical and Geoenvironmental Engineering,* 128(7): 580-589.

Juang, C.H., Ou, C., Lu, C., and Luo, Z. (2011). “Probabilistic framework for assessing liquefaction hazard at a given site in a specified exposure time using standard penetration testing.” *Canadian Geotechnical Journal,* 47:674-687.

Kayen, R., Moss, R., Thompson, E., Seed, R., Cetin, K., Kiureghian, A., Tanaka, Y., and Tokimatsu, K. (2013). “Shear-wave velocity–based probabilistic and deterministic assessment of seismic soil liquefaction potential.” *Journal of Geotechnical and Geoenvironmental Engineering*, 139(3): 407-419.

Maurer, B.W., Green, R.A., Cubrinovski, M., and Bradley, B.A. (2014). “Evaluation of the liquefaction potential index for assessing liquefaction hazard in Christchurch, New Zealand.” *Journal of Geotechnical and Geoenvironmental Engineering,* 140(7): 04014032.

Maurer, B.W., Green, R.A., and Taylor, O.S. (2015a). “Moving towards an improved index for assessing liquefaction hazard: lessons from historical data.” *Soils and Foundations*, 55(4): 778-787.

Maurer, B.W., Green, R.A., Cubrinovski, M., and Bradley, B. (2015b). “Fines-content effects on liquefaction hazard evaluation for infrastructure during the 2010-2011 Canterbury, New Zealand earthquake sequence.” *Soil Dynamics and Earthquake Engineering*, 76: 58-68.

Maurer, B.W., Green, R.A., Cubrinovski, M., and Bradley, B. (2015c). “Assessment of CPT-based methods for liquefaction evaluation in a liquefaction potential index framework.” *Géotechnique*, 65(5): 328-336.

Maurer, B.W., Green, R.A., Cubrinovski, M., and Bradley, B. (2015d). "Calibrating the Liquefaction Severity Number (LSN) for Varying Misprediction Economies: A Case Study in Christchurch, New Zealand." *Proc. 6th International Conference on Earthquake Geotechnical Engineering*, Christchurch, New Zealand, 1-4 November 2015.

Maurer, B.W., Green, R.A., van Ballegooy, S., Bradley, B.A., and Upadhyaya, S. (2017a). "Performance comparison of probabilistic and deterministic liquefaction triggering models for hazard assessment in 23 global earthquakes." *Geo-Risk 2017: Reliability-based design and code developments* (J. Huang, G.A. Fenton, L. Zhang, and D.V. Griffiths, eds.), ASCE Geotechnical Special Publication 283, 31-42.

Maurer, B.W., Green, R.A., van Ballegooy, S., and Wotherspoon, L. (2017b). "Assessing liquefaction susceptibility using the CPT Soil Behavior Type Index," *Proc. 3rd Intern. Conf. on Performance-Based Design in Earthquake Geotechnical Engineering* (PBDIII), Vancouver, Canada, 16-19 July.

Maurer, B.W., Green, R.A., van Ballegooy, S., and Wotherspoon, L. (2019). "Development of region-specific soil behavior type index correlations for evaluating liquefaction hazard in Christchurch, New Zealand." *Soil Dynamics and Earthquake Engineering*, 117:96-105.

Moss, R.E.S, Seed, R.B., Kayen, R.E., Stewart, J.P., Der Kiureghian, A., and Cetin, K.O. (2006). "CPT-based probabilistic and deterministic assessment of in situ seismic soil liquefaction potential." *Journal of Geotechnical and Geoenvironmental Engineering*, 132(8):1032-1051.

NZGD (2016). *New Zealand Geotechnical Database*. <https://www.nzgd.org.nz/Default.aspx> Accessed 8/24/16. New Zealand Earthquake Commission (EQC).

Oommen, T., Baise, L. G., and Vogel, R. (2010). "Validation and application of empirical liquefaction models." *Journal of Geotechnical and Geoenvironmental Engineering, 136*(12): 1618-1633.

Papathanassiou, G., Pavlides, S., and Ganas, A. (2005). "The 2003 Lefkada earthquake: Field observation and preliminary microzonation map based on liquefaction potential index for the town of Lefkada." *Engineering Geology*, 82(1): 12-31.

Papathanassiou, G. (2008). "LPI-based approach for calibrating the severity of liquefaction-induced failures and for assessing the probability of liquefaction surface evidence." *Engineering Geology*, 96(1-2): 94-104.

Papathanassiou, G., Mantovani, A., Tarabusi, G., Rapti, D., and Caputo, R. (2015). "Assessment of liquefaction potential for two liquefaction prone areas considering the May 20, 2012 Emilia (Italy) earthquake." *Engineering Geology*, 189: 1-16.

Robertson, P.K. and Wride, C.E. (1998). “Evaluating cyclic liquefaction potential using cone penetration test.” *Canadian Geotechnical Journal*, 35(3): 442-459.

Sana, H. and Nath, S.K. (2016). “Liquefaction potential analysis of the Kashmire valley alluvium, NW Himalaya.” *Soil Dynamics and Earthquake Engineering*, 85: 11-18.

Seed, H.B. and Idriss, I.M. (1971). “Simplified procedure for evaluating soil liquefaction potential.” *Journal of the Soil Mechanics and Foundations Division*, 97(SM9): 1249–1273.

Sönmez, H. (2003). “Modification of the liquefaction potential index and liquefaction severity mapping for a liquefaction-prone area (Inegol, Turkey).” *Engineering Geology*, 44(7): 862–871.

Toprak, S. and Holzer, T. L. (2003). "Liquefaction potential index: Field assessment." *Journal of Geotechnical and Geoenvironmental Engineering*, 129(4): 315-322.

Ulmer, K.J. (2019). “Development of an energy-based liquefaction evaluation procedure.” Ph.D. Dissertation in preparation, Virginia Tech, Blacksburg, VA.

Upadhyaya, S., Maurer, B.W., Green, R.A., and Rodriguez-Marek, A. (2018). “Effect of non-liquefiable high fines-content, high plasticity soils on liquefaction potential index (LPI) performance.” *Geotechnical Earthquake Engineering and Soil Dynamics V: Liquefaction Triggering, Consequences, and Mitigation* (S.J. Brandenberg and M.T. Manzari, eds.), ASCE Geotechnical Special Publication 290, 191-198.

Upadhyaya, S., Green, R.A., Rodriguez-Marek, A., Maurer, B.W., Wotherspoon, L., Bradley, B.A., and Cubrinovski, M. (2019a). “Influence of corrections to recorded peak ground accelerations due to liquefaction on predicted liquefaction response during the M_w 6.2, February 2011 Christchurch earthquake.” *13th Australia New Zealand Conference on Geomechanics 2019*, April 1-3, Perth, Australia.

Upadhyaya, S., Green, R.A., Maurer, B.W., and Rodriguez-Marek, A. (2019b). “Selecting factor of safety against liquefaction for design based on cost considerations.” *7th International Conference on Earthquake Geotechnical Engineering*, June 17-20, Rome, Italy.

Upadhyaya, S., Green, R.A., Maurer, B.W., Rodriguez-Marek, A., and van Ballegooy, S. (2019c). "Ishihara-inspired Liquefaction Severity Number (*LSNish*)." Unpublished manuscript (included in this dissertation).

van Ballegooy, S., Malan, P.J., Jacka, M.E., Lacrosse, V.I.M.F., Leeves, J.R., Lyth, J.E., and Cowan, H. (2012). "Methods for characterising effects of liquefaction in terms of damage severity." *Proc. 15th World Conference on Earthquake Engineering* (15 WCEE), Lisbon, Portugal, September 24-28.

van Ballegooy, S., Cox, S.C., Thurlow, C., Rutter, H.K., Reynolds T., Harrington, G., Fraser, J., and Smith, T. (2014a). *Median water table elevation in Christchurch and surrounding area after the 4 September 2010 Darfield earthquake: Version 2*. GNS Science Report 2014/18.

van Ballegooy, S., Malan, P., Lacrosse, V., Jacka, M.E., Cubrinovski, M., Bray, J.D., O'Rourke, T.D., Crawford, S.A., and Cowan, H. (2014b). "Assessment of liquefaction-induced land damage for residential Christchurch." *Earthquake Spectra*, 30(1): 31-55.

van Ballegooy, S., Green, R.A., Lees, J., Wentz, F., and Maurer, B.W. (2015). "Assessment of various CPT based liquefaction severity index frameworks relative to the Ishihara (1985) H_1-H_2 boundary curves." *Soil Dynamics and Earthquake Engineering*, 79(Part B): 347-364.

Whitman, R.V. (1971). "Resistance of soil to liquefaction and settlement." *Soils and Foundations*, 11: 59-68.

Wotherspoon, L.M, Orense, R.P, Bradley, B.A., Cox, B.R., Wood, C. and Green, R.A. (2014). *Geotechnical characterisation of Christchurch strong motion stations*, Earthquake Commission Biennial Grant Report; 2014, project no. 12/629.

Wotherspoon, L.M., Orense, R.P., Green, R.A., Bradley, B.A., Cox, B.R. and Wood, C.M. (2015). "Assessment of liquefaction evaluation procedures and severity index frameworks at Christchurch strong motion stations." *Soil Dynamics and Earthquake Engineering* 79(Part B): 335-346.

Yalcin, A., Gokceoglu, C., and Sönmez, H. (2008). "Liquefaction severity map for Aksaray city center (Central Anatolia, Turkey)." *Natural Hazards and Earth Systems Sciences*, 8(4): 641–649.

Zhang, G., Robertson, P.K., and Brachman, R.W.I. (2002). "Estimating liquefaction-induced ground settlements from CPT for level ground." *Canadian Geotechnical Journal*, 39(5): 1168-1180.

Zhu, J., Baise, L.G., and Thompson, E.M. (2017). “An updated geospatial liquefaction model for global application.” *Bulletin of the Seismological Society of America*, 107(3): 1365-1385.

Zou, K.H. (2007). “Receiver operating characteristic (ROC) literature research.” On-line bibliography available from: <http://www.spl.harvard.edu/archive/spl-pre2007/pages/ppl/zou/roc.html> accessed 10 March 2016.

Tables

Table 5.1 Optimum *LSNish* thresholds for different severities of surficial liquefaction manifestation

Manifestation severity category	**Threshold *LSNish***
Any manifestation	4.2
Marginal manifestation	3.1
Moderate manifestation	10.1
Severe manifestation	23.0

Table 5.2 Optimum *P*(*S*) threshold for different severities of surficial liquefaction manifestation

Manifestation severity category	**Threshold *P*(*S*)**
Any manifestation	0.4
Marginal manifestation	0.3
Moderate manifestation	0.6
Severe manifestation	0.7

Figures

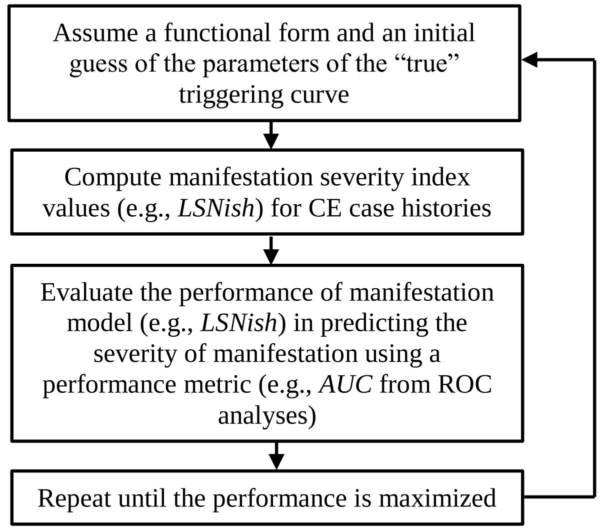

Figure 5.1 Flowchart showing the approach for deriving a "true" liquefaction triggering curve within the *LSNish* model.

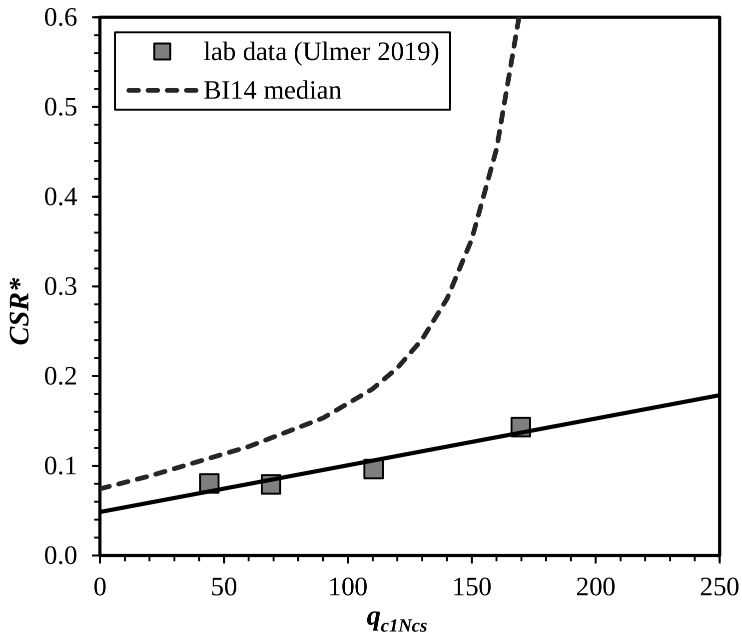

Figure 5.2 CSR^* versus q_{c1Ncs} data from laboratory tests of Ulmer (2019) along with the best fit $CRR_{M7.5}$ curve (solid black line) as well as the BI14 median $CRR_{M7.5}$ curve.

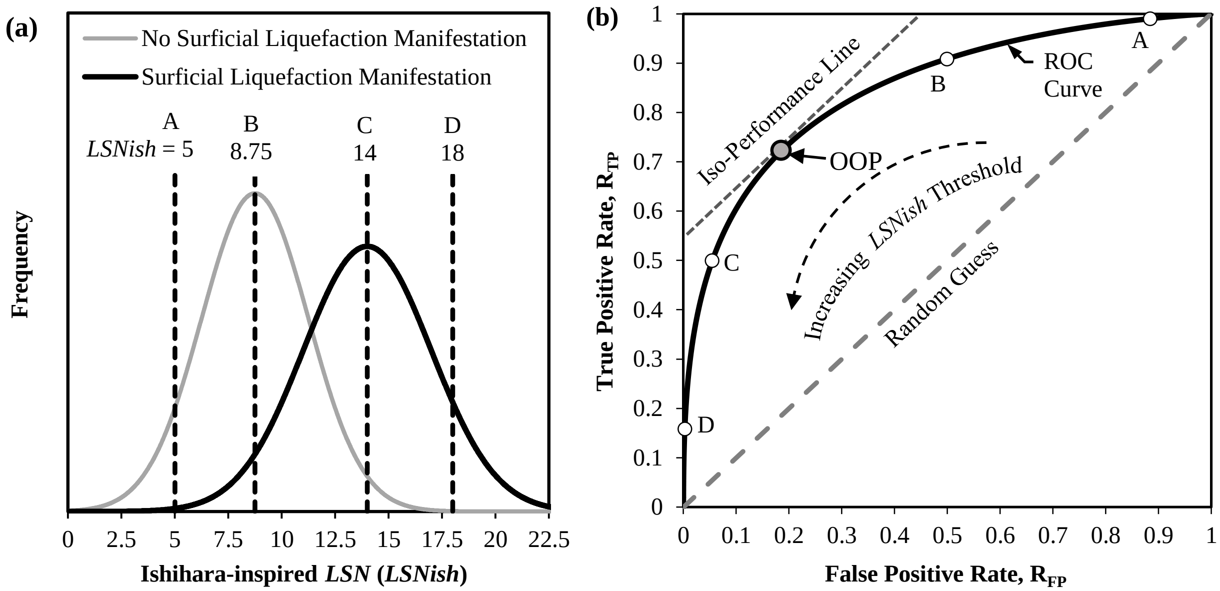

Figure 5.3 Conceptual illustration of ROC analyses: (a) frequency distributions of surficial liquefaction manifestation and no surficial liquefaction manifestation observations as a function of *LSNish*; (b) corresponding ROC curve (after Maurer et al. 2015b,c,d).

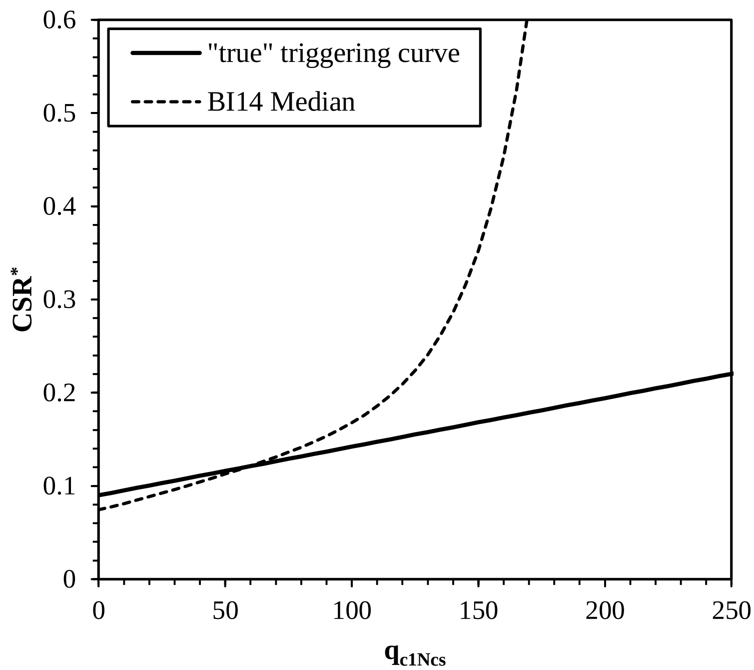

Figure 5.4 "True" triggering curve derived within the *LSNish* model plotted along with the BI14 median $CRR_{M7.5}$ curve.

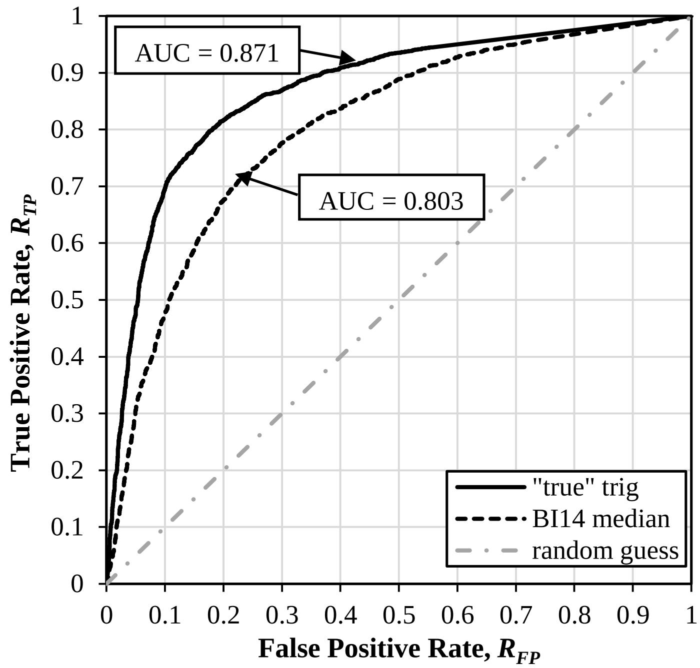

Figure 5.5 ROC curves for the “true” triggering curve and the BI14 $CRR_{M7.5}$ curve, operating in conjunction with *LSNish*.

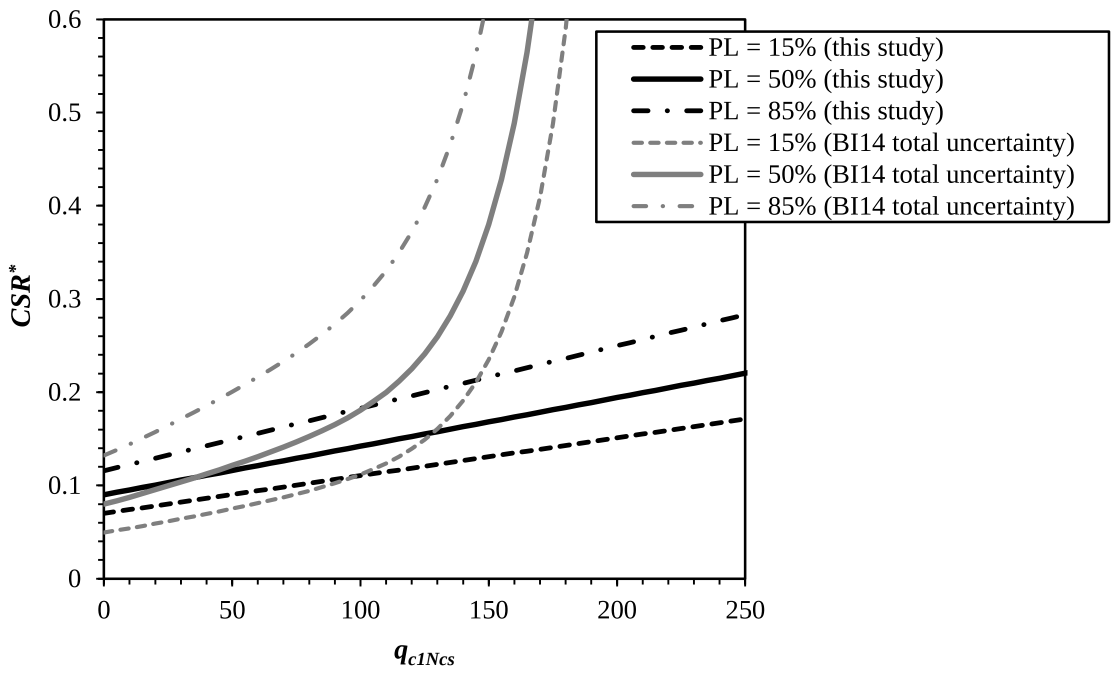

Figure 5.6 Probabilistic “true” liquefaction triggering curves derived within the *LSNish* model. Also shown are the BI14 total uncertainty $CRR_{M7.5}$ curves for clean sand (FC ≤ 5%), regressed by Green et al. (2016).

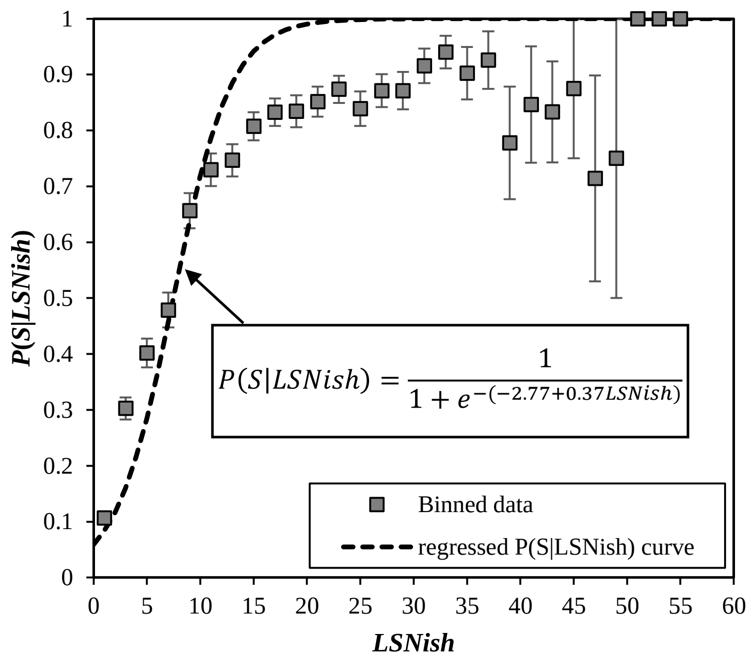

Figure 5.7 Probability of surficial liquefaction manifestation as a function of *LSNish* along with the observed binned data.

Supplementary Material

Table S1. Summary of 50 world-wide CPT liquefaction case histories.

No.	CPT ID	Earthquake Event	Country	Magnitude (M_w)	PGA (g)	Liq?	GWT (m)	Sounding depth (m)	Original references
1	Hinode Minami Elementary School	2011 Tohoku	Japan	9	0.17	No liq	1.1	20	Cox et al. (2013), Boulanger and Idriss (2014)
2	Tangshan (T13)	1976 Tangshan	China	7.6	0.58	Liq	1.1	15.94	Shibata and Teparaska (1988); Moss et al. (2009; 2011)
3	Alameda Bay Farm Island (Dike)	1989 Loma Prieta	United States	6.93	0.24	No liq	5.5	11.94	Mitchell et al. (1994)
4	Marine Lab (C4)	1989 Loma Prieta	United States	6.93	0.28	Liq	2.8	13.65	Boulanger et al. (1995; 1997)
5	MBARI 4 (CPT-1)	1989 Loma Prieta	United States	6.93	0.28	No liq	1.9	13.65	Boulanger et al. (1995; 1997)
6	General Fish (CPT-6)	1989 Loma Prieta	United States	6.93	0.28	No liq	1.7	13.69	Boulanger et al. (1995; 1997)
7	Woodward Marine (14-A)	1989 Loma Prieta	United States	6.93	0.28	Liq	1.2	6.1	Boulanger et al. (1995; 1997)
8	Port of Oakland (POO7-2)	1989 Loma Prieta	United States	6.93	0.28	Liq	3	10.95	Mitchell et al. (1994); Kayen et al. (1998)
9	Port of Oakland (POO7-3)	1989 Loma Prieta	United States	6.93	0.28	No liq	3	15.93	Mitchell et al. (1994); Kayen et al. (1998)
10	Pajaro Dunes (PD1-44)	1989 Loma Prieta	United States	6.93	0.22	Liq	3.4	9.9	Bennett & Tinsely (1995); Toprak & Holzer (2003)
11	Radovich (RAD-98)	1989 Loma Prieta	United States	6.93	0.38	No liq	3.5	14.1	Bennett & Tinsely (1995); Toprak & Holzer (2003)
12	MBARI 3 (RC-6)	1989 Loma Prieta	United States	6.93	0.28	No liq	2.6	9.57	Boulanger et al. (1995; 1997)
13	MBARI 3 (RC-7)	1989 Loma Prieta	United States	6.93	0.28	No liq	3.7	11.16	Boulanger et al. (1995; 1997)
14	SFO Bay Bridge (SFOBB-1)	1989 Loma Prieta	United States	6.93	0.28	Liq	3	14.95	Mitchell et al. (1994); Kayen et al. (1998)
15	SFO Bay Bridge (SFOBB-2)	1989 Loma Prieta	United States	6.93	0.28	Liq	3	10.8	Mitchell et al. (1994); Kayen et al. (1998)
16	Silliman (SIL-68)	1989 Loma Prieta	United States	6.93	0.38	Liq	3.5	12.8	Bennett & Tinsely (1995); Toprak & Holzer (2003)
17	Southern Pacific Bridge (SPR-48)	1989 Loma Prieta	United States	6.93	0.33	Liq	5.3	10.8	Bennett & Tinsely (1995); Toprak & Holzer (2003)

18	Marine Lab (UC-1)	1989 Loma Prieta	United States	6.93	0.28	Liq	2.4	18	Boulanger et al. (1995; 1997)
19	Sandhold Road (UC-2)	1989 Loma Prieta	United States	6.93	0.28	No liq	1.7	15	Boulanger et al. (1995; 1997)
20	Sandhold Road (UC-3)	1989 Loma Prieta	United States	6.93	0.28	No liq	1.7	15	Boulanger et al. (1995; 1997)
21	Sandhold Road (UC-6)	1989 Loma Prieta	United States	6.93	0.28	No liq	1.7	14.95	Boulanger et al. (1995; 1997)
22	Woodward Marine (UC-9)	1989 Loma Prieta	United States	6.93	0.28	Liq	1.2	16.6	Boulanger et al. (1995; 1997)
23	State Beach Kiosk (UC-14)	1989 Loma Prieta	United States	6.93	0.28	Liq	1.8	22	Boulanger et al. (1995; 1997)
24	State Beach Path (UC-16)	1989 Loma Prieta	United States	6.93	0.28	Liq	2.5	22	Boulanger et al. (1995; 1997)
25	State Beach (UC-18)	1989 Loma Prieta	United States	6.93	0.28	No liq	3.4	19.95	Boulanger et al. (1995; 1997)
26	Adapazari Site B (CPT-B1)	1999 Kocaeli	Turkey	7.51	0.4	Liq	3.3	20.54	PEER (2000a)
27	Adapazari Site D (CPT-D1)	1999 Kocaeli	Turkey	7.51	0.4	Liq	1.5	24.74	PEER (2000a)
28	Degirmendere DN-1	1999 Kocaeli	Turkey	7.51	0.4	Liq	1.7	20.16	Youd et al. (2009)
29	Hotel Spanca SH-4	1999 Kocaeli	Turkey	7.51	0.37	Liq	0.5	20.26	PEER (2000a)
30	Honjyo Central Park (HCP-1)	1995 Hyogoken-Nambu	Japan	6.9	0.7	No liq	2.5	13.82	Suzuki et al. (2003)
31	Imazu Elementary School (IES-1)	1995 Hyogoken-Nambu	Japan	6.9	0.6	Liq	1.4	16.2	Suzuki et al. (2003)
32	Kobe Art Institute (KAI-1)	1995 Hyogoken-Nambu	Japan	6.9	0.5	No liq	3	5.1	Suzuki et al. (2003)
33	Kobe Customs Maya Office A (KMO-A)	1995 Hyogoken-Nambu	Japan	6.9	0.6	Liq	1.8	24.25	Suzuki et al. (2003)
34	Kobe Customs Maya Office A (KMO-B)	1995 Hyogoken-Nambu	Japan	6.9	0.6	Liq	1.8	19.79	Suzuki et al. (2003)
35	New Wharf Construction Offices (NWC-1)	1995 Hyogoken-Nambu	Japan	6.9	0.45	Liq	2.6	12.78	Suzuki et al. (2003)

36	Sumiyoshi Elementary (SES-1)	1995 Hyogoken-Nambu	Japan	6.9	0.6	No liq	1.9	8.33	Suzuki et al. (2003)
37	Siporex Kogyo Osaka Factory (SKF-1)	1995 Hyogoken-Nambu	Japan	6.9	0.4	Liq	1.5	10.59	Suzuki et al. (2003)
38	Brady Farm (BDY004)	1987 Edgecumbe	New Zealand	6.6	0.4	No liq	1.53	11.47	Christensen (1995), Moss et al. (2003)
39	Gordon Farm (GDN001)	1987 Edgecumbe	New Zealand	6.6	0.43	Liq	0.5	7.89	Christensen (1995), Moss et al. (2003)
40	Gordon Farm (GDN002)	1987 Edgecumbe	New Zealand	6.6	0.43	No liq	0.9	6.22	Christensen (1995), Moss et al. (2003)
41	Whakatane Hospital (HSP001)	1987 Edgecumbe	New Zealand	6.6	0.26	No liq	4.4	6.29	Christensen (1995), Moss et al. (2003)
42	Keir Farm (KER001)	1987 Edgecumbe	New Zealand	6.6	0.31	Liq	2.5	16.62	Christensen (1995) Moss et al. (2003)
43	Landing Road Bridge (LRB007)	1987 Edgecumbe	New Zealand	6.6	0.27	Liq	1.2	15.44	Christensen (1995), Moss et al. (2003)
44	Morris Farm (MRS001)	1987 Edgecumbe	New Zealand	6.6	0.42	Liq	1.6	13.14	Christensen (1995), Moss et al. (2003)
45	Morris Farm (MRS003)	1987 Edgecumbe	New Zealand	6.6	0.41	No liq	2.08	13.86	Christensen (1995), Moss et al. (2003)
46	Robinson Farm (RBN001)	1987 Edgecumbe	New Zealand	6.6	0.44	Liq	0.8	12.69	Christensen (1995), Moss et al. (2003)
47	Robinson Farm (RBN002)	1987 Edgecumbe	New Zealand	6.6	0.44	No liq	0.7	11.99	Christensen (1995)
48	Robinson Farm (RBN003)	1987 Edgecumbe	New Zealand	6.6	0.44	No liq	0.9	12	Christensen (1995)
49	Robinson Farm (RBN004)	1987 Edgecumbe	New Zealand	6.6	0.44	Liq	0.61	14.52	Christensen (1995), Moss et al. (2003)
50	Sewage Pumping Station (SPS001)	1987 Edgecumbe	New Zealand	6.6	0.26	Liq	1.3	13.47	Christensen (1995), Moss et al. (2003)

Supplemental data references

Bennett, M. J., and Tinsley, J. C., III (1995). *Geotechnical data from surface and subsurface samples outside of and within liquefactionrelated ground failures caused by the October 17, 1989, Loma Prieta earthquake, Santa Cruz and Monterey Counties, California*. U.S. Geological Survey Open-File Rep. 95-663, U.S. Geological Survey.

Boulanger, R. W., Idriss, I. M., and Mejia, L. H. (1995). *Investigation and evaluation of liquefaction related ground displacements at Moss Landing during the 1989 Loma Prieta earthquake*. Report No. UCD/CGM-95/02, Center for Geotechnical Modeling, Department of Civil & Environmental Engineering, University of California, Davis, 231 pp., May.

Boulanger, R. W., Mejia, L. H., and Idriss, I. M. (1997). "Liquefaction at Moss Landing during Loma Prieta earthquake." *Journal of Geotechnical and Geoenvironmental Engineering*, 123(5): 453–67.

Boulanger, R. W. and Idriss, I. M. (2014). *CPT and SPT based liquefaction triggering procedures*. Report No. UCD/CGM-14/01, Center for Geotechnical Modeling, Department of Civil and Environmental Engineering, University of California, Davis, CA, 134 pp.

Christensen, S. A. (1995). "Liquefaction of Cohesionless Soils in the March 2, 1987 Edgecumbe Earthquake, Bay of Plenty, New Zealand, and Other Earthquakes." *Masters of Engineering Thesis*, Department of Civil Engineering, University of Canterbury, Christchurch, New Zealand.

Cox, B. R., Boulanger, R. W., Tokimatsu, K., Wood, C., Abe, A., Ashford, S., Donahue, J., Ishihara, K., Kayen, R., Katsumata, K., Kishida, T., Kokusho, T., Mason, B., Moss, R., Stewart, J., Tohyama, K., and Zekkos, D. (2013). "Liquefaction at strong motion stations and in Urayasu City during the 2011 Tohoku-Oki earthquake." *Earthquake Spectra*, 29(S1): S55-S80.

Holzer, T. L., Bennett, M. J., Ponti, D. J., and Tinsley, J. C., III (1999). "Liquefaction and soil failure during 1994 Northridge earthquake." *Journal of Geotechnical and Geoenvironmental Engineering*, 125(6): 438-452.

Kayen, R. E., Mitchell, J. K., Seed, R. B., and Nishio, S. (1998). "Soil liquefaction in the east bay during the earthquake." The Loma Prieta, California, Earthquake of October 17, 1989 –

Liquefaction. Thomas L. Holzer, editor, *U.S. Geological Survey Professional Paper 1551-B*, B61-B86.

Mitchell, J. K., Lodge, A. L., Coutinho, R. Q., Kayen, R. E., Seed, R. B., Nishio, S., and Stokoe, K. H., II (1994). *Insitu test results from four Loma Prieta earthquake liquefaction sites: SPT, CPT, DMT and shear wave velocity*. Report No. UCB/EERC-94/04. Earthquake Engineering Research Center, University of California at Berkeley.

Moss, R. E. S., Seed, R. B., Kayen, R. E., Stewart, J. P., Youd, T. L., and Tokimatsu, K. (2003). *Field case histories for CPT-based in situ liquefaction potential evaluation*. Geoengineering Research Rep. UCB/GE-2003/04.

Moss, R. E. S., Kayen, R. E., Tong, L.-Y., Liu, S.-Y., Cai, G.-J., and Wu, J. (2009). *Re-investigation of liquefaction and nonliquefaction case histories from the 1976 Tangshan earthquake*. Rep. No. 209/102, Pacific Earthquake Engineering Research (PEER) Center, Berkeley, CA.

Moss, R. E. S., Kayen, R. E., Tong, L.-Y., Liu, S.-Y., Cai, G.-J., and Wu, J. (2011). "Retesting of liquefaction and nonliquefaction case histories from the 1976 Tangshan earthquake." *Journal of Geotechnical and Geoenvironmental Engineering*, 137(4): 334-343.

PEER (2000a). *Documenting Incidents of Ground Failure Resulting from the Aug. 17, 1999, Kocaeli, Turkey Earthquake*. http://peer.berkeley.edu/publications/turkey/adapazari/.

Shibata, T., and Teparaska, W. (1988). "Evaluation of Liquefaction Potential of Soils Using Cone Penetration Testing." *Soils and Foundations*, 28(2): 49-60.

Suzuki, Y., Tokimatsu, K., Moss, R. E. S., Seed, R. B., and Kayen, R. E. (2003). *CPT-based liquefaction case histories from the 1995 Hyogoken-Nambu (Kobe) earthquake, Japan*. Geotechnical Engineering Research Report No. UCB/GE-2003/03.

Toprak, S., and Holzer, T. L. (2003). "Liquefaction potential index: Field assessment." *Journal of Geotechnical and Geoenvironmental Engineering*, 129(4): 315-322.

Youd, T. L., DeDen, D. W., Bray, J. D., Sancio, R., Cetin, K. O., and Gerber, T. M. (2009). "Zero displacement lateral spreads, 1999 Kocaeli, Turkey, earthquake." *Journal of Geotechnical and Geoenvironmental Engineering*, 135(1): 46-61.

Chapter 6: Summary and Conclusions

6.1 Summary of Contributions

The overarching goal of this dissertation was to develop improved methodologies for predicting liquefaction triggering and the consequent damage potential such that the impacts of liquefaction on natural and built environment can be minimized. This was achieved by addressing some of the shortcomings of the existing methodologies. Specifically, this dissertation focused on developing a framework that accounts for the mechanisms of liquefaction triggering and surface manifestation in a consistent and adequate manner. Towards this end, this dissertation made the following major contributions:

1. Development of a framework that relates optimal factor of safety (*FS*) against liquefaction triggering for decision making to the cost of mispredicting liquefaction triggering. The framework developed herein can be used to select project-specific optimal *FS* thresholds based on the costs of liquefaction risk-mitigation schemes relative to the costs associated with the consequences of liquefaction. Additionally, the framework could be similarly used to select optimal probability of liquefaction triggering (*PL*) thresholds for decision making based on the relative costs of misprediction.

2. Rigorous investigation of the predictive performance of three different manifestation severity index (*MSI*) models (e.g., *LPI*, *LPIish*, and *LSN*) as a function of the CPT soil behavior type index averaged over the upper 10 m of the profile (I_{c10}) using case histories from the 2010-2016 Canterbury earthquakes, wherein I_{c10} was used to infer the extent to which a profile contains high fines-content, high plasticity soil strata. It was shown that the relationship between computed *MSI* and the severity of surficial liquefaction manifestation is I_{c10}-dependent such that the severity of manifestation decreases with increasing I_{c10}. In this regard, I_{c10}-specific thresholds may be employed to more-accurately estimate the liquefaction damage potential at sites having high fines-content, high plasticity soils. Furthermore, probabilistic models were proposed for evaluating the severity of manifestations as a function of *MSI* and I_{c10}.

3. Development of Ishihara-inspired *LSN* (*LSNish*) - a new *MSI* that more fully accounts for the effects of non-liquefiable crust thickness and the effects of contractive/dilative

tendencies of the soil on the occurrence and severity of surficial liquefaction manifestation. *LSNish* was derived as a conceptual and mathematical merger of the *LSN* formulation and Ishihara's H_1-H_2 relationships.

4. Development of an improved and internally-consistent approach for predicting triggering and surface manifestation of liquefaction. It was shown that current models for predicting liquefaction response may not account for the mechanisms of liquefaction triggering and surface manifestation in a consistent and sufficient manner. Specifically, the manifestation models often assume that the triggering curves are "true" curves (i.e., free of factors influencing manifestation). However, as an artifact of the way triggering curves are being developed, they may inherently account for some of the factors influencing surface manifestations (e.g., dilative tendencies of dense soils). As a result, using the triggering curves in conjunction with the manifestation models likely results in the double-counting, omission, or general mismanagement of distinct factors that influence triggering and manifestation. Accordingly, an approach was presented to derive a "true" liquefaction triggering curve that is consistent with a defined manifestation model (e.g., *LSNish*). Both deterministic and probabilistic variants of the "true" triggering curves were developed, with the latter accounting for uncertainties in the field observations and in the parameters that control liquefaction triggering and surface manifestations.

6.2 Key Findings

The contributions listed above are the outcomes of the study presented in Chapters 2 through 5 of this dissertation. The following provides a summary of each of the chapters and the main findings:

Chapter 2 demonstrated how project-specific costs of mispredicting liquefaction triggering can be utilized in selecting an appropriate *FS* threshold for decision making. Specifically, relationships between optimal *FS* threshold and ratio of false-positive prediction costs to false-negative prediction costs (i.e., cost ratio, *CR*) were derived by performing receiver operating characteristic (ROC) analyses on different existing liquefaction triggering models and their associated case-history databases. The optimal *FS*-*CR* relationships were found to be specific to the triggering model and the database being used. Additionally, it was shown that these relationships were not very smooth likely due to limited number of case histories as well as the distribution of *FS* in the corresponding databases. Consequently, a generic optimal *FS*-*CR* curve was developed by combining the *FS* data from all the models. However, it was shown that, even the generic curve was not completely smooth, suggesting that additional case histories will be ultimately needed to derive a more refined relationship. Alternative to using *FS* to quantify liquefaction triggering potential, probabilistic variants of the triggering evaluation models were used to develop optimal *PL-CR* curves.

In Chapter 3, 9631 liquefaction case histories from the 2010-2016 Canterbury, New Zealand, earthquakes were utilized to investigate the predictive performances of three different *MSI* models (i.e., *LPI*, *LPIish*, and *LSN*), as a function of the soil behavior type index (I_c) averaged over the upper 10 m of a soil profile (I_{c10}), wherein I_{c10} is used to infer the extent to which a profile contains high fines-content, high plasticity soils. It was shown that, for each *MSI* model: (1) the relationship between computed *MSI* and the severity of surficial liquefaction manifestation is I_{c10}-dependent, such that at any given *MSI* value, the severity of manifestation decreases as I_{c10} increases; and (2) the predictive efficiency of the *MSI* model (i.e., the ability to segregate cases based on observed manifestation severity using *MSI* thresholds) decreases as I_{c10} increases. These findings suggest that I_{c10}-specific severity thresholds may be used to more-accurately estimate the severity of surficial liquefaction manifestations. However, even when I_{c10}-specific thresholds are employed, the *MSI* models are unlikely to efficiently predict the severity of manifestations. Additionally, probabilistic models were proposed for evaluating the severity of surficial liquefaction manifestation as a function of *MSI* and I_{c10}. Finally, the approaches presented herein are indirect ways to correct the predictions made by existing *MSI* models, given that they perform poorly at sites with high I_{c10}. An improved *MSI* model is ultimately needed such that the effects of high fines-content high plasticity soils are incorporated within the model itself.

In Chapter 4, a new *MSI* model was developed such that it accounts for the influences of non-liquefiable crust/capping layer thickness as well as post-triggering volumetric strain potential in predicting the occurrence and severity of surficial liquefaction manifestations. This model was derived as a conceptual and mathematical merger of Ishihara's H_1-H_2 boundary curves and the *LSN* formulation, hence termed *LSNish*. It should however be noted that *LSNish* still does not account for the effects of interbedded high fines-content high plasticity on the severity of surficial liquefaction manifestation, which is a complex phenomenon and will need additional research in the future. Consequently, *LSNish* was evaluated using 7167 liquefaction case histories from the

Canterbury, New Zealand, earthquakes, comprised of predominantly clean to silty sand profiles and its predictive efficiency was compared to those of *LPI*, *LPIish*, and *LSN*. It was found that despite more fully accounting for factors that influence surficial liquefaction manifestations, *LSNish* did not demonstrate improved performance over existing models. This could be due to *LSNish* double counting the dilative tendency of dense soil which inhibits surficial manifestation, since the shape of the liquefaction triggering curve inherently accounts for such effects. This same issue is a shortcoming of *LSN*. A proper accounting and clear separation of distinct factors influencing triggering and manifestation could improve the performance of *LSNish*, as further investigated in the following chapter.

Chapter 5 presented an internally-consistent approach to developing models that predict triggering and surface manifestation of liquefaction. Specifically, this chapter demonstrated a methodology to derive a "true" liquefaction triggering curve consistent with a defined manifestation model (i.e., *LSNish*) such that factors influential to triggering and manifestation are handled more rationally and consistently. This methodology avoids the need to select a single "critical" layer because the cumulative response of the entire soil profile is tied to the observed surficial manifestation (or lack thereof). Utilizing 7167 liquefaction case histories from the 2010-2016 Canterbury Earthquakes, comprised of predominantly clean to silty sand profiles, deterministic and probabilistic variants of the "true" triggering curve were developed within the *LSNish* formulation. It was shown that *LSNish* performed significantly better when used in conjunction with the "true" triggering curve derived herein than with an existing triggering curve for the compiled Canterbury case histories. Additionally, operating within the *LSNish* framework, the "true" triggering curve was shown to be equally efficient as the existing triggering curve when applied to 50 global case histories.

6.3 Engineering Significance

The study presented herein advances the state-of-the-art in liquefaction risk assessments through the development of improved methodologies for predicting the occurrence and damage potential of liquefaction. The findings from this study will lead to a better understanding of the mechanisms of liquefaction triggering and related phenomenon, thereby adding to the body of knowledge in liquefaction research and practice. Moreover, the methodologies adopted in this study are more objective and standardized, and easily implementable in engineering practice.

- A simple, yet rational approach was presented by which the project-specific consequences, or costs of mispredicting liquefaction triggering can be used to select an appropriate *FS* threshold for decision making.
- An approach for correcting the predictions made by the existing *MSI* models in profiles having high fines-content, high plasticity soil strata was presented, given that the *MSI* models perform poorly in such conditions.
- A new *MSI* model was developed that more fully accounts for factors influencing surface manifestation.
- Most importantly, a framework was proposed for developing liquefaction triggering models consistent with a defined manifestation model such that factors influential to triggering and manifestation are handled more rationally and consistently. While significant advances have been made in terms of predicting liquefaction triggering and related phenomenon, the fundamental approach to developing triggering models has remained the same since it was first proposed in 1971. This approach has historically been, and presently is, less than completely rational. As such, the framework proposed herein represents the most significant conceptual advance in ~50 years.

6.4 Recommendations for Future Research

While this dissertation represents significant conceptual advance in liquefaction risk assessments, additional work will be needed to further improve and validate the methodologies/framework presented herein. One of the most significant contributions of this dissertation is the development of an internally-consistent framework for predicting liquefaction triggering and the severity of surficial liquefaction manifestations. However, there are several components of the framework that could be improved through further research into the mechanics of liquefaction triggering and surficial manifestation. In particular, the following issues need to be addressed by future research:

- The approach to deriving a “true” liquefaction triggering curve presented herein was demonstrated using the *LSNish* formulation, since it accounts for the factors influencing manifestation in a more-appropriate manner compared to other existing manifestation models. However, this does not imply that *LSNish* is a perfect model. Uncertainties remain as to what factors influence surface manifestation and how exactly these factors control the mechanism of manifestation. Ultimately, the manifestation model could be improved to better capture the many influential factors that are currently not considered (or are inadequately considered). These include the properties of both liquefied and non-liquefied strata (e.g., depth, thickness, density, fines-content, plasticity, permeability, post-triggering strain potential) as well as the stratification/sequencing and cross-interactions between these strata within a soil profile.

- In deriving the “true” triggering curve, it was shown that the liquefaction case history data was not sufficient to constrain both the shape and the position of the curve. Thus, several assumptions were made to constrain the parameters of the triggering curve. For example, the shape/slope of the triggering curve was constrained to be consistent with trends shown by laboratory data. However, more research will be needed to validate such assumptions as well as better constrain the parameters of the triggering curve.
- In addition, the probabilistic framework for evaluating the severity of surficial liquefaction manifestation presented in Chapter 5 could be expanded to evaluate the probability of other forms of damage/consequences of liquefaction (e.g., settlement, collapse of structures).

Appendix A: Selecting factor of safety against liquefaction for design based on cost considerations

Sneha Upadhyaya[1]; Russell A. Green[2]; Brett W. Maurer[3]; and Adrian Rodriguez-Marek[2]

[1]Graduate Student, Department of Civil and Environmental Engineering, Virginia Tech, USA.
[2]Professor, Department of Civil and Environmental Engineering, Virginia Tech, USA.
[3]Assistant Professor, Department of Civil and Environmental Engineering, University of Washington, USA.

A.1 Abstract

The stress-based simplified procedure is the most widely used approach for evaluating liquefaction triggering-potential of sandy soils. In deterministic liquefaction evaluations, "rules of thumb" are typically used to select the minimum acceptable factor of safety (FS) against liquefaction triggering, sometimes guided by the strain potential of the soil once liquefied. This approach does not fully consider the value of the infrastructure that will potentially be impacted by the liquefaction response of the soil. Accordingly, in lieu of selecting FS based solely on precedent, Receiver Operator Characteristic (ROC) analyses are used herein to analyze the Standard Penetration Test (SPT) liquefaction case-history database of Boulanger & Idriss (2014) to relate FS to the relative consequences of misprediction. These consequences can be expressed as a ratio of the cost of a false-positive prediction to the cost of a false-negative prediction, such that decreasing cost-ratios indicate greater consequences of liquefaction, all else being equal. It is shown that FS = 1 determined using the Boulanger & Idriss (2014) procedure inherently corresponds to a cost ratio of ~0.1 for loose soils and ~0.7 for denser soils. Moreover, the relationship between FS and cost ratio provides a simple and rational approach by which the project-specific consequences of misprediction can be used to select an appropriate FS for decision making.

A.2 Introduction

The most commonly used approach for liquefaction-triggering evaluations is the stress-based simplified procedure originally developed by Whitman (1971) and Seed & Idriss (1971). Although probabilistic variants of this procedure have been developed, deterministic evaluations still represent the standard of practice. In a deterministic liquefaction evaluation procedure, the normalized cyclic stress ratio (CSR^*), or seismic demand, and the normalized cyclic resistance ratio ($CRR_{M7.5}$), or soil capacity, are used to compute a factor of safety (FS) against liquefaction:

$$\mathrm{FS} = \frac{\mathrm{CRR}_{\mathrm{M7.5}}}{\mathrm{CSR}^*} \tag{A.1}$$

where CSR^* is the cyclic stress ratio normalized to a M7.5 event and corrected to an effective overburden stress of 1 atm and level-ground conditions. $CRR_{M7.5}$ is the cyclic resistance ratio normalized to the same conditions as CSR^* and is computed using semi-empirical relationships that are a function of in-situ test metrics, which have been normalized to overburden pressure and corrected for fines-content (e.g., Whitman 1971, Seed & Idriss 1971, Robertson & Wride 1998, Cetin et al. 2004, Moss et al. 2006, Idriss & Boulanger 2008, Kayen et al. 2013, Boulanger & Idriss 2014, among others). These normalized in-situ metrics include Standard Penetration Test (SPT) blow count (N_{160cs}); Cone Penetration Test (CPT) tip resistance (q_{c1Ncs}); and shear-wave velocity (V_{s1}).

Liquefaction is predicted to trigger when $FS \leq 1$ (i.e., when the demand equals or exceeds the capacity). In current practice, “rules of thumb” are often used to select an appropriate FS for design. While such rules-of-thumb should, in theory, account for the consequences, or costs, of misprediction, they have generally been based largely on heuristic techniques and intuition. Due to the lack of a standardized approach to selecting FS, various guidelines have been proposed, often without any consideration of misprediction consequences. These include the costs of false-negative predictions (i.e., liquefaction is observed, but is not predicted), which are the costs of liquefaction-induced damage; and the costs of false-positive predictions (i.e., liquefaction is predicted, but not is not observed), which could be those associated with ground improvement. Clearly, these costs can vary among different engineering projects. For example, the costs associated with mispredicting liquefaction beneath a one-story residential building will be likely very different than those from a similar misprediction beneath a large earthen dam.

Accordingly, the focus of the study presented herein is to investigate the relationship between the costs of misprediction and appropriate FS values using a standardized, quantitative approach. Towards this end, Receiver Operating Characteristic (ROC) analyses are used to analyze the SPT case-history database compiled by Boulanger & Idriss (2014) [BI14] to relate the FS computed using their SPT-based liquefaction triggering procedure to the ratio of false-positive costs to false-negative costs. This ratio is henceforth referred to as the cost ratio (CR). The resulting relationships between CR and FS provide insights into previously proposed FS guidelines and can be used to develop optimal, project-specific FS values for decision making.

A.3 Data and Methodology

This study utilizes the SPT-based case-history database compiled by BI14, which is comprised of 136 "liquefaction" cases (including 3 "marginal" cases) and 116 "no liquefaction" cases. Figure A.1 shows the BI14 deterministic $CRR_{M7.5}$ curve along with the associated case history data. Histograms of the FS of the case histories are shown in Figure A.2, where the case histories are divided into three groups: $N_{1,60cs} \leq 15$ blows/30 cm, 15 blows/30 cm < $N_{1,60cs}$ < 30 blows/30 cm, and $N_{1,60cs} \geq 30$ blows/30 cm. The reason for this grouping will become apparent subsequently.

To investigate the relationship between FS and the costs of mispredicting liquefaction triggering, ROC analyses were performed on the FS distributions shown in Figure A.2. A brief overview of ROC analysis is presented in the following section.

A.3.1 Overview of ROC analyses

Receiver Operating Characteristics (ROC) analyses have been widely adopted to evaluate the performance of diagnostic models, including extensive use in medical diagnostics (e.g., Zou 2007) and to a much lesser degree in geotechnical engineering (e.g., Oommen et al. 2010, Maurer et al. 2015a,b,c, 2017a,b,c, Green et al. 2015, 2017, Zhu et al. 2017, Upadhyaya et al. 2018). In particular in cases where the distribution of "positives" (e.g., liquefaction cases) and "negatives" (e.g., no liquefaction cases) overlap (e.g., Fig. A.2a,b), ROC analyses can be used (1) to identify the optimum diagnostic threshold; and (2) to assess the relative efficacy of competing diagnostic models, independent of the thresholds used. A ROC curve is a plot of the True Positive Rate (R_{TP}) (i.e., liquefaction is predicted and was observed) versus the False Positive Rate (R_{FP}) (i.e., liquefaction is predicted, but was not observed) for varying threshold values (e.g., FS). A conceptual illustration of ROC analysis, including the relationship among the distributions for positives and negatives, the threshold value, and the ROC curve, is shown in Figure A.3.

In ROC curve space, a diagnostic test that has no predictive ability (i.e., a random guess) will result in a ROC curve that plots as a 1:1 line through the origin. In contrast, a diagnostic test that has perfect predictive ability will result in a ROC curve that plots along the left vertical and upper horizontal axes, connecting at the point (0,1). This latter case indicates the existence of a threshold value that perfectly segregates the dataset (e.g., all cases with liquefaction have FS ≤ 1 and all cases without liquefaction have FS > 1). The area under the ROC curve (AUC) can be used as a metric to evaluate the predictive performance of a diagnostic model, whereby higher AUC indicates better predictive capabilities (Fawcett 2005). As such, a random guess returns an AUC of 0.5 whereas a perfect model returns an AUC of 1.

The optimum operating point (OOP) in a ROC analysis is defined as the threshold value (e.g., FS) that minimizes the misprediction cost, where cost is computed as:

$$\text{cost} = C_{FP} \times R_{FP} + C_{FN} \times R_{FN} \tag{A.2}$$

where C_{FP} and R_{FP} are the cost and rate of false-positive predictions, respectively, and C_{FN} and R_{FN} are the cost and rate of false-negative predictions, respectively. Normalizing Eq. (A.2) with respect to C_{FN}, and equating R_{FN} to 1-R_{TP}, cost may alternatively be expressed as:

$$\text{cost}_n = \frac{\text{cost}}{C_{FN}} = CR \times R_{FP} + (1 - R_{TP}) \tag{A.3}$$

where CR is the cost ratio defined by CR = C_{FP}/C_{FN} (i.e., the ratio of the cost of a false-positive prediction to the cost of a false-negative prediction).

As may be surmised, Eq. (A.3) plots in ROC space as a straight line with slope of CR and can be thought of as a contour of equal performance (i.e., an iso-performance line). Thus, each CR corresponds to a different iso-performance line. One such line, with CR =1 (i.e., false positives costs are equal to false-negative costs) is shown in Figure A.3b. The point where the iso-performance line is tangent to the ROC curve corresponds to the OOP (e.g., the "optimal" FS corresponding to a given CR). Thus, by varying the CR values, a relationship between optimal FS and CR can be developed.

A.4 Results and Discussion

ROC analyses were performed on the case history distributions shown in Figures A.2a and A.2b (note that a ROC analysis could not be performed on the distribution shown in Figure A.2c because there are not any liquefaction case histories where $N_{1,60cs} \geq 30$ blows/30 cm). The resulting ROC curves are shown in Figure A.4a. Using Eq. (A.3) in conjunction with these curves, relationships between CR and optimal FS were developed and are shown in Figure A.4b. Moreover, the optimal FS for a range of CR are listed in Table A.1.

As may be observed from Figure A.4b, the optimal FS is inversely proportional to the CR (i.e., the lower the CR, the higher the degree of conservatism required). Additionally, it can be observed that the BI14 deterministic $CRR_{M7.5}$ curve (i.e., FS = 1) shown in Figure A.1 has an associated CR of ~0.1 for $N_{1,60cs} \leq 15$ blows/30 cm and ~0.71 for 15 blows/30 cm < $N_{1,60cs}$ < 30 blows/30 cm. This implies a more conservative positioning of the $CRR_{M7.5}$ curve for looser soils than for denser soils. Whether this was intentional or not, this can be justified because of the higher strain potential of loose soils versus dense soils once liquefaction is triggered. In a similar vein, Martin & Lew (1999) propose FS guidelines for California considering different damage-potential modes of liquefaction (i.e., "settlement," "surface manifestation," and "lateral spreading") where larger minimum required FS values are recommended for soils having $N_{1,60cs} \leq 15$ blows/30 cm versus soils having $N_{1,60cs} \geq 30$ blows/30 cm (Table A.2).

As an example, if we evaluate the recommended minimum required FS for post-liquefaction consolidation settlement listed in Table A.2 using Figure A.4b, the FS = 1.1 for $N_{1,60cs} \leq 15$ blows/30 cm has an associated CR of ~0.1 (i.e., the cost associated with a false-positive prediction is about one tenth the cost of a false-negative prediction). If we assume that the FS varies linearly from 1.1 to 1.0 for $N_{1,60cs}$ ranging from 15 to 30 blows/30 cm, the associated CR ranges from 0 to ~0.71. Again, the higher upper limit of the CR for denser soils can be justified based on the lower strain potential of the soil once it liquefies.

Although consideration of the strain potential of the liquefied soil should be taken into account in determining the minimum required FS for a project, the value of the infrastructure that will potentially be impacted by the liquefaction should also be considered (e.g., large earthen dam vs. a low-rise storage structure). This is where optimal FS-CR relationships shown in Figure A.4b can be used to select project-specific FS. Specifically, the costs of liquefaction risk mitigation schemes relative to the costs associated with allowing the infrastructure to sustain damage (e.g., Green et al. 2019) can be taken directly into account in selecting the FS. This is conceptually illustrated in Figure A.5 using a hypothetical optimal FS-CR curve. In this figure, the initial FS for a site is computed to be 1.0, which has an associated CR = 0.8. However, the minimum required FS for the site is specified as 1.2, which has an associated CR = 0.1. To determine whether performing ground improvement to increase the FS from 1.0 to 1.2 is worth the expense, the difference between the CR for the unimproved and improved ground can be compared to the cost of ground improvement divided by C_{FN} (i.e., $CR_{improved} – CR_{unimproved}$ vs. Cost of Ground Improvement/C_{FN}). If ($CR_{improved} – CR_{unimproved}$) ≥ Cost of Ground Improvement/C_{FN}, then ground improvement is worth the expense (i.e., using a minimum required FS = 1.2 is justified). However, if ($CR_{improved} – CR_{unimproved}$) < Cost of Ground Improvement/C_{FN}, then it would be more economical to leave the site unimproved (i.e., use a minimum required FS = 1.0) and pay for the cost of repairs associated with liquefaction, if it occurs.

The limitation of using the optimal FS-CR curves in Figure A.4b to select project-specific minimum required FS are the limited ranges of the FS represented by the curves (i.e., $N_{1,60cs} \leq 15$ blows/30 cm: $0.7 \leq FS \leq 1.3$; 15 blows/30 cm < $N_{1,60cs}$ < 30 blows/30 cm: $0.89 \leq FS \leq 1.075$). More specifically, the issue is the maximum value of the FS that can be determined using the curves (i.e., FS = 1.3 for $N_{1,60cs} \leq 15$ blows/30 cm and FS ≈ 1.075 for 15 blows/30 cm < $N_{1,60cs}$ < 30 blows/30 cm), because it is doubtful that an FS less than 1.0 will be used as a design criterion. These upper bound limits on FS are dictated by the largest FS for the "liquefaction" case histories in distributions shown in Figure A.2. And, although the distributions may become "smoother" as additional case histories are compiled, it is doubtful that the maximum FS represented by the optimal FS-CR curves will increase significantly. The reason is that the deterministic $CRR_{M7.5}$ curves are conservatively "placed" so that none of the "liquefaction" case histories have large FS; if they do, the deterministic $CRR_{M7.5}$ curve would be re-drawn to reduce the FS of the "liquefaction" case histories.

Inherently, selecting a minimum required FS for a project that is greater than 1.3 for $N_{1,60cs} \leq 15$ blows/30 cm or greater than 1.075 for 15 blows/30 cm < $N_{1,60cs}$ < 30 blows/30 cm (e.g., FS = 1.5, Martin & Lew 1999) implies that the costs associated with allowing the infrastructure to sustain damage due to liquefaction are intolerable, regardless of the value of the impacted infrastructure. However, it needs to be realized that FS is based on both the capacity of the soil to resist liquefaction (i.e., $CRR_{M7.5}$) and the demand imposed on the soil due to earthquake shaking (i.e., CSR^*). For the case histories shown in Figure A.1, best estimates of the ground motions actually experienced at the sites were used to compute CSR^*. However, for design specifications, ground motions having a given return period (T_R) are commonly used to compute CSR*, where longer return period motions are specified for "critical" versus "standard" structures (e.g., ASCE 2005, 2017). Accordingly, the probability that liquefaction will be triggered at a site that is associated with common design specifications is a function of both FS and the T_R of ground motions specified in design criteria, although this probability is not necessarily quantified. Based on this, the minimum required FS listed in Table A.2, for example, could be used to form the basis of design specifications for both standard and critical facilities because the T_R of the design ground motions can be used to adjust the (unquantified) probability of liquefaction triggering to an acceptable level. Although this approach to specifying design criteria for liquefaction triggering may seem ad hoc, it does represent the current state-of-practice and will likely continue to do so until more formal probabilistic approaches for evaluating liquefaction triggering potential are developed (e.g., Green et al. 2018).

A.5 Conclusions

Utilizing the SPT liquefaction case-history database compiled by Boulanger & Idriss (2014), relationships between the optimal factor of safety against liquefaction (FS) and the ratio of false-positive prediction costs to false-negative prediction costs (i.e., cost ratio, CR) were developed. It was shown that an inverse relationship exists between CR and FS, such that as CR decreases, the corresponding optimal FS for decision making increases. The relationships were used to provide insights into FS specifications for California. The CR associated with minimum required FS for looser soils is lower than that for denser soils, due to the strain potential of the respective soils once liquefaction is triggered. However, these specifications do not consider the value of the infrastructure that will potentially be impacted by the liquefaction response of the soil; optimal FS-CR relationships can be used for this purpose. Specifically, optimal FS-CR relationships can be used to select the minimum required FS based on the costs of liquefaction risk-mitigation schemes relative to the costs associated with allowing the infrastructure to sustain damage.

A.6 Acknowledgements

This research was funded by National Science Foundation (NSF) grants CMMI-1435494, CMMI-1724575, CMMI-1751216, and CMMI-1825189, as well as Pacific Earthquake Engineering Research Center (PEER) grant 1132-NCTRBM and U.S. Geological Survey (USGS) award G18AP-00006. However, any opinions, findings, and conclusions or recommendations expressed

in this paper are those of the authors and do not necessarily reflect the views of NSF, PEER, or USGS.

References

American Society of Civil Engineering (ASCE), 2005. *ASCE/SEI 43-05: Seismic design criteria for structures, systems, and components in nuclear facilities*, American Society of Engineers, Reston, VA.

American Society of Civil Engineering (ASCE), 2017. *ASCE 7-16: Minimum design loads and associated criteria for buildings and other structures*, American Society of Engineers, Reston, VA.

Boulanger, R.W. & Idriss, I.M. 2014. *CPT and SPT based liquefaction triggering procedures*. Report No. UCD/CGM-14/01, Center for Geotechnical Modelling, Department of Civil and Environmental Engineering, UC Davis, CA, USA.

Cetin, K.O., Seed, R.B., Der Kiureghian, A., Tokimatsu, K., Harder, L.F., Jr., Kayen, R.E. & Moss, R.E.S. 2004. Standard penetration test-based probabilistic and deterministic assessment of seismic soil liquefaction potential. *Journal of Geotechnical and Geoenvironmental Engineering*, ASCE, 130(12): 1314–1340.

Fawcett, T. 2006. An introduction to ROC analysis. *Pattern recognition letters*, *27*(8): 861-874.

Green, R.A., Maurer, B.W., Cubrinovski, M. & Bradley, B.A. 2015. Assessment of the Relative Predictive Capabilities of CPT-Based Liquefaction Evaluation Procedures: Lessons Learned from the 2010-2011 Canterbury Earthquake Sequence. *Proc. 6th Intern. Conf. on Earthquake Geotechnical Engineering* (6ICEGE), Christchurch, New Zealand, 2-4 November.

Green, R.A., Upadhyaya, S., Wood, C.M., Maurer, B.W., Cox, B.R., Wotherspoon, L., Bradley, B.A. & Cubrinovski M. 2017. Relative efficacy of CPT- versus Vs-based simplified liquefaction evaluation procedures. *Proc. 19th Intern. Conf. on Soil Mechanics and Geotechnical Engineering*, Seoul, Korea, 17-22 September.

Green, R.A., Bommer, J.J., Rodriguez-Marek, A., Maurer, B., Stafford, P., Edwards, B., Kruiver, P.P., de Lange, G. & van Elk, J. 2018. Addressing limitations in existing 'simplified' liquefaction triggering evaluation procedures: Application to induced seismicity in the Groningen gas field," *Bulletin of Earthquake Engineering*, https://doi.org/10.1007/s10518-018-0489-3.

Green, R.A., Wotherspoon, L.M. & Cubrinovski, M. 2019. Chapter 8: Damage and restoration to river stopbanks, *Earthquake-Flood Multi-Hazard Impacts on Lifeline Systems* (Sonia Giovinazzi, Deidre Hart, and Craig Davis, eds.), ASCE Monograph. (*in press*)

Idriss, I.M. & Boulanger, R.W. 2008. *Soil liquefaction during earthquakes*. Monograph MNO-12, Earthquake Engineering Research Institute, Oakland, CA, 261 pp.

Kayen, R., Moss, R., Thompson, E., Seed, R., Cetin, K., Kiureghian, A., Tanaka, Y. & Tokimatsu, K. 2013. Shear-wave velocity–based probabilistic and deterministic assessment of seismic soil liquefaction potential. *Journal of Geotechnical and Geoenvironmental Engineering*, 139(3): 407-419.

Martin, G.R. & Lew, M. (eds). 1999. *Recommended procedures for implementation of DMG Special Publication 117 guidelines for analysing and mitigating liquefaction in California*. Southern California Earthquake Center, University of Southern California, Los Angeles, CA.

Maurer, B.W., Green, R.A., Cubrinovski, M. & Bradley, B. 2015a. Fines-content effects on liquefaction hazard evaluation for infrastructure during the 2010-2011 Canterbury, New Zealand earthquake sequence. *Soil Dynamics and Earthquake Engineering*, 76: 58-68.

Maurer, B.W., Green, R.A., Cubrinovski, M., & Bradley, B. 2015b. Assessment of CPT-based methods for liquefaction evaluation in a liquefaction potential index framework. *Géotechnique* 65(5): 328-336.

Maurer, B.W., Green, R.A., Cubrinovski, M. & Bradley, B. 2015c. Calibrating the liquefaction severity number (LSN) for varying misprediction economies: A case study in Christchurch, New Zealand. *Proc. 6th International Conference on Earthquake Geotechnical Engineering*, Christchurch, New Zealand, 1-4 November 2015.

Maurer, B.W., Green, R.A., van Ballegooy, S., Bradley, B.A. & Upadhyaya, S. 2017a. Performance comparison of probabilistic and deterministic liquefaction triggering models for hazard assessment in 23 global earthquakes. *Geo-Risk 2017: Reliability-based design and code developments* (J. Huang, G.A. Fenton, L. Zhang, and D.V. Griffiths, eds.), ASCE Geotechnical Special Publication 283: 31-42.

Maurer, B.W., Green, R.A., van Ballegooy, S. & Wotherspoon, L. 2017b. Development of region-specific soil behavior type index correlations for evaluating liquefaction hazard in Christchurch, New Zealand. *Soil Dynamics and Earthquake Engineering*, (*in press*).

Maurer, B.W., Green, R.A., van Ballegooy, S. & Wotherspoon, L. 2017c. Assessing liquefaction susceptibility using the CPT Soil Behavior Type Index. *Proc. 3rd Intern. Conf. on Performance-Based Design in Earthquake Geotechnical Engineering* (PBDIII), Vancouver, Canada, 16-19 July.

Moss, R.E.S, Seed, R.B., Kayen, R.E., Stewart, J.P., Der Kiureghian, A. & Cetin, K.O. 2006. CPT-based probabilistic and deterministic assessment of in situ seismic soil liquefaction potential. *Journal of Geotechnical and Geoenvironmental Engineering*, ASCE, 132(8):1032-1051.

Oommen, T., Baise, L.G. & Vogel, R. 2010. Validation and application of empirical liquefaction models. *Journal of Geotechnical and Geoenvironmental Engineering, 136*(12): 1618-1633.

Robertson, P.K. & Wride, C.E. 1998. Evaluating cyclic liquefaction potential using cone penetration test. *Canadian Geotechnical Journal*, 35(3): 442-459.

Seed, H.B. & Idriss, I.M. 1971. Simplified procedure for evaluating soil liquefaction potential. *Journal of the Soil Mechanics and Foundations Division,* 97(SM9): 1249–1273.

Upadhyaya, S., Maurer, B.W., Green, R.A, & Rodriguez-Marek, A. 2018. Effect of non-liquefiable high fines-content, high plasticity soils on liquefaction potential index (LPI) performance. *Geotechnical Earthquake Engineering and Soil Dynamics V: Liquefaction Triggering, Consequences, and Mitigation* (S.J. Brandenberg and M.T. Manzari, eds.), ASCE Geotechnical Special Publication 290: 191-198.

Whitman, R.V. 1971. Resistance of soil to liquefaction and settlement. *Soils and Foundations*, 11: 59–68.

Zhu, J., Baise, L.G. & Thompson, E.M. 2017. An updated geospatial liquefaction model for global application. *Bulletin of the Seismological Society of America*, 107(3), doi: 10.1785/0120160198.

Zou, K.H. 2007. Receiver operating characteristic (ROC) literature research. On-line bibliography available from: <http://www.spl.harvard.edu/archive/spl-pre2007/pages/ ppl/zou/roc.html> accessed 10 March 2016.

Tables

Table A.1 Optimal FS for a range of CR.

CR	Optimal FS	
	$N_{1,60cs} \leq 15$	$15 < N_{1,60cs} < 30$
0.00-0.10	1.29	1.07
0.10-0.36	0.94	1.07
0.36-0.60	0.94	1.03
0.60-0.72	0.78	1.03
0.72-0.80	0.78	0.94
0.80-1.63	0.75	0.94
1.63-2.00	0.75	0.89

Table A.2 Minimum required FS for liquefaction hazard assessment for California (Martin & Lew 1999).

Consequences of Liquefaction	$N_{1,60cs}$	FS
Settlement	≤15	1.1
	≥30	1.0
Surface Manifestation	≤15	1.2
	≥30	1.0
Lateral Spreading	≤15	1.3
	≥30	1.0

Figures

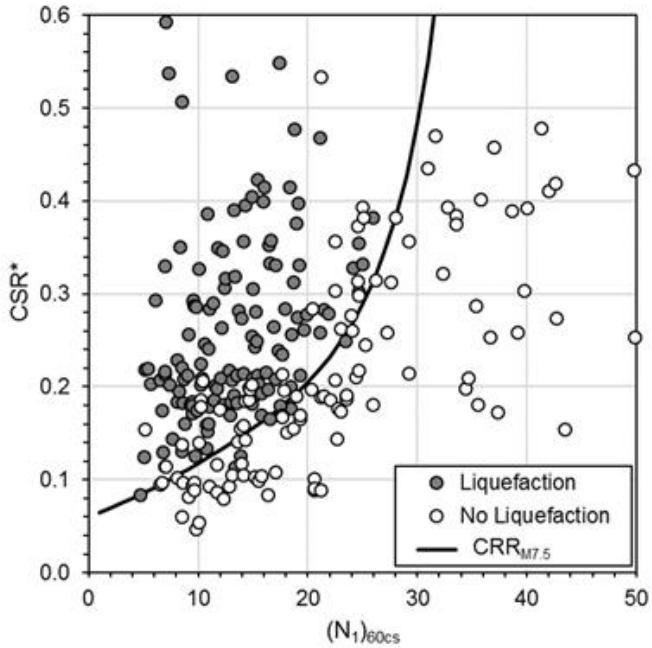

Figure A.1 BI14 deterministic $CRR_{M7.5}$ curve and associated case history data.

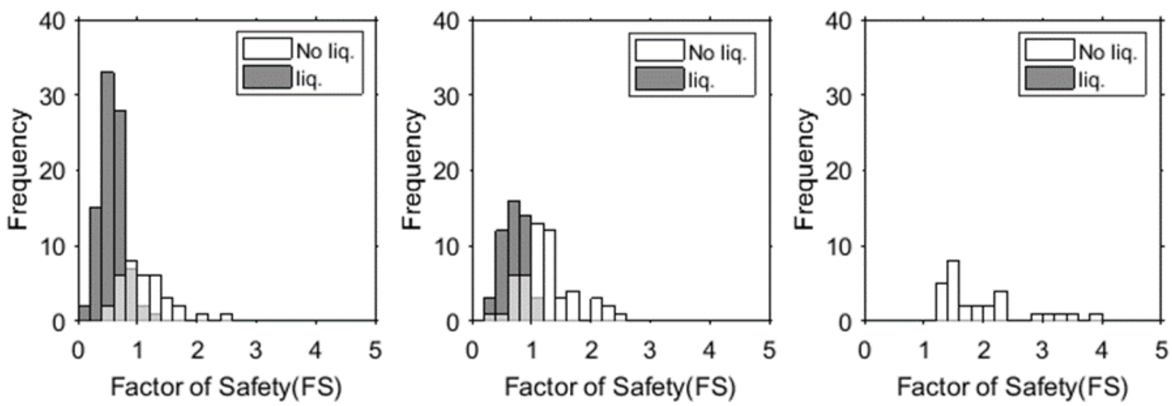

Figure A.2 Histograms of FS for the BI14 SPT case history database: (a) $N_{1,60cs} \leq 15$ blows/30 cm; (b) 15 blows/30 cm < $N_{1,60cs}$ < 30 blows/30 cm; and (c) $N_{1,60cs} \geq 30$ blows/30 cm. The light grey bars indicate the overlapping of the histograms of liquefaction and no liquefaction case histories.

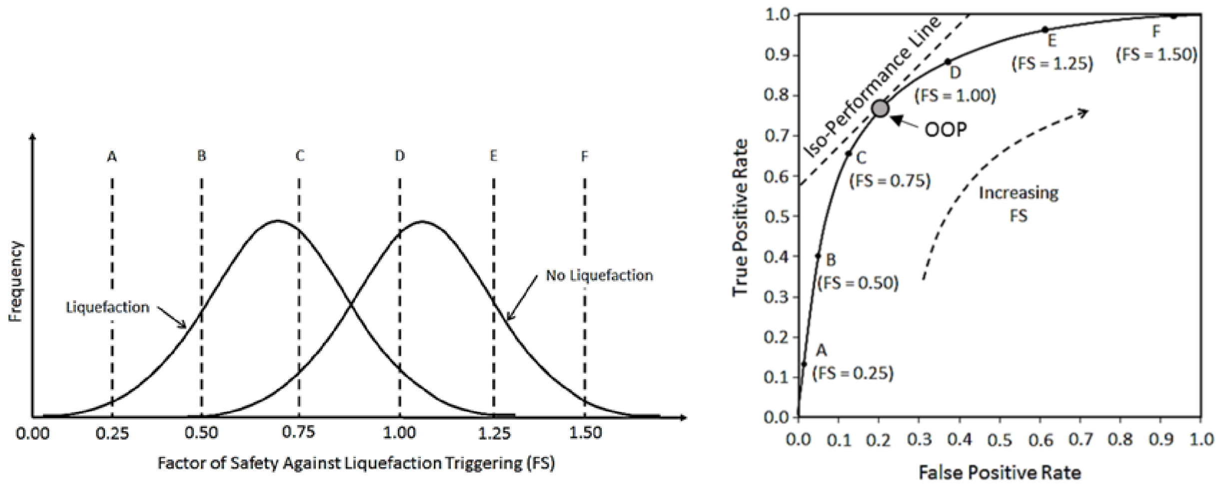

(a) (b)

Figure A.3 Conceptual illustration of ROC analyses: (a) frequency distributions of liquefaction and no liquefaction observations as a function of FS; (b) corresponding ROC curve.

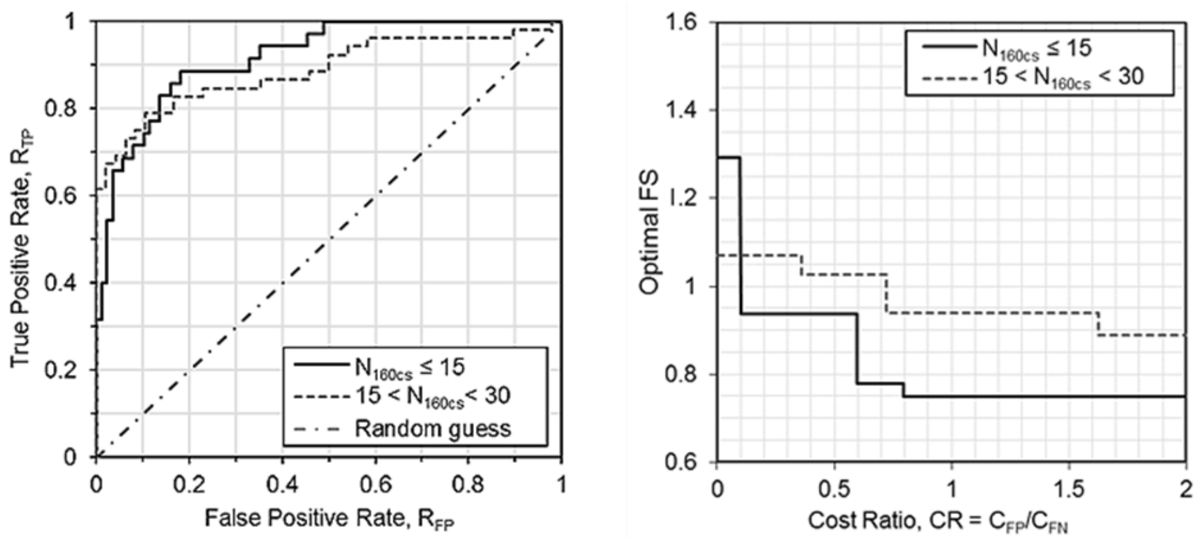

(a) (b)

Figure A.4 ROC analyses of the BI14 SPT case history data shown in Figure A.2a ($N_{1,60cs} \leq 15$ blows/30 cm) and Figure A.2b (15 blows/30 cm < $N_{1,60cs}$ < 30 blows/30 cm): (a) ROC curves; and (b) optimal FS vs CR.

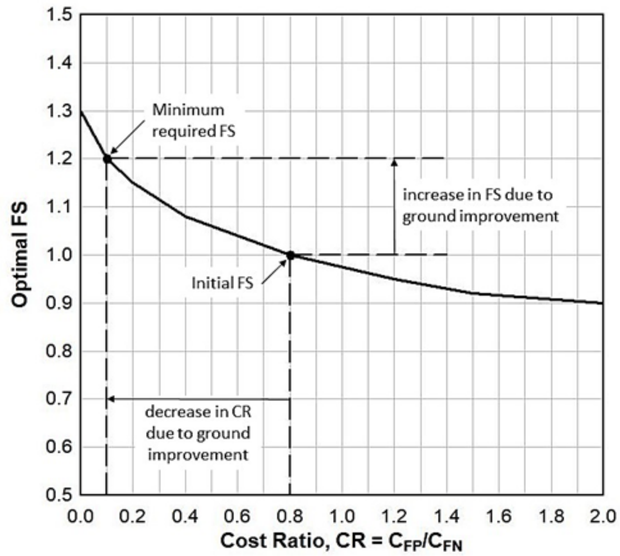

Figure A.5 Conceptual illustration, using a hypothetical optimal FS-CR curve, on how to determine whether performing ground improvement to increase the FS from 1.0 to 1.2 is worth the expense.

Appendix B: Influence of corrections to recorded peak ground accelerations due to liquefaction on predicted liquefaction response during the M_w 6.2, February 2011 Christchurch earthquake

Sneha Upadhyaya[1]; Russell A. Green[2]; Adrian Rodriguez-Marek[2]; Brett W. Maurer[3]; Liam M. Wotherspoon[4]; Brendon A. Bradley[5]; and Misko Cubrinovki[5]

[1]Graduate Student, Department of Civil and Environmental Engineering, Virginia Tech, USA.

[2]Professor, Department of Civil and Environmental Engineering, Virginia Tech, USA.

[3]Assistant Professor, Department of Civil and Environmental Engineering, University of Washington, USA.

[4]Associate Professor, Department of Civil and Environmental Engineering, University of Auckland, NZ.

[5]Professor, Department of Civil and Natural Resources Engineering, University of Canterbury, NZ.

B.1 Abstract

Evaluations of Liquefaction Potential Index (LPI) in the 2010-2011 Canterbury earthquake sequence (CES) in New Zealand have shown that the severity of surficial liquefaction manifestations is significantly over-predicted for a large subset of sites. While the potential cause for such over-predictions has been generally identified as the presence of thick, non-liquefiable crusts and/or interbedded non-liquefiable layers in a soil profile, the severity of surficial liquefaction manifestations at sites that do not have such characteristics are also often significantly over-predicted, particularly for the M_w 6.2, February 2011 Christchurch earthquake. The over-predictions at this latter group of sites may be related to the peak ground accelerations (PGAs) used in the liquefaction triggering evaluations. In past studies, the PGAs at the case history sites were estimated using a procedure that is conditioned on the recorded PGAs at nearby strong motion stations (SMSs). Some of the soil profiles on which these SMSs were installed experienced severe liquefaction, often with an absence of surface manifestation, and the recorded PGAs are inferred to be associated with high-frequency dilation spikes after liquefaction was triggered. Herein the influence of using revised PGAs at these SMSs that are in accord with pre-liquefaction motions on the predicted severity of surficial liquefaction at nearby sites is investigated. It is shown that

revising the PGAs improved these predictions, particularly at case history sites where the severity of the surface manifestations was previously over-predicted and could not be explained by other mechanisms.

B.2 Introduction

The 2010-2011 Canterbury, New Zealand, earthquake sequence (CES) began with the 4 September 2010, M_w 7.1 Darfield earthquake and included up to ten events that triggered liquefaction. However, most notably, widespread liquefaction was induced by the M_w 7.1, 4 September 2010 Darfield and the M_w 6.2, 22 February 2011 Christchurch earthquakes. The ground motions from these events were recorded across Christchurch and its environs by a dense network of strong motion stations (SMSs). Also, due to the severity and spatial extent of liquefaction resulting from the 2010 Darfield earthquake, the New Zealand Earthquake Commission (EQC) funded an extensive subsurface characterization program for Christchurch, with over 25,000 Cone Penetration Tests (CPT) performed to date. The combination of well-documented liquefaction response during multiple events, densely-recorded ground motions for the events, and detailed subsurface characterization provided an unprecedented opportunity to investigate liquefaction triggering and related phenomena. Towards this end, multiple studies have investigated the accuracy of various liquefaction triggering evaluation procedures and liquefaction severity index models (e.g., Green et al. 2014, 2015; Maurer et al. 2014, 2015; van Ballegooy et al. 2014b). Among others, Maurer et al. (2014, 2015) evaluated the performance of the Liquefaction Potential Index (LPI) (Iwasaki et al. 1978) during the 2010-2011 CES and found that it systematically over-predicted the severity of surficial liquefaction manifestations for a significantly large number of sites. Moreover, Maurer et al. (2014, 2015) found that such over-predicted case histories generally were comprised of soil profiles having thick, non-liquefiable crusts and/or interbedded non-liquefiable soils high in fines content, which could have suppressed the surficial manifestation of liquefied layers. However, the severity of surficial liquefaction manifestations was also over-predicted for a number of soil profiles that do not have these characteristics, especially for the M_w 6.2, February 2011 Christchurch earthquake.

One reason for these latter over-predictions may be related to the peak ground accelerations (PGAs) used in the liquefaction triggering evaluations. The PGAs at CPT sites in most prior CES studies have been estimated using the Bradley (2013b) procedure, which combines the unconditional PGA distribution as estimated by the Bradley (2013a) ground motion prediction equation, the recorded PGAs at the SMSs, and the spatial correlations of intra-event residuals to compute the conditional PGAs at sites of interest. Thus, for sites that are located far enough away from an SMS, the conditional PGAs are similar to the unconditional PGAs, and for the sites that are located near an SMS, the PGAs approach the recorded PGA at the SMS. However, the soil profiles at some of the SMSs were found to have severely liquefied during the 2011 Christchurch earthquake, as evidenced by the cyclic mobility/dilation spikes and reduced high frequency content of the horizontal components of the recorded ground motions after liquefaction was triggered (Bradley & Cubrinovski 2011). Thus, the recorded PGAs at these SMSs typically corresponded to the amplitude of these high-frequency dilation spikes, which are often higher than the PGAs of the pre-liquefaction portion of the ground motions and likely higher than the PGAs that would have been experienced at the sites if liquefaction had not been triggered. Wotherspoon et al. (2014, 2015) identified four such SMSs where the recorded PGAs were higher than the pre-liquefaction PGAs and suggested reduced PGAs for those SMSs, as summarized in Table B.1. An example acceleration time history at the North New Brighton School (NNBS) SMS is also shown in Figure B.1, which indicates the cyclic mobility/dilation spikes caused by the liquefaction of the underlying soils and the interpreted pre-liquefaction PGA.

Accordingly, the objective of this study is to investigate the influence of using the pre-liquefaction PGA at the SMSs on the predicted severity of surficial liquefaction manifestations at nearby case history sites during the 2011 Christchurch earthquake. Towards this end, the PGAs for a select group of case history sites that are located close to the SMSs listed in Table B.1 are estimated following the Bradley (2013b) procedure, using both the actual recorded PGAs and the pre-liquefaction PGAs at the SMSs. Both sets of PGAs are then used to predict the severity of surficial liquefaction manifestations via LPI and the prediction accuracies are assessed.

B.3 Data and Methodology

As discussed previously, revising the PGAs at the four SMSs listed in Table B.1 to the pre-liquefaction PGAs mostly affects nearby sites. Thus, only CPT soundings that are located within 1 km from at least one of the four SMSs listed in Table B.1 are analyzed in this study. Maurer et al. (2015) found that sites with an average soil-behavior-type index (I_c) for the upper 10 m of the soil profile (I_{c10}) less than 2.05 generally correspond to sites having predominantly clean sands to silty sands. Thus, only soundings that have $I_{c10} < 2.05$ were considered in this study, with the intent of removing cases where the over-predictions are potentially due to other causes (e.g., interbedded non-liquefiable layers high in fines content). Using all of the above criteria, 416 CPT soundings were selected for further analysis.

The severity of surficial liquefaction manifestation at each of the 416 CPT sounding locations for the 2011 Christchurch earthquake was classified in accordance with Green et al. (2014) via post-earthquake ground reconnaissance and high-resolution aerial and satellite imagery. The CPT soundings and imagery were extracted from the New Zealand Geotechnical Database (NZGD 2016). The PGA at the site of each CPT sounding was estimated using two different approaches: a) the Bradley (2013b) procedure in conjunction with the actual recorded PGAs at the SMSs, similar to prior CES studies; and (b) the Bradley (2013b) procedure in conjunction with the revised pre-liquefaction PGAs at four SMSs (see Table B.1). The PGAs at the selected case history sites resulting from approaches (a) and (b) are referred to herein as "existing" PGAs and "new" PGAs respectively. The depth of ground water table immediately prior to the earthquake was estimated using the event-specific model of van Ballegooy et al. (2014a). Finally, LPI was computed for each site using both sets of PGAs, where the factor of safety against liquefaction (FS_{liq}) was computed using the Boulanger & Idriss (2014) deterministic liquefaction evaluation procedure (LEP). Inherent to this process, soils with $I_c > 2.5$ were considered to be non-liquefiable (Maurer et al. 2017, 2018).

The accuracy of LPI predictions for both sets of PGAs were assessed following the procedure used by Maurer et al. (2014), in which ranges of LPI values assigned to different categories of surficial liquefaction manifestation severity (e.g., Table B.2) are used to compute an error (E), where E = computed LPI – (min or max) of expected range (i.e. min if computed LPI is less than the lower limit of the expected range and max if computed LPI is higher than the upper limit of the expected range). For example: if the computed LPI is 20 for a site with no observed surficial liquefaction manifestations, E = 20 - 4 = 16. Similarly, if the computed LPI is 7 for a site with severe surficial manifestations, E = 7 - 15 = -8. The prediction errors are then classified into one of the nine categories as shown in Table B.3. Note that although Maurer et al. (2014) suggested the LPI ranges shown in Table B.2 based on the Robertson & Wride (1998) LEP, they were generally found to be applicable in this study as well, which uses the Boulanger & Idriss (2014) LEP.

B.4 Results and Discussion

Table B.4 summarizes the number of case histories in each error category resulting from using the two sets of PGAs (i.e. existing and new PGAs). Moreover, histograms of these results are presented in Figure B.2.

It can be seen that using the new PGAs decreased the total number of over-predictions (i.e. "Slight to moderate O-P" to "Excessive O-P) from 262 to 56. However, the new PGAs also increased the number of under-predictions (i.e. "Slight to moderate U-P" to "Excessive U-P") from 13 to 90, but these were mostly slight-to-moderate under-predictions. Moreover, the rate at which the over-predictions changed to accurate predictions is significantly higher than the rate at which the accurate prediction changed to under-predictions. Overall, the number of accurate predictions increased from 141 to 270.

These findings suggest that corrections to the recorded PGAs for SMS sites that experience liquefaction is warranted in evaluating liquefaction procedures or documenting liquefaction case histories. Specifically, the high frequency cyclic mobility/dilation spikes after liquefaction triggering can result in over-estimated PGA values (hence, overly conservative seismic demand) for liquefaction triggering evaluations, which in turn can lead to over-predictions of the severity of surficial liquefaction manifestations. The revised PGAs used in this study were proposed by Wotherspoon et al. (2014, 2015) and corresponded to the PGAs of the recorded motions prior to the onset of liquefaction, where judgement was used to determine the timing of liquefaction triggering. More formal approaches for determining this timing are under development (e.g., Kramer et al. 2016, 2018).

An example case history is presented next that illustrates the influence of using the pre-liquefaction PGA at a nearby SMS on the predicted severity of surficial liquefaction manifestation.

Case History Site: NNB-POD03-CPT05

This case history site is located ~0.4 km from the NNBS SMS and is predominantly comprised of clean sands, as inferred from the I_c profile (Figure B.3). The PGA estimated at this site during the M_w 6.2, February 2011 Christchurch earthquake prior to making any adjustments to the recorded PGAs was 0.531 g. The depth to the ground water table was estimated to be approximately 2 m. No evidence of surficial liquefaction manifestation was observed at this site following the 2011

Christchurch earthquake. However, the LPI value computed using the existing PGAs was 13, which corresponds to expected moderate surface manifestation. Thus, the severity of surficial liquefaction manifestation is over-predicted at this site and the prediction error is moderate-to-severe over-prediction (e.g. Table B.3). The new PGA estimated at this site using the revised (pre-liquefaction) PGAs at the SMSs was 0.334 g. The computed LPI value associated with this new PGA was 2 which corresponds to no surficial liquefaction manifestations. Thus, it is seen that using the pre-liquefaction PGA at the SMSs to compute the PGA at this site corrected the prediction of the severity of surficial liquefaction manifestation at this site.

Figure B.3 contains the profiles of normalized and fines-content corrected CPT tip resistance (q_{c1Ncs}) and I_c for the case history site, as well as the profiles of FS_{liq} and LPI computed using both the existing and new PGAs.

B.5 Conclusions

This study investigated the influence of revising the recorded PGAs at the liquefied SMSs to the PGA of the pre-liquefaction portion of the ground motion on the predicted severity of surficial liquefaction at nearby sites. By analyzing 416 case-history sites located within 1 km of such SMSs, it was shown that using the new PGAs estimated by revising the PGAs at the SMSs correctly predicted a significant number of case histories that were previously over-predicted, likely due to over-estimated PGAs. Finally, the findings of this study highlight the need to accurately estimate PGAs for liquefaction evaluation by accounting for the effects that liquefaction of the underlying soils may have on recorded ground motions.

B.6 Acknowledgements

This research was funded by National Science Foundation (NSF) grants CMMI-1435494, CMMI-1724575, and CMMI-1825189 and by QuakeCoRE. However, any opinions, findings, and conclusions or recommendations expressed in this paper are those of the authors and do not necessarily reflect the views of NSF or QuakeCoRE.

References

Boulanger, R.W. & Idriss, I.M. 2014. *CPT and SPT based liquefaction triggering procedures*. Report No. UCD/CGM. -14/01, Center for Geotechnical Modelling, Department of Civil and Environmental Engineering, UC Davis, CA, USA.

Bradley, B.A. 2013a. A New Zealand-specific pseudo-spectral acceleration ground-motion prediction equation for active shallow crustal earthquakes based on foreign models. *Bulletin of the Seismological Society of America* 103(3): 1801-1822.

Bradley, B.A. 2013b. Site-Specific and spatially-distributed ground motion intensity estimation in the 2010-2011 Christchurch earthquakes. *Soil Dynamics and Earthquake Engineering* 48: 35-47.

Bradley, B.A. & Cubrinovski, M. (2011). Near-source Strong Ground Motions Observed in the 22 February 2011 Christchurch Earthquake. *Seismological Research Letters* 82: 853-865.

Green, R.A., Cubrinovski, M., Cox, B., Wood, C., Wotherspoon, L., Bradley, B. & Maurer, B.W. 2014. Select liquefaction case histories from the 2010-2011 Canterbury earthquake sequence. *Earthquake Spectra* 30(1): 131-153.

Green, R.A., Maurer, B.W., Cubrinovski, M. & Bradley, B.A. 2015. Assessment of the Relative Predictive Capabilities of CPT-Based Liquefaction Evaluation Procedures: Lessons Learned from the 2010-2011 Canterbury Earthquake Sequence. *Proc. 6th Intern. Conf. on Earthquake Geotechnical Engineering* (6ICEGE), Christchurch, New Zealand, 2-4 November.

Iwasaki, T., Tatsuoka, F., Tokida, K. & Yasuda, S. 1978. A practical method for assessing soil liquefaction potential based on case studies at various sites in Japan. *Proceedings of the 2nd International Conference on Microzonation*, Nov 26-Dec 1, San Francisco, CA, USA.

Kramer, S.L., Sideras, S.S. & Greenfield, M.W. 2016. The timing of liquefaction and its utility in liquefaction hazard evaluation. *Soil Dynamics and Earthquake Engineering 91:133-146.*

Kramer, S.L., Sideras, S.S., Greenfield, M.W. & Hushmand, B. 2018. Liquefaction, ground motions, and pore pressures at the Wildlife Liquefaction Array in the 1987 Superstition Hills earthquake. *Proc. Geotechnical Earthquake Engineering and Soil Dynamics V* (GEESD V), *Liquefaction Triggering, Consequences, and Mitigation* (S.J. Brandenberg and M.T. Manzari, eds.), ASCE Geotechnical Special Publication (GSP) 290: 384-402.

Maurer, B.W., Green, R.A., Cubrinovski, M. & Bradley, B.A. 2014. Evaluation of the liquefaction potential index for assessing liquefaction hazard in Christchurch, New Zealand. *Journal of Geotechnical and Geoenvironmental Engineering* 140(7): 04014032.

Maurer, B.W., Green, R.A., Cubrinovski, M. & Bradley, B.A. 2015. Fines-content effects on liquefaction hazard evaluation for infrastructure during the 2010-2011 Canterbury, New Zealand earthquake sequence. *Soil Dynamics and Earthquake Engineering* 76: 58-68.

Maurer, B.W., Green, R.A., van Ballegooy, S. & Wotherspoon, L. 2017. Assessing Liquefaction Susceptibility Using the CPT Soil Behavior Type Index. *Proc. 3rd Intern. Conf. on Performance-Based Design in Earthquake Geotechnical Engineering* (PBDIII), Vancouver, Canada, 16-19 July.

Maurer, B.W., Green, R.A., van Ballegooy, S. & Wotherspoon, L. 2018. Development of Region-Specific Soil Behavior Type Index Correlations for Evaluating Liquefaction Hazard in Christchurch, New Zealand. *Soil Dynamics and Earthquake Engineering* (*in press*)

NZGD 2016. *New Zealand Geotechnical Database*. <https://www.nzgd.org.nz/Default.aspx> Accessed 8/24/16. New Zealand Earthquake Commission (EQC).

Robertson, P.K. & Wride, C.E. 1998. Evaluating cyclic liquefaction potential using cone penetration test. *Canadian Geotechnical Journal* 35(3): 442-459.

van Ballegooy, S., Cox, S.C., Thurlow, C., Rutter, H.K., Reynolds T., Harrington, G., Fraser, J. & Smith, T. 2014a. *Median water table elevation in Christchurch and surrounding area after the 4 September 2010 Darfield earthquake: Version 2*. GNS Science Report 2014/18.

van Ballegooy, S., Malan, P., Lacrosse, V., Jacka, M.E., Cubrinovski, M., Bray, J.D., O'Rourke, T.D., Crawford, S.A. & Cowan, H. 2014b. Assessment of liquefaction-induced land damage for residential Christchurch. *Earthquake Spectra* 30(1): 31-55.

Wotherspoon, L.M, Orense, R.P, Bradley, B.A., Cox, B.R., Wood, C. & Green, R.A. 2014. *Geotechnical characterisation of Christchurch strong motion stations*, Earthquake Commission Biennial Grant Report; 2014, project no. 12/629.

Wotherspoon, L.M., Orense, R.P., Green, R.A., Bradley, B.A., Cox, B.R. & Wood, C.M. 2015. Assessment of liquefaction evaluation procedures and severity index frameworks at Christchurch strong motion stations. *Soil Dynamics and Earthquake Engineering* 79(Part B): 335–346.

Tables

Table B.1 Revised PGA values at four SMSs for M_w 6.2, February 2011 Christchurch earthquake as recommended by Wotherspoon et al. (2015).

SMS Name	SMS ID	PGA (g)	
		Recorded	Revised
Christchurch Botanical Gardens	CBGS	0.50	0.32
Christchurch Cathedral College	CCCC	0.43	0.35
North New Brighton School	NNBS	0.67	0.32
Christchurch Resthaven	REHS	0.52	0.36

Table B.2 LPI ranges used to assess the prediction accuracy (Maurer et al. 2014).

Manifestation severity category	Expected LPI range
No liquefaction	$0 \leq LPI < 4$
Marginal liquefaction	$4 \leq LPI < 8$
Moderate liquefaction	$8 \leq LPI < 15$
Severe liquefaction	$LPI \geq 15$

Table B.3 LPI prediction error classification (Maurer et al. 2014)**.**

Error category	Prediction error (E)
Excessive under-prediction	$E < -15$
Severe to excessive under-prediction	$-15 \leq E < -10$
Moderate to severe under-prediction	$-10 \leq E < -5$
Slight to moderate under-prediction	$-5 \leq E < -1$
Accurate prediction	$-1 \leq E < 1$
Slight to moderate over-prediction	$1 \leq E < 5$
Moderate to severe over-prediction	$5 \leq E < 10$
Severe to excessive over-prediction	$10 \leq E < 15$
Excessive over-prediction	$E > 15$

Table B.4 Summary of number of case histories in each error category using the existing and new PGAs.

Error category	Number of Case Histories	
	existing PGA	new PGA
Excessive U-P	0	0
Severe to excessive U-P	0	1
Moderate to severe U-P	4	14
Slight to moderate U-P	9	75
Accurate Prediction	141	270
Slight to moderate O-P	81	39
Moderate to severe O-P	104	11
Severe to excessive O-P	54	2
Excessive O-P	23	3
Total U-P	13	90
Total O-P	262	56

U-P = Under-predictions; O-P = Over-predictions

Figures

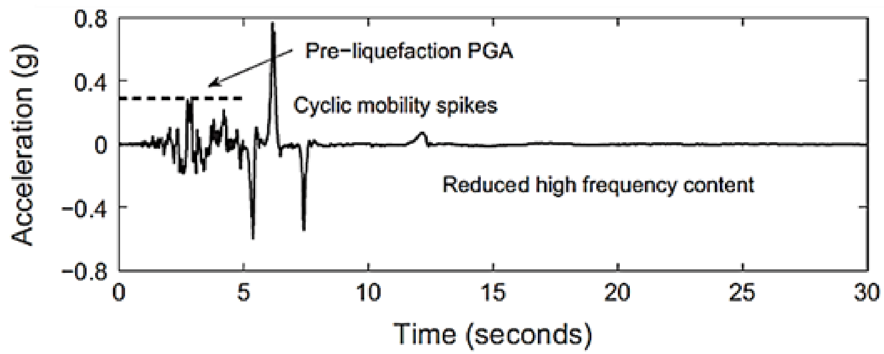

Figure B.1 Ground motion record at NNBS during the M_w 6.2 Christchurch earthquake showing cyclic mobility/dilation spikes and the pre-liquefaction PGA (Wotherspoon et al. 2015).

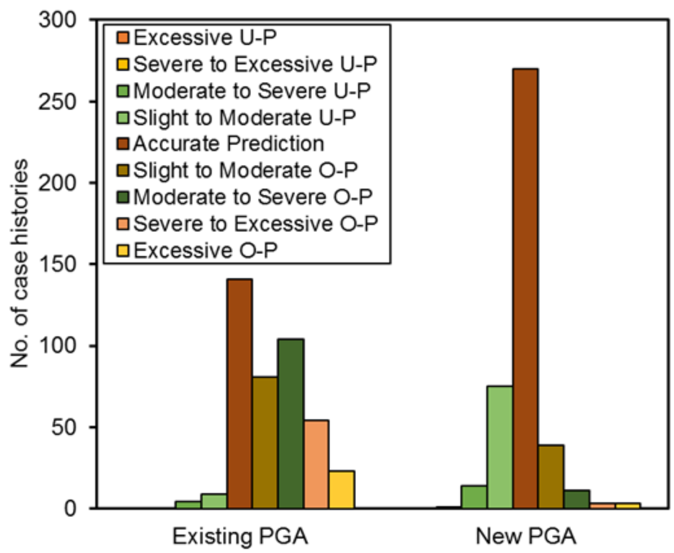

Figure B.2 Histogram showing the number of case histories in each error category using the existing and new PGAs.

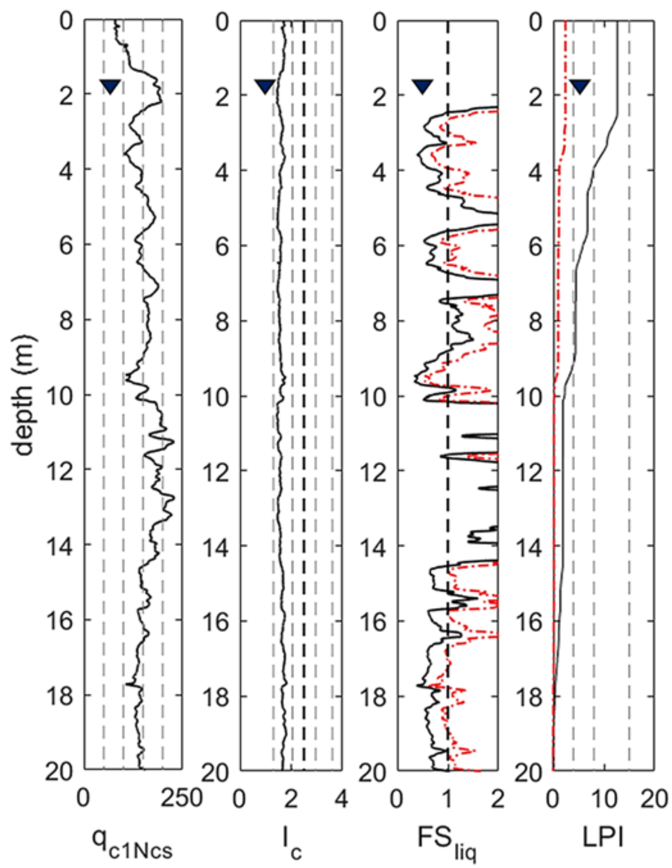

Figure B.3 Profiles of q_{c1Ncs}, I_c, FS_{liq}, and LPI versus depth for NNB-POD03-CPT05 for the M_w 6.2 February 2011 Christchurch earthquake. The solid black and red dotted lines on the profiles of FS_{liq} and LPI correspond to the existing and new PGAs at the site.